IONIC TRANSPORT
IN
PEG-MX POLYMERIC ELECTROLYTES

A Thesis Submitted
in Partial Fulfilment of the Requirements
for the Degree of

DOCTOR OF PHILOSOPHY

by
SHIULI GUPTA

to the
MATERIALS SCIENCE PROGRAM
INDIAN INSTITUTE OF TECHNOLOGY, KANPUR
January 1994

Certificate

It is certified that the work contained in the thesis entitled IONIC TRANSPORT IN PEG–MX BASED POLYMER ELECTROLYTES , by Shiuli Gupta, has been carried out under my supervision and that this work has not been submitted elsewhere for a degree.

January, 1994

Prof. Keshava Shahi
Materials Science Program
Indian Insititute of Technology, Kanpur

Synopsis

During the past two decades, the polymeric electrolytes (PEs) have attracted considerable attention because of their potential applications in various electrochemical devices, especially high energy density batteries. The properties that make them so attractive are their easy processibility, thin and thick film forming ability, mechanical flexibility so as to give good contact with the battery electrodes even during charge discharge operations, light weight and a wide potential window in the solid state.

A large variety of polymer hosts such as poly(ethylene oxide) (PEO), poly (propylene oxide) (PPO), poly(ethylene succinate) (PESc), poly(ethylene imine) (PEI), polyphosphazenes (MEEP) etc. have been employed to develop new ionically conducting polymer–salt complexes. Of all these systems, the PEO based electrolytes have been most extensively investigated, and some promising materials, e.g. PEO–$LiClO_4$, PEO–$LiCF_3SO_3$ etc. have been developed as a result. However, there are very few studies on poly(ethylene glycol) (PEG)-based systems, even though the PEG is quite similar PEO except that its repeat unit, viz. $-(CH_2 - CH_2O) - OH$, has an additional -OH group. The hydroxyl end-group has been known to stabilize complexes.

The aim of this work was therefore to investigate PEG-based systems with a view to (i) develop new polymeric electrolytes for possible applications in devices, (ii) contribute towards a better overall understanding of ion–transport mechanism in polymeric electrolytes.

During the course of this investigation it was realized that while the σ vs T behaviour is reasonably well understood in terms of configurational entropy model that leads to the well known empirical V-T-F type of behaviour, the σ vs composition (salt concentration, X) behaviour is not understood at all. An attempt has therefore been made to extend the configurational entropy model to include the effect of the salt, and hence explain, at least qualitatively, the observed σ–X behaviour.

To achieve the above objectives, the following systems were chosen for investigation:

$$\text{PEG–LiX (X = Cl,Br, } ClO_4 \text{)}$$

Li-salts were the obvious choice because of the well known advantage of Li (anode) based batteries which have high energy density.

The thesis comprises 6 chapters, Chapter 1 gives a brief review of solid electrolytes or fast–ion conductors, their classification and the relative importance of polymeric electrolyes as solid–state battery materials. A brief description of various kinds of conducting polymers is given and the concept of polymer–salt complexes is introduced. A summary of recent developments in the field of polymer–salt complexes is also given followed by the Statement of the Problem.

Chapter 2 deals with the theory of polymeric electrolytes. The first section discusses the thermodynamics of the complex formation and the factors that affect complex formation. A discussion on the temperature and composition dependence of σ is given. Besides, the various theories of transport in polymers, viz., the Cohen-Turnbull and the WLF approach to the free volume theory and the Configurational Entropy model are briefly outlined.

In Chapter 3 a brief description of the experimental techniques used in this work is given. The polymer films were prepared by solvent casting (methanol and acetonitrile). Self supporting films of $\simeq$ 0.5 mm thickness were obtained

and characterized by Complex Impedance Analysis, FTIR, XRD, DSC, SEM and solid state NMR techniques.

Chapter 4 deals with the structural and phase characterization studies using such techniques as DTA/DSC, XRD and FTIR. The FTIR studies on PEG–LiX systems showed a shift in the bands at 1100 cm^{-1} region, which could be attributed to the fact that the –C–O–C bands were involved in the complex formation. The XRD studies indicated the absence of LiX pure phases in the complexes. As expected, the XRD peaks corresponding to PEG phase, were found to decrease in intensity with the increase in the salt concentration. The DSC studies on these complexes indicate two thermal events; one around 62–65 $^{\circ}C$ corresponding to the melting of the host polymer PEG and the other at $\sim 200^{\circ}C$ corresponding to the melting of the crystalline polymer–salt complex phase. Based on these limited DSC, XRD and SEM studies partial phase diagrams of the PEG–LiCl and PEG–LiBr systems have been suggested. The SEM studies on quenched samples showed the absence of spherulitic structure above $\sim 60^{\circ}C$.

Chapter 5 reports the ionic transport studies such as electrical conductivity (σ) vs salt concentration (X) and temperature (T), dielectric constant (ϵ') and loss (ϵ'') and solid state NMR on the PEG–LiX (X = Cl,Br, ClO_4) systems.

The σ vs X studies on PEG–LiX (X = Cl, Br, ClO_4) are characterized by a pair of maxima (say at X_1 and X_3, $X_3 > X_1$) and a minimum (say at X_2 such that $X_1 < X_2 < X_3$). It has generally been found that the σ_{max} $(X_3) > \sigma_{max}$ (X_1), and that the locations of extrema shift towards higher salt concentrations, i.e. the values of X_1, X_2 and X_3 increase, as temperature increases. These features are exhibited not just by PEG–LiX systems investigated in this work, but a fairly large number of polymer–salt complexes and are not explained by the existing theories and models. The configurational entropy model that leads to the well known VTF type of σ vs T relation, has been extended to include the effect of the salt in the polymer to obtain the following relation

$$\sigma(X,T) = A(T)X \exp[\frac{-K_\sigma}{T_r - T_\sigma X}] \qquad (1)$$

which describes the conductivity as function of both temperature (T) and composition (X). In the above equation A(T) = constant ($T^{-1/2}$) is a weakly temperature–dependent constant, and
$K_\sigma = E_a/k$ = apparent *activation* temperature
$T_r = T - T_o$ = reduced temperature, and
$T_\sigma = \delta T_{cx}/\delta X$ = change in the glass transition temperature per mole fraction of salt.

The modified Eq (1) not only predicts the existence of a pair of maxima and a minimum between them, but also several other minute features observed in the σ–X isotherms. For instance, the modified Eq (1) predicts that (i) X = X_1 and X_3 are points of local maxima and X_3 a minimum, i.e. $\delta^2\sigma/\delta X^2 < 0$ at X_1 and X_3 and >0 at X_2, (ii) X_2 lies between X_1 and X_3, i.e. $X_1 < X_2 < X_3$, (iii) $\sigma(X_3) > \sigma(X_1)$, (iv) the locations of all three extrema shift to higher values of salt concentrations i.e. X_1, X_2 and X_3 increase,as the temperature (T) or reduced temperature T_r (= $T - T_o$) increases, (v) at low salt concentrations i.e. $X << T_r/T_\sigma$, σ vs X isotherms should be linear and their slope would increase exponentially as T or T_r increases and thus a plot of $\delta\sigma/\delta X$ vs $1/T - T_o$ should also be linear whose slope yields the apparent activation temperature (K_σ) or energy $E_a = kK_\sigma$. All these predictions are in confirmity with the experimental results.

Besides, from the known K_σ and T_o values of the host polymer and T_σ for a particular polymer–salt complex, the locations of maxima (X_1,X_3) and the minimum (X_2) have been calculated and are found to be comparable with the corresponding observed values, except for X_3 values. The inadequacy of the extended model at high salt concentrations is attributed to the (i) failure of underlying assumptions, viz., that $K_\sigma = kE_a$ is independent of the salt concentrations and is an exclusive property of the host polymer and (ii) the polymer salt complexes are essentially amorphous. The available experimental results suggest that E_a remains practically constant upto 0.05–0.08 mole fraction of salt but increases thereafter. Similarly, the crystalline phase may appear at higher salt concentrations. Microscopically, the above features may be

explained in terms of formation of neutral ion pairs and charged triple ion pairs.

The observed conductivity vs temperature behaviour consists of two regions; a low temperature ($T < 60°C$) region associated with an Arrhenius activation energy of $\sim$ 1.03 eV and a high temperature region ($T > 60°C$) with an activation energy of $\sim$ 0.45 eV. The dielectric studies in the range 180–300 K indicate the presence of two relaxation processes. ^{7}Li NMR linewidth studies suggest two regions of motional narrowing in the 160–340 K region. The ^{7}Li spin-lattice relaxation studies also showed two relaxation regions. The activation energies obtained from the dielectric loss and NMR linewidth vs temperature studies are found to be comparable.

The last and the 6th Chapter presents the effect of ionic size and dispersion of Al_2O_3 on the conductivity (σ) of the polymer–salt complexes. The effect of anion size on σ is examined by investigating the salts LiX (X = Cl, Br, I and ClO_4) complexed with PEG. The conductivity is highest for the largest and most polarizable anion, viz., ClO_4^-. The effect of cation size was studied by using the salts MI (M = Li, Na, K and Cs) with PEG. Here also, larger the cation higher is the conductivity. Lithium being, as usual, exception to this rule. PEG–LiX salts exhibit by and large the highest conductivity.

Acknowledgements

First and foremost I wish to thank Prof. K. Shahi for his valuable guidance, without which this thesis would not have been possible. The unrestricted and progrssive laboratory environment that he provided made the entire course of this research work very stimulating.

I am also thankful to Profs. D.C. Aggarwal, Jitendra Kumar, K.N. Rai and Y.N. Mahapatra of the Materials Science Deparment, I.I.T. Kanpur, for their constant support throughout the course of this thesis work, and particularly to Prof. K.N. Rai for providing some of the impedance measurement facilities.

I also wish to thank Profs. S.C. Aggarwal, D.C. Khan, V. Singh and K. Bannerji of the Physics Department, I.I.T., Kanpur for helping me in understanding solid state physics through their courses.

I would also like to thank a few others who helped me throughout the course of my phD. work: Profs. D.P. Rao, Shobha Madan, R.K. Thareja, P.R.K. Rao, A.P. Shukla, K.V.G.K. Gokhale and S.K. Gupta.

I wish to thank Prof. S.V. Bhat and Mr. Nader Binesh from the Physics Department, I.I.Sc., Bangalore for their valuable help in the solid state NMR analysis.

I also wish to thank the members of the various laboratories outside I.I.T.,Kanpur, that were used during the course of this thesis : Mr. Naveen Suyal from the Hindustan Cables Ltd. and Dr. P.T. Rajgopalan from DMSRDE

(Defence Lab.) for the DSC measurements; and Mr. Surya Prakash of the Sophisticated Instruments Facility (SIF), I.I.Sc., Bangalore for the Solid State NMR measurements.

I wish to thank Mr. Umashanker from the XRD laboratory, Mr. Pal from the SEM laboratory, Mr. B. Sharma from the Materials Processing Laboratory, Mr. Jain from the Materials testing Laboratory and Mr. Chaturi Singh from the Electronics Laboratory of the Advanced Center for Materials Science, I.I.T., Kanpur.

I also wish to thank Mr. J.N. Sharma and the other members of the Glass Blowing Section, I.I.T., Kanpur and all the members of the Central Workshop, I.I.T., Kanpur for their valuable help.

I wish to thank Mr. Vishwanath Singh, Mr. Jawar Singh, Mr. Agnihotri, Mr. Gupta and all other members of the ACMS office for providing the necessary facilities like xeroxing, typing etc.

I also wish to thank my friends in the Solid State Ionics Lab.: Viji, Sujata, Mandira, Mangamma, Ashok Kumar, Manoravi, Padmanabhan and Venkat; and my other friends in the Materials Science Department : Subhashish, Atanu, Ajay, Shantanu, Bhangui, Ramani and Subhash . The other friends who helped me throughout my stay in this campus are : Hajra, Smita, Gaitri, Sudha, Amita, Deepti, Sujata, Ligy and Mrs. Sita Gokhale.

I wish to thank Venkatesh, Krishna Mohan Singh and Deepak Murthy without whose help I could not have prepared this manuscript.

Finally, I wish to thank my mother, Mrs. Krishna Gupta and my father Mr. Sudhakar Gupta for their constant encouragement and support during the entire course of my thesis work.

Shiuli Gupta

Pūrnamadah pūrnamidaṁ Pūrnāt pūrnamudachyate
Pūrnasya pūrnamadāya pūrnamevāvaśisyate
(from Shukla Yajurveda)

That, the Invisible Substratum is Absolute. This, the visible, manifested creation has sprung up from that Absolute. Comprehending the absoluteness of the Absolute, the Absolute verily remains the Absolute, even when the creation appears or disappears.

To my mind if modern science is proving anything again and again, it is the essential unity of things... the whole universe is simply an ocean of matter, of which you and I are like little whirlpool, taking the whirlpool form, and coming out as matter again... The whole of our lives is one... this is the unity from which we all have come and that must essentially be one.

–Swami Vivekananda

Contents

List of Figures

List of Tables

Notations

E_{a1} : Activation energy in low temperature

E_{a2} : Activation energy in high temperature

E_a : Apparent activation energy from V-T-F Equation

K_σ : Apparent activation temperature,E_a/k

PEO : Poly(ethylene oxide)

PEG : Poly(ethylene glycol)

PPO : Poly(propylene oxide)

T_o : Equilibrium glass transition temperature

T_{ox} : $T_o + T_\sigma X$

T_σ : $(\delta T_{ox}/\delta X)$

T_r : Reduced temperature $(T-T_o)$

X_2 : Composition at minimum of σ ($= T_r/T_\sigma$)

X_1 : Composition at first maximum of σ

: ($= 1/2T_\sigma$ [$(K_\sigma + 2T_r - \sqrt{K_\sigma^2 + 4K_\sigma T_r}]$

X_3 : Composition at second maximum of σ

: ($= 1/2T_\sigma$ [$(K_\sigma + 2T_r + \sqrt{K_\sigma^2 + 4K_\sigma T_r}]$

Equations Used :

Arrhenius Eq.	: $\sigma = \sigma_o \exp(-E/kT)$
Vogel-Tamman-Fulcher (V-T-F) Eq.	: $\sigma = A'\sqrt{T} \exp(-E_a/kT)$
(Modified) V-T-F Eq.	: σ (X,T) = AX exp $[\frac{-K_a}{T_r - T_o X}]$

Chapter 1

Introduction

1.1 Historical background

Typical ionic solids like alkali halides have very low ionic conductivities at or near ambient temperatures [$\sigma_{NaCl} = 10^{-18} ohm^{-1} cm^{-1}$]. This is because these ionic crystals have low degrees of disorder so that the defect concentrations rarely exceed 10^{-18} cm^{-3}, thus only a limited fraction of ions can move at a time and carry charge through the crystal lattice. However, it was found that the defect concentration and hence the ionic conductivity depends strongly on temperature. It was, in fact the studies on the temperature dependence of ionic conductivity of such ionic solids, which ultimately led to the discovery of *superionic conductors*.

Tubandt and Lorenz, observed that solid AgI had ionic conductivities comparable to those of the best conducting liquid electrolytes at temperatures higher than $400°C$ (Tubandt and Lorenz, 1914; Tubandt and Reinhold, 1934). They showed that AgI had a highly conducting solid phase (now known as the α-phase) stable between $147 - 555°C$. At the $\beta - -\alpha$ transition, the conductivity of AgI increases by more than three orders of magnitude upto $\sigma = 1.3$ ohm^{-1} cm^{-1}. The measurement of the conductivity of AgI may be

regarded as the starting point for the investigation of such solid electrolytes. Tubandt and coworkers identified the high temperature phases of various ionic crystals as belonging to the same class of materials– α and β CuBr, α–CuI, α–Ag_2S, α–Ag_2Te. The chalcogenide phases were found to be mixed ionic and electronic conductors (Tubandt and Reinhold, 1934). In a later work, Strock (1934) proposed that the highly mobile cations were supposed to move in a *liquid like* manner within the rigid framework of the anion lattice.

Ketlaar (1934) in the same year found that in another highly conducting compound $\alpha - Ag_2HgI_4$, the three cations per unit cell were distributed at random over the four equivalent sites, leaving one site vacant, indicating that a disordered structure is related to high conductivity. Subsequently, Reuter and K.Hardel (1961) discovered Ag_3SI and Owens and Argue (1967) and Bradley and Greene (1967) independently discovered $RbAg_4I_5$. In the same year Geller (Geller, 1975) determined the structure of MAg_4I_5 [M = Rb, K, NH_4 etc.]. Their structures belong to the enantiomorphic cubic space groups $P4_13(O^7)$ and $P4_33(o^6)$. Geller (1967) also reported that $RbAg_4I_5$ under goes transitions to non- cubic phases below room temperature. This was a landmark, since the σ value of $RbAg_4I_5$ at $250K$ is $10^{-1}ohm^{-1}cm^{-1}$ (Owens and Argue, 1967) or 17 orders of magnitude larger than that of NaCl at the same temperature. That the solid electrolyte can in fact be a practical substitute for aqueous electrolytes was perhaps first demonstrated by Takahashi and Yamamoto (1966a, 1966b) using Ag_3SI i.e. $[Ag; Ag_3SI; I_2, C]$.

In the previous two decades considerable work has been done in the field of superionic conductors. Various new materials have been identified as potential solid electrolytes for high energy density batteries. This is an important development, as the existing batteries employ aqueous electrolytes and suffer from various inherent disadvantages such as – limited shelf life, low specific energy density, and limited temperature range. They also lack ruggedness and cannot be discharged quickly. The electrolytes in solid state not only eliminate a container which is required for liquid electrolytes but also make handling convenient. These electrolytes have been found to have high

energy and power carrying capacity.

1.2 Materials Aspects of Solid Electrolytes

The search for new solid electrolytes have been made based on the following considerations (Hagenmuller and VanGool, 1977)

- *In a MX material the M species can have high conductivity if the number of available sites of identical or slightly higher energy is largely in excess of the number of M particles present e.g.* $\alpha - AgI$ *and* $RbAg_4I_5$.
- *the interionic repulsive energy is minimized when the mobile ions have the smallest possible charge, i.e., monovalent.*
- *fast ionic mobility is easier for mobile species with low coordination numbers, i.e., a mobile ion finds it much easier to leave a tetrahedrally surrounded position than a site with higher coordination.*
- *the weaker the bonding energy of the M-X bond, the higher is the ionic mobility.*
- *a larger and more polarizable anion leads to higher mobility of the cation, and a small cation may be considered more mobile. A very small cation may be too strongly bound and hence may have low mobility, e.g., mobility of* $Li^+ < Na^+$ *in* β*-aluminas.*
- *since high ionic conductivity is associated with a liquid like behavior, materials with relatively low melting points are better conductors. Eg.* — CaF_2 *and* $\beta - PbF_2$ *whose melting points are lower than those of zirconia and thoria show much higher conductivities at the same temperature.*
- *the presence of homovalent or heterovalent foreign ions in the lattice may increase the conductivity.*

- *presence of insulating dispersed phases like alumina, silica, flyash etc. may increase the conductivity.*

- *amorphous ionic materials have higher conductivities than crystallized materials. Eg. $LiAlSiO_4$ has higher conductivity in the glassy state and complexes of $LiClO_4$,$LiBF_4$, $LiCF_3SO_3$ with PEO (polyethylene oxide) show much higher conductivities than the corresponding crystalline solids.*

The discovery of $MAgI_4$ family of solid electrolytes and the demonstration of AgI / Ag_3SI / I_2 all solid state cell as a potential substitute of conventional aqueous cells/batteries, stimulated a tremendous interest in solid electrolytes (Chandra, 1981) . During the past few decades, a large number of Ag^+ and Cu^+ based solid electrolytes were developed as a result (see Table 1.1) and some of them tested in cells/batteries (Shahi, 1977; Shahi and Chandra, 1975; K.Funke, 1987; Geller, 1975),However, it was realized soon that Ag^+ or Cu^+ based cells have low energy density and hence limited utility. The emphasis therefore shifted to lithium and to some extent sodium, ion based electrolytes, because for high energy density the metallic element corresponding to the mobile ion should have low equivalent weight and be highly electropositive.

The lithium based solid electrolytes may be grouped into the following categories (Shahi, 1983)

- Crystalline electrolytes, e.g. Li_3N, Li_2SO_4, LiX (X = F, Cl, Br, I).

- Mixed crystal type electrolytes : $Li_3N - LiI - LiOH$, $Li_2S - LiX$ (X = Cl,Br,I)

- Dispersed phase solid electrolytes : $LiCl - Al_2O_3$ (25 %), $LiCl - SiO_2$ (60 %).

- Ceramic electrolytes : Li-β-alumina, LISICON ($Li_{14}Zn(GeO_4)_4$).

- Glassy electrolytes : Li_5AlO_4, Li_5GaO_4, $LiNbO_3$.

Table 1.1: **Solid Electrolyte Materials**

Type of Electrolyte	Max. σ	Reference
	$(\Omega^{-1}cm^{-1})$	
Inorganic Cationic Conductors		
Halogenide Solid Electrolytes		
$RbAg_4I_5$	0.27 at 25°C	Owens and Argue (1967)
		Bradley and Greene (1967)
α-AgI	1.31 at 419 K	Tubandt and Lorenz (1914)
		Strock (1934)
$PyAg_5I_6$	0.077 at 25°C	Geller and Owens (1972)
α-Cu_2HgI_4		Ketlaar (1938)
$(C_6H_12N_4CH_3)_3Cu_{17}I_{20}$	0.001 at 20°C	Takahashi, Yamamoto and Ikeda (1973)
Sulphate based electrolytes		
Li_2SO_4		A.Lunden (1988)
$Li_2SO_4 - Li_2WO_4$		Lunden, Schroeder and Ljungmark (1988)
$\beta - Li_2SO_4 - Na_2SO_4$		Chaklanobis, Shahi and Syal (1990)
Mixed Crystal Type Electrolytes		
AgI-AgBr	4.3×10^{-6} at 25°C	Shahi and Wagner (1983)
NaBr-KBr	1.3×10^{-5} at 500°C	Manoravi and Shahi (1991a)
KBr-NaI	2.3×10^{-4} at 500°C	Manoravi and Shahi (1991b)
NaBr-NaI		Manoravi and Shahi (1991c)
$Li_2S - LiX$ (X=Cl,Br,I)	0.03 at 300°C	Schoch, Hartmann and Weppner (1986)

Table 1.1: **Solid Electrolyte Materials (continued)**

Type of Electrolyte	Max. σ	Reference
	$(\Omega^{-1}cm^{-1})$	
Li-based Electrolytes		
LiI	1×10^{-1} at 300K	Jackson and Young (1969)
LiI.$4CH_3OH$	4×10^{-3} at 25°C	Hartwig, Rabenau and Weppner (1981)
$Li_{14}Zn(GeO_4)_4$	1.3×10^{-1} at 300°C	
Li_3N		Rabenau (1982)
$Li_4B_7O_{12}(Cl_{0.68}Br_{0.32})$	1×10^{-3} at 200°C	Shannon, Taylor, *et al.* (1977)
$Li_{1-x}Si_{1-x}P_xO_4$	1×10^{-2} at 300°C	Gratzer, Bittner, *et al.* (1971)
$Li_{2+x}C_{1-x}B_xO_3$	x=0.25, 1×10^{-2}	Shannon, Taylor, *et al.* (1977)
		Huggins (1977)
Composite Electrolytes		
LiI + Al_2O_3 (40 mol%)	100* at 25°C	Liang (1973)
AgI + Al_2O_3 (0.06μ,30 mol%)	50* at 25°C	Shahi and Wagner (1981a)
AgI + SiO_2 (0.007μ,10 mol%)	45* at 25°C	Shahi and Wagner (1981b)
LiBr + Al_2O_3 (0.06μ,20 mol%)	50* at 127°C	Khandkar and Wagner (1986)
AgCl + Al_2O_3 (fibers, 3.0μ,4vol%)	15-200 nS/cm at 25°C	Dudney (1988)
$SrCl_2$ + Al_2O_3 (2.6μ,30%)	5×10^{-4} at 500°C	Fujitsu, Koumoto and Yanagida (1986)
Inorganic Anionic Conductors		
α and $\beta - PbF_2$	6×10^{-5} at 150°C	Kennedy, Meles and Hunter (1973)
ThO_2	1×10^{-5} at 1000°C	Rudolph (1959)
$(ThO_2)_{0.90}(YO_{1.5})_{0.1}$	1×10^{-2} at 1000°C	Baurle (1966)
ZrO_2 + CaO (14 m/o)	0.05 at 1000°C	Etsell and Fleugas (1970)

Table 1.1: **Solid Electrolyte Materials (continued)**

Type of Electrolyte	Max. σ	Reference
	$(\Omega^{-1}cm^{-1})$	
β - Aluminas (BA)		
Na-β-Alumina	$10^{-3} - 10^{-2}$	Yao and Kummer (1967)
Mixed $Na^+ - Cd^{2+}$-BA		Wittingham and Huggins (1971)
K,Rb,and Tl - Na BA		Kummer (1972)
NH_4^+/H_3O^+ BA		Farrington, Frase and Thomas (1984)
Eu^{2+} BA		Ghosal, Mangle, *et al.* (1983)
Pb^{2+} BA		Seevers, DeNuzzio, *et al.* (1983)
Ionically Conducting Glasses		
$75AgI.25Ag_2SO_4$	6×10^{-2} at $20°C$	Kunze (1972)
$66Ag_2S.33Ag_3S_3$	1×10^{-4} at $20°C$	Kawamoto, Nagura and Tsuchikashi (1974)
$50Na_2S.50SiS_2$	1×10^{-7} at $20°C$	Andeen, Ravaina and Souquet (1976)
$M_2O : B_2O_3 : P_2O_5$ (M=Li,Ag)		Torell (1982)
Ionically Conducting Polymers		
PEO–LiSCN	7×10^{-5} at $100°C$	Chabagno (1980)
PPO–$LiCF_3SO_3$	9×10^{-5} at $100°C$	Chabagno (1980)
PEG–$NiBr_2$	—	Mendolia and Farrington (1992)

- Polymeric electrolytes : PEO–$LiClO_4$, PPO–$LiCF_3SO_3$.

Although the crystalline solid electrolytes have been the subject of studies , the emphasis at present is on amorphous and polymer electrolytes. Some Li– based electrolytes are also listed in Table 1.1.

1.3 Polymer Electrolytes

An important advantage of polymer electrolytes is their simple processibility. The polymer host and the inorganic salt are dissolved in adequate compositions in suitable solvents and the two solutions are mixed. The solvent is then evaporated and the residue is the polymer–salt complex. This simple procedure allows easy preparation of polymer electrolyte in thin–film form, which in turn permit the fabrication of cells with variable geometry and high electrode/eletrolyte interfacial area. Furthermore, the viscoelasticity of polymer electrolytes, i.e., their ability to accommodate volume changes, minimizes the problems generally associated to all solid-state secondary batteries which arises from deformations and deteriorations of the interfaces during charge/discharge cycles. Finally, polymer electrolytes which are based on simple polyethers, are likely to have a wide electrochemical stability. For example the sweep voltammetry of a $(PEO)_7LiBF_4$ polymer electrolyte at 100^oC (Scrosati, 1988), using a Pt indicator electrode and a Li reference electrode shows that the electrolyte may allow the use of electrodic couples having operating voltages upto 4V. All these favorable aspects have led to extensive research and development in the field of polymer electrolytes.

Some of the fundamental aspects of polymers (electrolytes) are highlighted through the following questions.

1. What are polymeric materials exactly ?

2. Are they conducting-ionically or electronically?

3. Can the conductivity be enhanced by the addition of solvents or external ions?

1.3.1 What are polymeric materials exactly?

The main structural features of a polymeric compound is the presence in it of chain molecules in which a large number of atoms are combined consecutively. It has two kinds of bonds : chemical and intermolecular,which differ greatly in energy and length . The atoms in the chain are joined to each other by strong chemical bonds about 1-1.5 A in length. Much weaker intermolecular forces interact between the chains at distances of about 3-4 A. Crosslinked (three dimensional) polymers have chemical bonds (crosslinks) between their chains. If the number of crosslinks is much smaller than the number of bonds between the atoms in the chain or, which is the same, if the chain lengths between the modes of the spatial network are sufficiently large, the compound retains the properties of a polymer. However, structures like diamond, B_4C, SiC which have a network of atoms connected by chemical bonds will not be called *polymeric* materials. Structures like graphite and many inorganic compounds with crystalline lamellar lattice in which the bond energies in the plane differ considerably from that between the atoms in different planes, may be considered polymeric.

This discussion is however, limited to organic polymers. An organic macromolecule may consist of monomers of identical or of different chemical structures. Polymers consisting of identical monomers are called *homopolymers.* Polymeric compounds containing several types of monomeric units in their chain are known as *copolymers* or *mixed polymers.* Monomeric residues may combine with each other into a macromolecule to form polymers of linear, branched or crosslinked (3-d) structures. *Linear polymers* are polymers whose macromolecules are longchains with a high degree of asymmetry. A *branched*

polymer is a long chain (usually called the *main* or *backbone* chain) with side branches (side chains) the number and length of which may vary. *Crosslinked* or three *dimensional*, polymers consist of long chains connected up into a three-dimensional network by chemical crosslinks.

Copolymers may also be linear, branched or crosslinked. According to the structure of their main chain all polymers fall into *homochain* and *heterochain polymers*. The *homochain polymer* are composed of atoms of the same species, e.g., C,S,P etc. In *heterochain polymers* the main chain is made of different atoms.

Can polymers be conducting?

The answer to this is yes, they are conducting, mainly electronically or due to the presence of ionic impurities present in very minute quantity. However the conductivity (σ) values are very low.

Can the conductivity be enhanced by external sources?

Mobile ions have been introduced in polymers via non-aqueous polar solvents or directly within the network of solvating macromolecules. The various ways by which this can be achieved are as follows:

- Ion exchange membranes: Macromolecules with attached ionophoretic groups have been commercially available, when crosslinked for use as ion exchange membranes or resins.

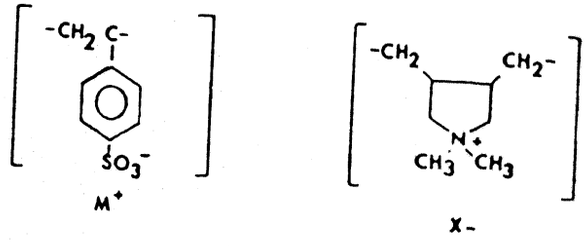

They show unipolar conduction of either M^+ or X^-. However in the dry state the conductivities are very low ($\sigma = 10^{-12} - 10^{-15} ohm^{-1} cm^{-1}$) as the polar moieties tend to segregate into stable immobile clusters. Aprotic solvents such as propylene carbonate (PC) do not loosen these clusters appreciably but water can be used to solvate them. Such polymers swollen by protic solvents are also called polyelectrolytes. The ionic conductivity is a function of the water content, and they may be considered as classical conductors in which ion transport is through the aqueous medium in which the polymer is dispersed. Polyelectrolytes have been reviewed extensively (Seanor, 1982; Wilson and Prosser, 1982; Miller, 1966).

- Gels: The conductivity of the polymer may be improved by *gelling* an aprotic electrolyte with a suitable macromolecule. Polymers with a dipole moment form gels with organic salt solutions in the range 20-90% electrolyte (Feuillade and Perche, 1975; Armand, 1980; Tsunemi, Ohno and Tsuchida, 1983)

  Some of the polymers used are : $(CH_2 - CF_2)_n, (CH_2 - CF_2)_m (CF_2 - CFCF_3)_n$

  Some of the organic salt solutions: $PC : LiBF_4; PC : LiClO_4; dioxalane : LiClO_4; THF : LiClO_4$

  The conductivities range from $10^{-5} - 10^{-3} - 1/cm^{-1}$ over the temperature range $25 - 100°C$. The electrochemical behavior of such gels have not been explored in detail, but the cationic transport number $t_+ = 0.35$, as the diffusion of the $Li(solvent)_4$ species is more hindered.

- Solvating polymer: It was observed that polymers with heteroatoms with free electron pairs can act as donors for a cation M^+. Some of these solvating polymers are:

  1. Poly(ethylene oxide) PEO
     $(CH_2 - CH_2 - O)_n$ (Armand, 1980; Fenton, Parker and Wright, 1973)
  2. Poly(ethylene oxide, crosslinked)
     $[(CH_2 - CH_2 - O)(trifunctionalurethane)]_n$ (Killis, LeNest, *et al.*, 1982)

(CH_2CH_2-O) radiation crosslinked (MacCallum, Smith and Vincent, 1984)

3. Poly(ethylene glycol,siloxane) crosslinked
   $[(OCH_2-CH_2)_pSiCH_{3q}OSi(CH_3)_{2r}O$, trif.urethane$]_n$ (Bouridah, Dalard, *et al.*, 1985)

4. Poly(propylene oxide) PPO
   $(CH_2-C(CH_3)H-O)_n$ (Armand, 1980; Chabagno, 1980)

5. Poly(ethylene succinate) PES
   $(-C_2H_4-O-CO-C_2H_4-CO-O)_n$ (Dupon, Papke, *et al.*, 1984)

6. Poly(aziridine)
   $(CH_2-CH_2-NH)_n$ (Davis and Chiang, June 3-6 1984)

7. Poly(N methyl aziridine)
   $(CH_2-CH_2-NCH_3-)_n$ (Armand, 1983)

8. Poly(methylene sulfide)
   $[(CH_2)_p-S)]_n$ p=2.5 (Shriver, Papke, *et al.*, 1981)

9. Poly(bis methoxy-ethoxy-ethoxy) phosphazene
   $[(CH_3O-C_2H_4-OC_2H_4O)_2PN]_n$ (Blonsky and Shriver, 1984)

10. Poly (ethylene adipate)
    $C_2H_4-O-CO-C_4H_8$ (Armstrong and Clarke, 1984)

PEO, which is by far the most studied material has in fact a complexing power comparable to that of crown ethers. The properties of these complexes have been studied extensively MacCallum and Vincent (1987), Armand and Gandini (June 1991), Chandra(1992). Salts of all alkali metal. including NH_4^+ have been incorporated in PEO. The only restriction being in the choice of a large anion with a delocalized charge, a criterion also used for aprotic liquid solvents. In addition to monovalent alkali metals and silver salts, salts of divalent metals like $Mg^{2+}, Cu^{2+}, Ni^{2+}, Pb^{2+}$ have also been used.

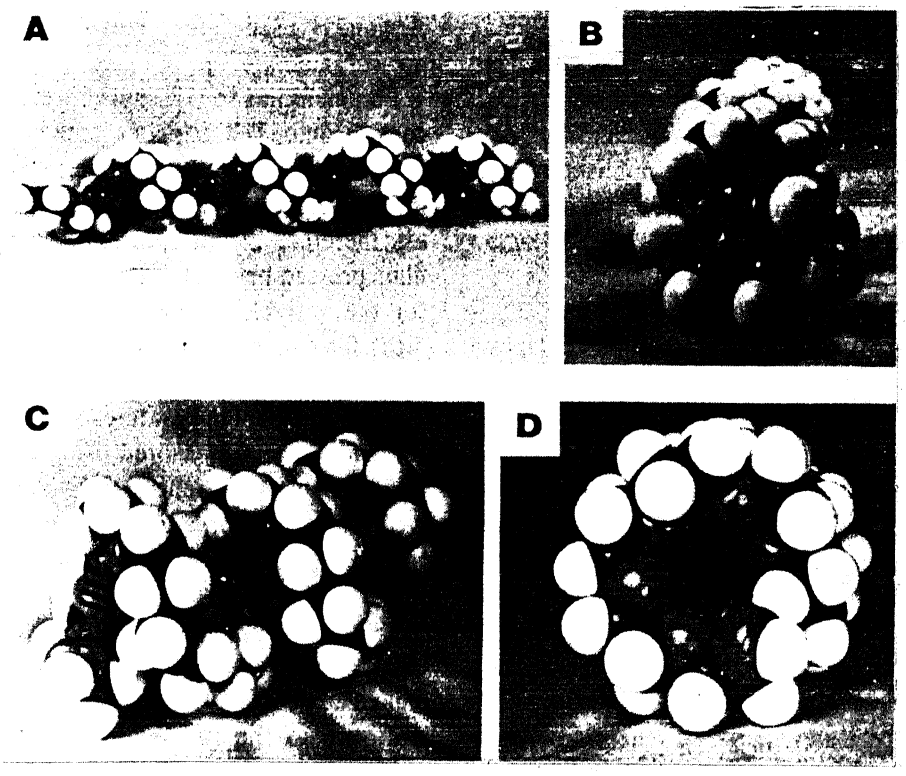

Figure 1.1: Molecular models of poly(ethylene oxide) conformations, (A) and (B) : of crystalline PEO; (C) and (D): PEO–salt complexes.(from Papke (1981).

The solvating polymers and their complexes with alkali metal salts will be discussed in detail in this work. Fig 1.1 shows the picture of molecular models of polethylene oxide and its complex.

1.4 Recent Developments

The thrust of work in improving the conductivity of these electrolytes has been in synthesizing new polymer hosts (Watanabe, 1992; Watanabe, Waganaka, *et al.*, 1992) A new polymer host: poly[2-(2-methoxyethoxy)ethyl glycidyl ether] (PMEEGE) has been developed, with the view that the flexible ether side

chain along with the flexible main chain will solvate the ions more effectively, and the short side chain would contribute to the fast ion transport owing to their fast molecular motion (Watanabe, Waganaka, *et al.*, 1992). Besides this organogels and mixtures of poly pyridinium and $AlCl_3$ complexes are also under scrutiny. In order to increase the salt *plasticizer* effect, bulkier anions based on carbanions bearing electron -withdrawing groups– $(CF_3SO_2)_3CLi$, lithium tris(trifluorosulfonyl)methyl has been used (Sanchez, 1992) as salt with PEO. A new polymer bearing a perfluorinated sulfonate function, from diallyl amine and hexafluoropropane sultone has been reported (Goulart, Sanchez and Armand, 1992) which is a good polyelectrolyte, the electron withdrawing substituents facilitating good dissociation.

Recently, the polymer salt complexes of divalent salts have been investigated (Farrington and Linford, 1987; Huq, Saltzberg and Farrington, 1989; Huq and Farrington, 1988). These systems exhibit widely varying properties. For example PEO-based electrolytes containing $CdBr_2$ are reported to have cationic transport number (t_+) of nearly unity while those of Ca or Co salts exhibit negligible cationic transport (Glasse, Latham, *et al.*, 1992). Polyether - transition metal salt systems are particularly interesting, because, in many cases distinct ionic species can be identified and quantified using visible spectroscopy (Huq, Saltzberg and Farrington, 1989; Huq and Farrington, 1988).

The semicrystalline nature of high molecular weight PEO leads to lower conductivities (conductivity being directly related to amorphous nature) and also complications in the interpretation of mechanism. Thus oligomeric polyether liquids like PEG are being used instead of PEO (Mendolia and Farrington, 1992; Cameron, Ingram and Sarmouk, 1990). Another recent development has been the study on *mixed alkali* effect in polymer electrolytes (Teeters and Norton, 1990; Huang and Frech, 1992). Raman studies prove that the mixed cations have a non- additive effect on the association-dissociation of the anions in the polymer complexes. The T_g values show a small minimum in the mixed alkali region. Solid electrolyte batteries based on these polymer–salt systems, mainly the PEO based complexes, have been fabricated (Hooper and North,

1983; Gauthier, Fauteux, *et al.*, 1985; Bonino, Ottaviani and Scrosati, 1988).

Molecular dynamic simulation and dielectric relaxation studies are the other areas being pursued very actively in recent times. A systematic investigation of structural, thermodynamic and transport properties as function of temperature, ion concentration and the solvent dielectric constant at the microscopic level has been accomplished using theoretical models (Forsyth, Payne, *et al.*, 1992; Xie and Farrington, 1993; Thomas, 1992). The solvent is modeled by Strockmayer particles (i.e., spherical Lennard–Jones particles with point dipole), and the behaviour of the ion in such a dipolar fluid has been simulated, Forsyth, Payne, *et al.* (1992).

Relaxation phenomena have been described by the stretched exponential or Kohlrausch – William – Watts (KWW) distribution function. The temperature and pressure variation of the power of the stretched exponential, β_{SE} for the polymer electrolytes have been studied (Fontanella, Wilson, *et al.*, 1992; Ichikawa and MacKnight, 1992; Ichikawa, Dickinson, *et al.*, 1992) . Plots of M″ versus log(frequency) for polymer–salt complexes have been found to exhibit two distinct peaks. The lower frequency peak represents the conductivity relaxation while the higher frequency peak the dielectric relaxation. Recently some modulus studies on PPO with sodium salts have been reported (Xue and Angell, 1987; Torell and Angell, 1988).Variation of ϵ'' with temperature has been studied to obtain activation energies and a "reciprocal frequency factor" (Fontanella, Wintersgill and Calame, 1985)

Recently new ionic conductors–*polymer–in–salt* materials are being investigated by Angell, Liu and Sanchez . In these electrolytes the salts are mixed with small quantities of the polymer (polypropylene oxide and polyethylene oxide). These materials have been found to have glass transitions low enough to remain rubbery at room temperature while preserving good lithium–ion conductivities and high electrochemical stability.

The field of polymer-based electrolytes are thus of growing importance in the field of solid state ionics. The focus of studies is at the moment on the

determination of the exact mechanism of conduction in these electrolytes. A constant effort is also underway to synthesize new polymers which include crosslinked networks, block or comb branch copolymers, or plasticization with lower oligomers. Design of polymer electrolyte batteries with practicable voltage output near the ambient will be the ultimate outcome of such research.

1.5 Statement of the Problem

It is apparent from the previous section that the field of polymeric electrolytes is growing in importance over the past two decades. A large variety of polymer hosts such as poly(ethylene oxide) (PEO), poly (propylene oxide) (PPO), poly(ethylene succinate) (PESc), poly(ethylene imine) (PEI), polyphosphazenes (MEEP) etc. have been employed to develop new ionically conducting polymer–salt complexes. Of all these systems, the PEO based electrolytes have been most extensively investigated, and some promising materials, e.g. PEO–$LiClO_4$, PEO–$LiCF_3SO_3$ etc. have been developed as a result. However, there are very few studies on poly(ethylene glycol) (PEG)-based systems, even though the PEG is quite similar to PEO except that its repeat unit, viz. $-(CH_2-CH_2O)-OH$, has an additional -OH group. The hydroxyl end-group has been known to stabilize complexes.

The aim of this work was therefore to investigate PEG-based systems with a view to (i) develop new polymeric electrolytes for possible applications in devices, (ii) contribute towards a better overall understanding of ion–transport mechanism in polymeric electrolytes.

During the course of this investigation it was realized that while the σ vs T behaviour is reasonably well understood in terms of configurational entropy model that leads to the well known empirical V-T-F type of behaviour, the σ vs composition (salt concentration, X) behaviour is not understood at all. An attempt has therefore been made to extend the configurational entropy model

to include the effect of the salt, and hence explain, at least qualitatively, the observed σ–X behaviour.

To achieve the above objectives, the following systems were chosen for investigation:

$$\text{PEG–LiX (X = Cl,Br, } ClO_4 \text{)}$$

Li-salts were the obvious choice because of the well known advantage of Li (anode) based batteries which have high energy density.

Chapter 2

Theory of Polymer Electrolytes

2.1 Thermodynamics of Complex Formation

Polymer electrolytes are thus essentially solutions of inorganic salts in polymer.The solubility of a salt in a particular solvent is determined by the energy and entropy changes associated with the transfer of its constituent ions from the crystal lattice to their equilibrium positions in solution.

The terms which must be considered in order to evaluate the thermodynamic parameters of electrolyte solvation include (MacCallum and Vincent, 1987) :

1. Energy of cavity formation within the solvent host,

2. Short-range specific interactions between the ions and the solvent molecules or solvating groups within their immediate neighbourhood, for example hydrogen bonding, coordinate bond formation etc.

3. Long range electrostatic forces.

In the polymer electrolytes reported so far, the *solvent* is a macromolecular array of Lewis bases of low polarity. These are commonly based on the oxygen atoms of a polyether or a polyester, or on the nitrogen atoms of a polyaziridine. Complexation is highly facilitated when the geometry of the ligand is pre-arranged to form cyclic structures where the ion is part of a five, more rarely six membered ring. This has been obtained in analogy with host-guest chemistry (Armand, 1987) of general alkali metal-organic ligands . There being two kinds of ions – cations and anions (of the inorganic salt), interactions of both with the solvent may be considered.

Unlike in polar protic media, where hydrogen bonding plays an important role in anion solvation, in polyethers specific anion solvation is absent. The stability of anions in aprotic media is related to their charge density and basicity, and thus follows the order

$$BF_4^- > ClO_4^- > SCN^-, I^- > Br^- > Cl^- > CH_3COO^-$$

Thus the most suitable anions for polymer electrolytes will be large, *soft* ions such as BF_4^- or ClO_4^-, such ions have low ion-dipole stabilization energies, but the ion-solvent interactions due to mutual polarisability are relatively large.

The term which deviates the energetics of solvation in polymer electrolytes is that arising from the solvation of the cation. This can occur by simple electrostatic interaction between the positive charge on the ion and the negative end of the solvent dipole, or by a partial sharing of a lone pair of electrons leading to the formation of a coordinate bond.

The steps involved in the cation solvation of these complexes (Papke, Ratner and Shriver, 1982a) are shown schematically in Fig. 2.1. Since the solvent-free complex is thermodynamically stable, ΔG for step (5) must be negative. The enthalpy associated with step (3), a gas phase interaction of the cation with four ether oxygen repeat units of PEO, is important in understanding the mechanism of ion transport.

Scheme 1. Thermodynamic cycle for cation solvation in poly(ethylene oxide) with a 4:1 oxygen:cation mol ratio

$$[M^+(g) + X^-(g)] + -(CH_2CH_2O-)_4(g) \xrightarrow{(3)} M-(CH_2CH_2O)^+_4(g) + X^-(g)$$

$$(1) \uparrow \Delta H_L \quad MX(c) \qquad (2) \uparrow \quad -(CH_2CH_2O)_4(s) \xrightarrow{(5)} (4) \downarrow \quad M-(CH_2CH_2O)^+_4X^-(s)$$

$$\downarrow \text{solvent} \quad M^+(soln) + X^-(soln) \qquad \downarrow \text{solvent} \quad -(CH_2CH_2O)_4(soln) \xrightarrow{(6)} \uparrow \text{dry} \quad M-(CH_2CH_2O)^+_4(soln) + X^-(soln)$$

Scheme 2. Ion transport process in poly(ethylene oxide), gas phase

Dissociative process

$$M-(CH_2CH_2O)^+_4(g) \overset{\Delta H_1}{\rightleftharpoons} M-(-CH_2CH_2O-)^+_3(g)$$

Associative process

$$M-(CH_2CH_2O-)^+_4(g) \overset{\Delta H_2}{\rightleftharpoons} M-(-CH_2CH_2O-)^+_3(g)$$

Figure 2.1: **Thermodynamic Cycle of Complex Formation**

The enthalpy for step (1) is the lattice energy. Despite the large enthalpies involved in steps (2),(3) and (4), the lattice energy term is quite important and it was found that for the Na-salts there is a cutoff region around 730 kJ/mole below which all sodium salts dissolve in PEO to form complexes. For Li-salts it was 850 kJ/mole. Calculations (Fig. 2.1) show that the total ΔH for step (5) will remain positive by about 100-250 kJ. Thus for ΔG of (5) to be negative a positive entropy term must be present. This may be possible since in aqueous solutions $NaClO_4$ has been shown to have a positive entropy (Latimer, 1952).

Papke, Ratner and Shriver (1982a) estimated a $\Delta H < -750$ kJ/mole for the Na-O interaction there are four such bonds. Hence if the cation has to move by breaking all the Na-O bonds, the estimated activation energy should be = 300 kJ/mole. However, the observed activation energy as obtained from $\ln \sigma T$ Vs 1/T plots are 40-120 kJ/mole, suggesting that only one or possibly two oxygen-metal bonds are broken in the transition state for cation motion. Another possibility is an associative mechanism in which one or two *free* oxygens move close to the four coordinate cation and substitute existing one or two ether oxygen.

In practise, both these mechanisms, namely polymer motion and cation motion are responsible for ionic transport in polymer electrolytes. This has been supported by the various reported activation energies (Wright, 1976; Armand, Chabagno and Duclot, 1979; Chabagno, 1980) which range from 33 kJ/mole (0.35 eV) upto 192 kJ/mole (2 eV), which are slightly more than the energy corresponding to breaking of one or two M-O linkages (1 eV). The difference in energy may be accounted for by taking into consideration the motion of the polyether chain.

As a result of several studies (Shriver, Papke, *et al.*, 1981; Chabagno, 1980; Ratner, 1987) the criteria for formation of salt-polymer complexes may be summarized as follows :

(a) The salt should have relatively small lattice energy; this will be aided by

choosing anion X^- to be *soft*, large and the conjugate base of a strong acid.

(b) The polymer should have a low cohesive energy density, this will be favored by a low glass transition temperature T_g.

(c) The polymer should have a high concentration of polar groups.

(d) The polymer chain should be flexible to provide effective solvation of cations and to provide favorable solvation entropy.

The effect of (a) is reflected in the fact that the salts of strongly solvated ions like Li^+ with small anions like Cl^- can also form complexes. Stiff-chain polymers such as aramids or polyoxymethylene which violate condition (b) do not form complexes. The condition (c) however is not always followed as single polysiloxanes and polyphosphazenes (with Si and P, respectively) do not form very good electrolytes. The condition (d) is generally followed , an example of which is PEO, whose complexes have been studied extensively (Chabagno, 1980; Fauteux and Robitaille, 1986; Berthier, Gorecki, *et al.*, 1983).

The structure of PEO has been reported to be helical (Papke, Ratner and Shriver, 1982b), based on a $T_2GT_2\bar{G}$ polymer repeat conformation (T= trans, G= gauche, $\bar{G}$= gauche-minus). Small ions like Li^+ and Na^+ were suggested to lie in the helix. Direct structural studies using fiber X-ray (Hibma (1983)) and EXAFS (Catlow, Chadwick, *et al.*, 1983) demonstrated that K^+ and Rb^+ ions lie outside the helices.

The polymer polyethylene glycol has a structure similar to PEO. The molecule consists of a chain periods of three units i.e. two CH_2 groups and one oxygen atom. At the end of the chain there are two hydroxyl groups. Dipole moment studies on polyethylene glycol indicate that there is association of the molecules into multimers (Purohit and Sengwa, 1991). This intermolecular hydrogen bonding may be between the end hydroxyl groups of two neighbours and also between the end hydroxyl groups and the oxygen

atoms present in the chain. The intermolecular hydrogen bonding leads to an unstable configuration. Molar polarization studies indicate that there also is some intramolecular hydrogen bonding with the nearest ether oxygen atom in the chain. Hence the complete rotation of the repeating groups in the chain of the molecules is restricted so that these compounds do not have an exact conformation.

2.2 Phase Behavior

Phase diagram studies on PEO – alkali metal salt complexes (Fauteux and Robitaille, 1986; Robitaille, Marques, *et al.*, 1987; Minier, Berthier and Gorecki, 1984) indicate that several phases coexist in the polymer-salt systems. Below the melting point of PEO there are three phases : the crystalline *stoichiometric* complex (c phase); the pure crystalline PEO and a minority (10-15%) elastomeric phase. This amorphous phase is not in thermodynamic equilibrium and represents the locked-in entropy of entangled high molecular weight polymers. The ionic mobility is only present in this elastomeric phase. Upon heating crystalline PEO melts and then the c phase dissolves in the elastomeric one until it finally disappears at the liquidus-solidus line in the phase diagram. ^1H and ^7F NMR measurements show that the ionic conductivity is primarily in the elastomeric phase (Minier, Berthier and Gorecki, 1984).

In order to understand the elastomeric phase, Minier, Berthier and Gorecki (1983) studied the recrystallization of $(PEO)_n(NaI)$. They concluded that the recrystallization of the salt rich complex is rapid when starting from a concentrated elastomeric phase ($n < 6$) but is drastically reduced for $n = 10$ and much lesser for lower salt concentration like $n = 24$, where the salt concentration becomes too dilute. In the case of pure PEO however, the recrystallization process is slowed down as soon as the elastomeric phase contains even a small amount of NaI. These results show that the composition of the elastomeric phase (that is responsible for ionic conductivity) depends

upon the thermal history of the sample.

Studies on PEO complexes of NH_4SCN (Dupon, Papke, *et al.*, 1982) show that these complexes exhibit a strong hysterisis effect which is reflected in the conductivity versus temperature measurement. The crystalline phase melts upon raising the temperature but in the measurements during the cooling cycle, the elastomeric phase does not get sufficient time to crystallize, so that the observed conductivity is far higher in the cooling cycle.

Fig 2.2 gives the phase diagrams of some selected salt-polymer systems. In all these systems there is evidence for one or more intermediate compounds, as also one or more eutectic. The results on some of the phase diagram studies are summarized in Table 2.1.

2.3 Conductivity versus composition behavior

The polymer-salt systems can be grouped into three main categories on the basis of their conductivity versus composition behavior. The *first* category includes those systems which exhibit no maximum or minimum but a monotonically increasing conductivity as the salt concentration in the complex increases. Under the *second* category are those systems which exhibit a single maximum in the σ-X isotherms, and the *third* where a pair of *maxima* separated by, of course, a minimum is a prominent feature. These results are elaborated further below.

In a number of polymer-salt systems, the electrical conductivity is found to increase with increasing salt concentration (X). In other words there are no maxima or minima in the σ-X isotherms in the investigated composition and temperature range. The data on these systems are presented in the form of $\log\sigma$ versus log X plots. The slope of these plots is unity, e.g. in network PEO(1050)-$LiClO_4$, or sometimes greater than unity, for instance , in network

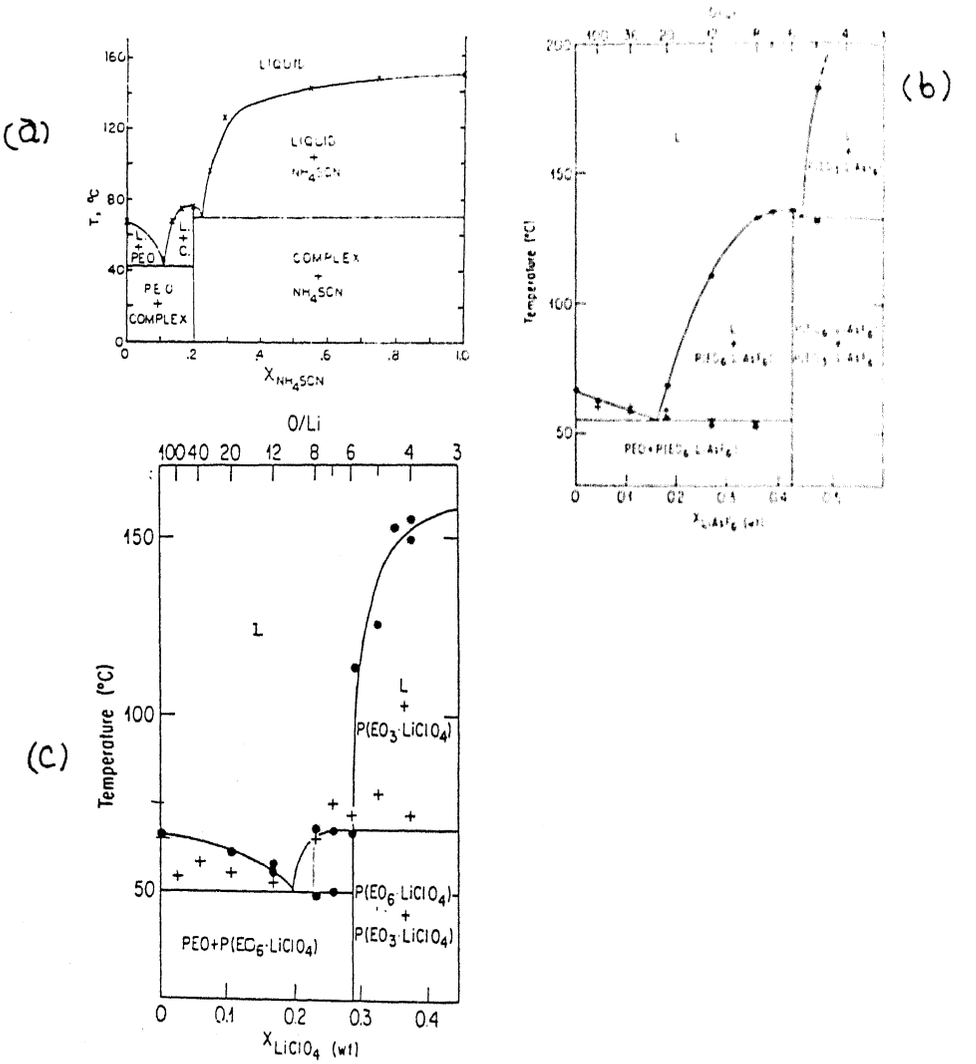

Figure 2.2: Some Polymer-salt phase diagrams; (a) PEO–NH_4SCN system (Stainer , 1985); (b) PEO–$LiAsF_6$ and (c) PEG–$LiClO_4$ systems (Robitaille, 1986)

Table 2.1: **The eutectic composition(s) and the intermediate compounds in some selected salt–polymer systems**

System	Eutectic Composition	Intermediate Comp.	Ref.
$PEO - NH_4SCN$	$(PEO)_8NH_4SCN$	$(PEO)_4NH_4SCN$	(a)
$PEO - NaSCN$	$(PEO)_{20}(NaSCN)$	$(PEO)_3NaSCN$	(b) and (c)
$PEO - NaI$	-	$(PEO)_3NaI$	(d) and (e)
PEO-KSCN	$(PEO)_4KSCN$		(f)
$PEO - LiClO_4$	$(PEO)_{10}LiClO_4$	$(PEO)_3LiClO_4$	(g)
		$(PEO)_6LiClO_4$	
$PEO - LiCF_3SO_3$	$(PEO)_{100}(LiCF_3SO_3)$	$(PEO)_{3.5}(LiCF_3SO_3)$	(g) and (e)
$PEO - LiAsF_6$	$(PEO)_{22}(LiAsF_6)$	$(PEO)_6(LiAsF_6)$	(e) and (h)
		$(PEO)_3(LiAsF_6)$	
$PEO - LiBH_4$	-	$(PEO)_{3.4}(LiBH_4)$	(i)
$PEO - HgCl_2$	-	$(PEO)_4(HgCl_2)$	(j)
$PEO - NH_2SO_2NH_2$	$(PEO)_2(NH_2SO_2NH_2)$	$(PEO)_{2.5}(NH_2SO_2NH_2)$	(k)
-	$(PEO)_4(NH_2SO_2NH_2)$	$(PEO)_5(NH_2SO_2NH_2)$	-
-	$(PEO)_{30}(NH_2SO_2NH_2)$	$(PEO)_{20}(NH_2SO_2NH_2)$	-

(a) Stainer et al (1985) ; (b) James et al (1979) ; (c)Lee et al (1986); (d)Berthier et al (1983); (e)Minier et al (1984); (f) Robitaille et al (1987); (g)Robitaille et al (1986); (h) Sorensen et al (1983); (i)Dupon et al (1984); (j)Blumberg et al (1964); (k)Ze de Bermudez et al (1992)

PPO-$NaB(C_6H_5)_4$ (Killis, LeNest, *et al.*, 1984). Fig 2.3 shows a representative conductivity- composition behavior of this category of polymer-salt systems. Several such results have been reported (Watanabe, Itoh, *et al.*, 1987; LeNest, Cheradame and Gandini, 1988; Killis, LeNest, *et al.*, 1984; Watanabe, Togo, *et al.*, 1984).

There is another class of polymer-salt systems (category II) in which the conductivity Vs composition ($\sigma - X$) behavior is characterized by the existence of a maximum. A typical result is shown in Fig 2.4 wherein the conductivity increases initially, attains a maximum value and then decreases as the salt concentration (X) in the polymer increases. The value of the optimum salt concentration corresponding to the maximum conductivity ranges from a low of 0.01 to as high as 0.5 mole fraction (m/f). There are a large number of polymer–salt systems which belong to this category (Lee and Crist, 1986; Albensson, Jacobsson, *et al.*, 1992; Mendolia and Farrington, 1992; Cai, Hu, *et al.*, 1992).

Lastly, there is a third variety of polymer-salt systems whose conductivity versus composition behavior is conspicuous by the presence of a *pair* of maxima separated by a minimum. σ-X result characteristic of this category (III) of systems are shown in Fig 2.5. A bulk of conductivity– composition data for polymer–salt complexes fall under this category. A closer inspection of all such data reveal that the concentrations X_1 and X_3 at which the $\sigma - X$ features extrema, shift to higher values as temperature increases, and also σ_{max} (X_1) is generally less than σ_{max} (X_3).

The above review by no means is exhaustive, and there are several other studies on polymer-salt systems (Sorensen and Jacobsen, 1982; Chiang, Davis, *et al.*, 1983; Bermudez, Armand, *et al.*, 1992; Dupon, Papke, *et al.*, 1982; Linden and Owen, 1988).

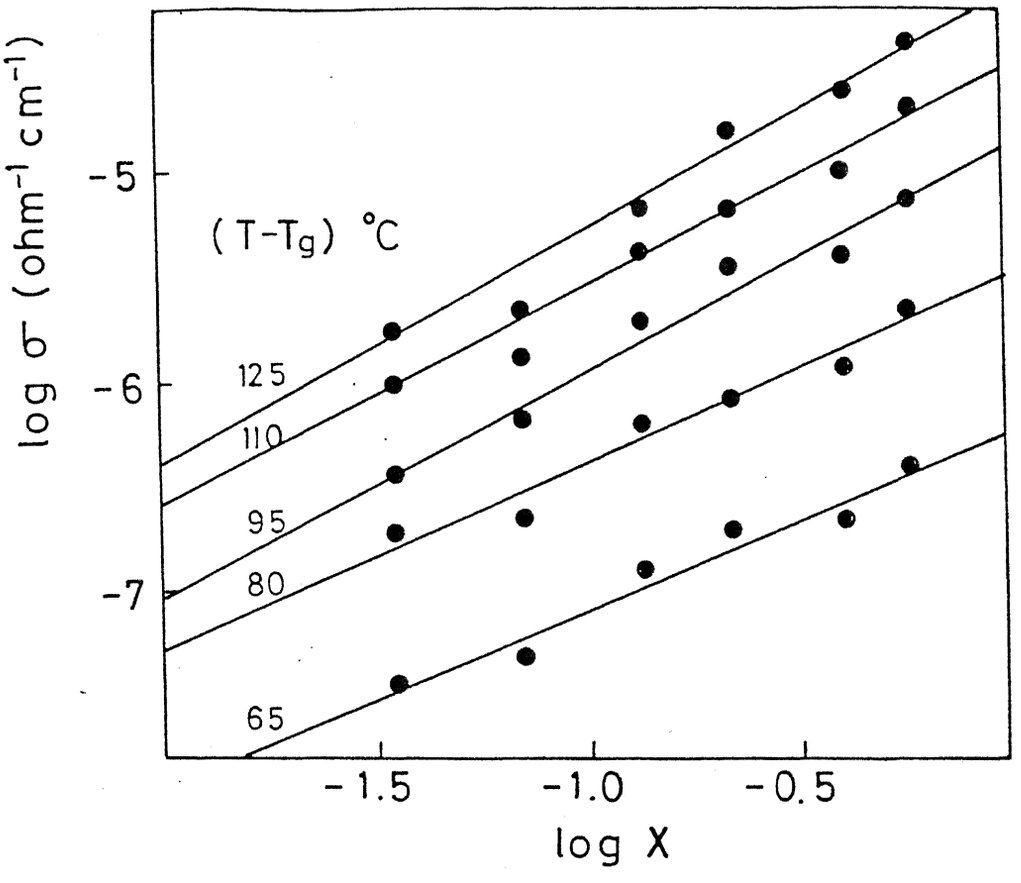

Figure 2.3: **The variation of log σ as a function of log X (mole fraction) at different temperatures for PEO-$NaB(C_6H_5)$ networks.**

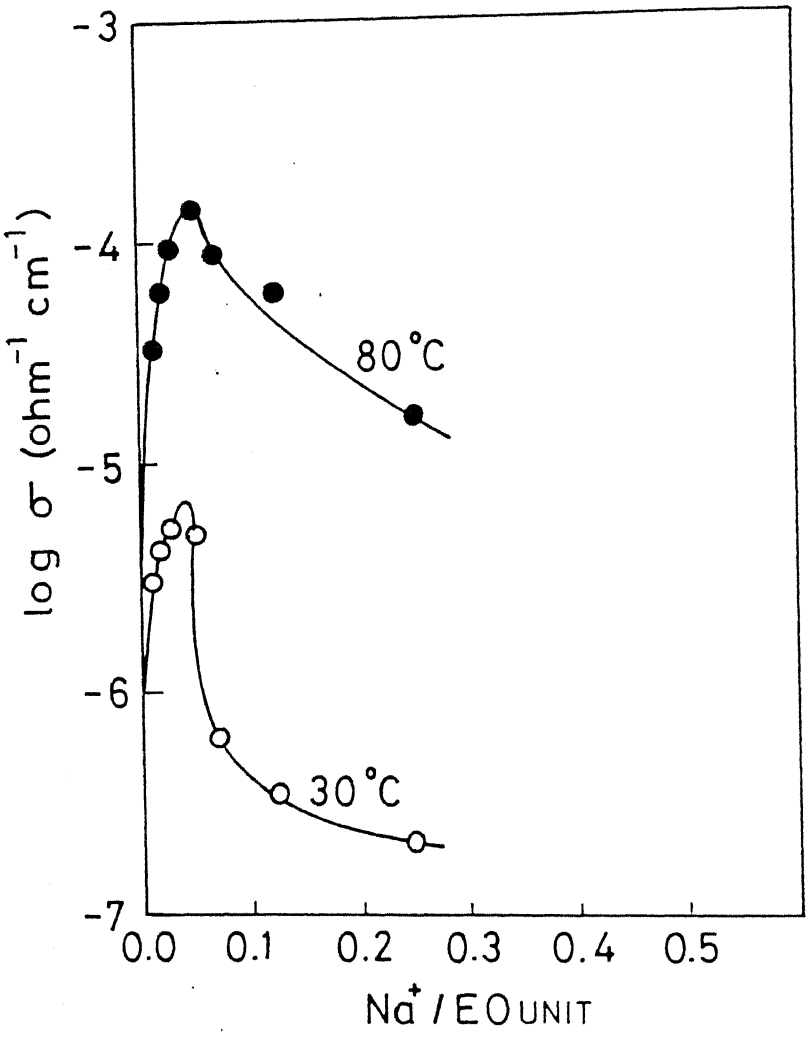

Figure 2.4: The log σ as a function of salt concentration (Na^+/EO unit), at two different temperatures for PEO(3)MI-$NaClO_4$.

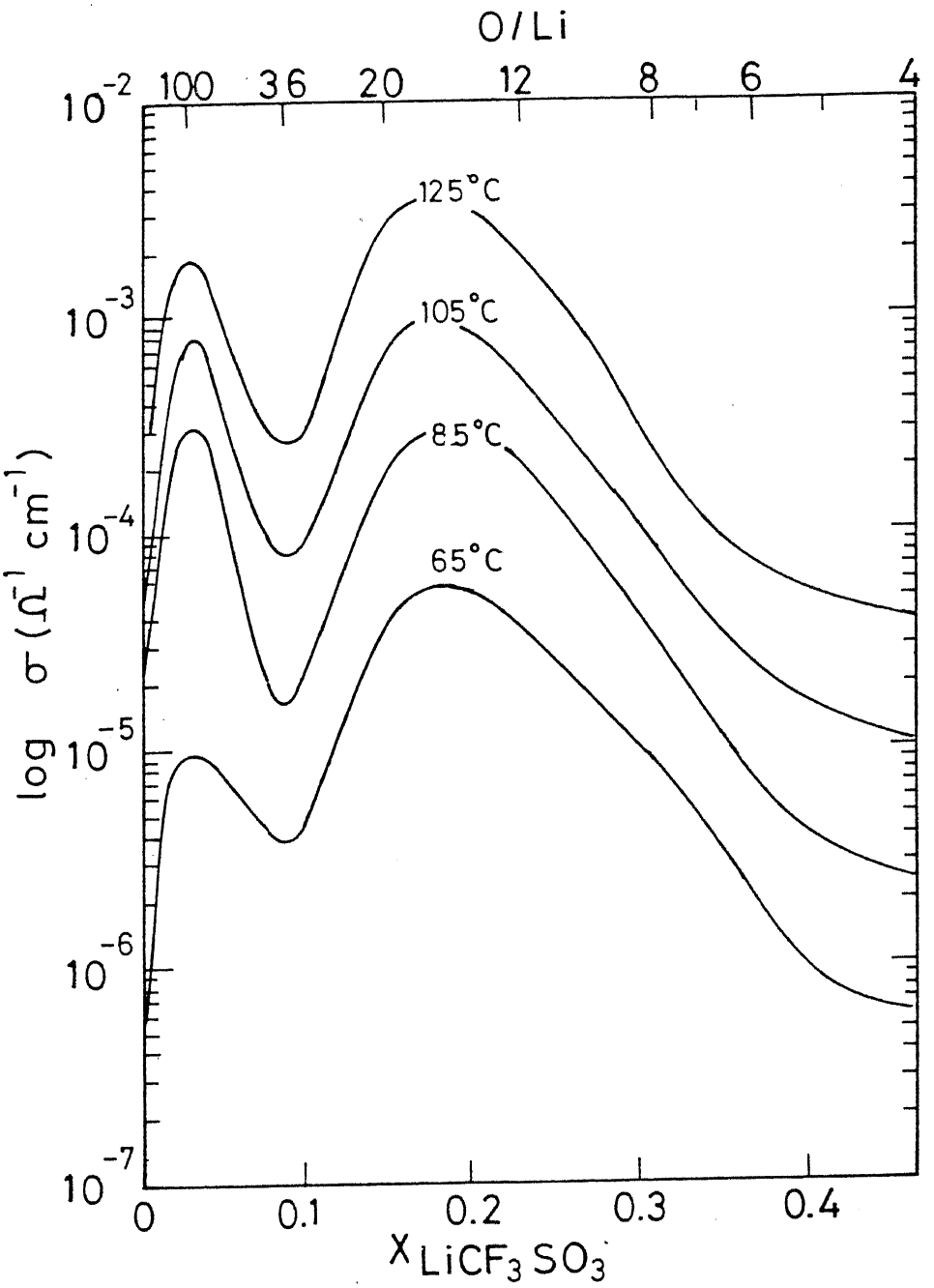

Figure 2.5: The log σ as a function of the salt concentration X (m/f) for PEO-$LiCF_3SO_3$ system at several different temperatures.

2.4 Conductivity versus temperature behavior

The electrical conductivity of solid electrolytes in general varies with temperature according to the Arrhenius equation :

$$\sigma = \sigma_o \exp[\frac{-E_a}{kT}] \tag{2.1}$$

Armand et al (Armand, Chabagno and Duclot, 1979) were the first to conclude that the $\sigma(T)$ variation of some polymer electrolytes ($(PEO)_n(LiSCN)$ and $(PEO)_n(CsSCN)$) followed the Vogel-Tamman-Fulcher (VTF) equation.

$$\sigma = \acute{A}T^{-1/2} \exp[\frac{E_a}{(T - T_o)}] \tag{2.2}$$

Thus a plot of $[\ln(\sigma.T^{1/2}/\acute{A})]^{-1}$ versus temperature (T) is found to be linear. The pre-exponential factor $\acute{A}$ is proportional to the carrier concentration (Fig. 2.6).

Generally speaking then, the conductivity versus temperature behavior of the salt–polymer complexes may be described by any of the following types (Ratner, 1987) :

(a) VTF behavior throughout the temperature range available.

(b) Arrhenius behavior at lower temperatures and VTF behavior at high temperatures.

(c) Arrhenius behavior throughout, but with two different activation, energies high E_a close to T_g , and a smaller E_a at higher temperatures.

(d) VTF behavior in the temperature ranges slightly above T_g, but Arrhenius behavior at higher temperatures.

(e) Behavior which is very unlike either Arrhenius or VTF at all temperatures.

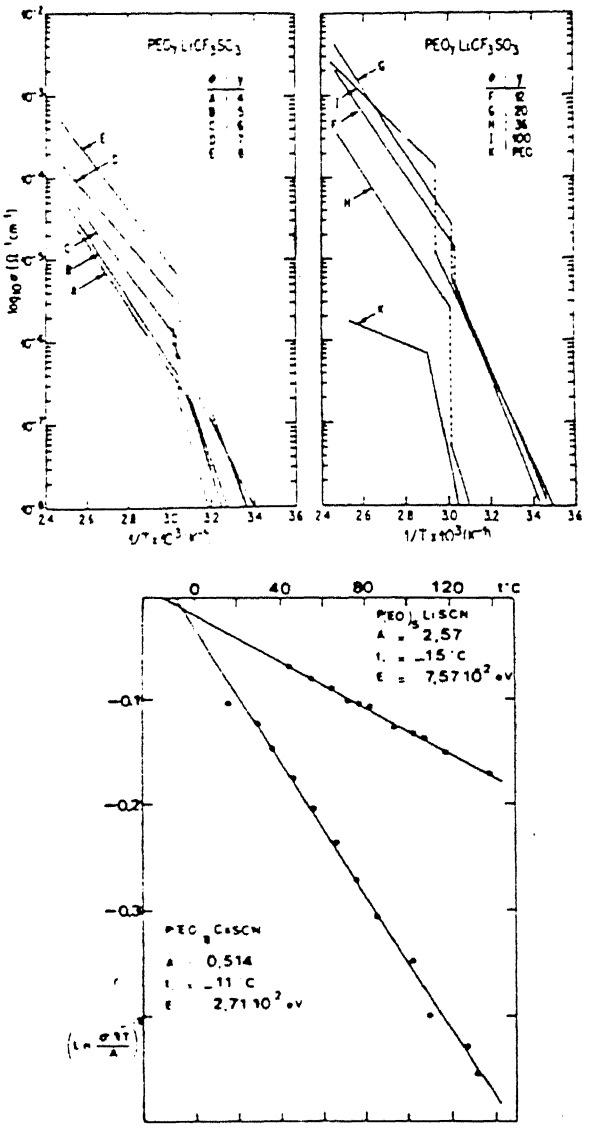

Figure 2.6: Temperature variation of conductivity of polymer electrolytes (a)Arrhenius behavior (b) VTF behavior

Most polymer electrolytes follow (a),(b), and/or (c). $(PEO)_{4.5}(LiBr)$ has been found to follow (e) but no proper explanation has been given. Behavior (d) has been explained by Kobayashi (Kobayashi, Uchiyama, *et al.*, 1985)

Since the VTF behavior describes the motion of the polymer only, and is related to the behavior near the glass transition temperature, it is necessary to understand the concept of the glassy state of the polymer.

2.4.1 The Nature of The Glassy State

The glassy state can be characterized by the changes which occur during the cooling of a polymer (or other glass–forming compound) at constant pressure. Once the material has passed through its melting point, a supercooled liquid or "melt" is obtained whose viscosity will increase as the temperature falls. Over a short temperature range, the viscosity of such a melt may approximate to an exponential function, but at low temperatures the viscosity increases more sharply than such a function would predict. Finally, when a viscosity is reached, which has been variously defined as $10^{11} - 10^{13}$ poises or as 10^{15} poises, and the rate of intermolecular rearrangement is slow compared with the time scale of the experiment, the material can be said to be in a glassy state.

In the temperature range of the glass transition, the properties of the melt change in a characteristic manner; the process can be illustrated by changes in volume (Fig. 2.4). If crystallization occurs, then at the melting temperature there is a discontinuous change, nearly always a fall, in volume (curve ABD). On the other hand, if the melt is cooled and crystallization prevented, there begins at point E the transition from a highly viscous supercooled melt to the rigid glass. At point F the solidification process is complete and a glassy state is formed. However, most polymers are partially crystalline and follow path ABE″F″ , i.e. , the presence of both a melting transition at E″ and a glass transition between E″ and F″.

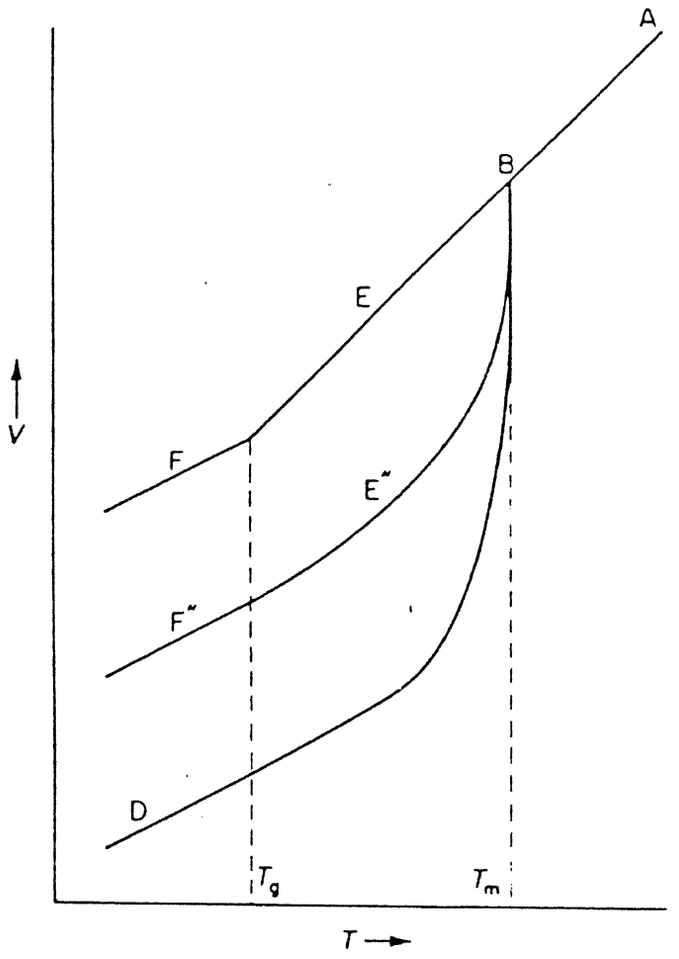

Figure 2.7: **Glass transition in polymers**

Thermodynamically, an n-th order transition is one in which the n^{th} derivatives of G with respect to T and P show a discontinuity and the $(n-1)^{th}$ derivatives become infinity. The glass transition cannot be regarded as a transition in the thermodynamic sence, but rather as a kinetic one. This is because there does not exist an internal thermodynamic equilibrium on both sides of the glass transition temperature, as is the case with a second order transition. Hence, the term "glass transition" is used for such transitions.

Since the glass transition temperature (T_g) is marked by very rapid increase in viscosity of the polymer melt, the factors controlling the polymer viscosity need to be taken into consideration. Several theories have been developed to account for the viscosity of liquids, we shall correlate them with the behavior of polymeric materials.

2.4.2 Doolittle's Free Volume Theory

A semi–empirical treatment was initiated by Doolittle and co-workers (Doolittle, 1951; Doolittle and Doolittle, 1957) who studied non-polymeric liquids and particularly treated the case of the n-paraffins. Doolittle defines free volume V_F as:

$$V_F = (V_T - V_o) \tag{2.3}$$

Where V_T is the volume of the liquid at any temperature T, and V_o the theoretical volume of closest packing at 0 K. Doolittle was able to obtain good values of V_o by extrapolating the density data for n-paraffins at 0 K. He then obtained a good fit to the following equation relating viscosity (η) with volume (V_o)

$$\eta = C \exp[\frac{BV_o}{(V - V_o)}] \tag{2.4}$$

where C is a constant and B also constant derived from the van der Waal's equation. This equation was valid only at high temperatures and high volumes.

2.4.3 The theory of Cohen and Turnbull

An equation similar to Doolittle's has been derived by Cohen and Turnbull (Cohen and Turnbull, 1959). According to them, the molecular processes occur by the movement of molecules into voids formed by redistribution of the free volume and which have a size greater than a critical value. Starting from the concept that the contribution of a molecule to diffusion D(V) is given by:

$$D(V) = ga(V)U \tag{2.5}$$

where g is a geometric factor,U the molecular velocity, and a(V) is roughly the diameter of the cage, they proposed that D(V) will be zero unless V exceeds a critical value V^* and becomes just large enough to permit another molecule to jump in. The final expression for diffusion thus obtained is,

$$D = ga^*U \exp(-\gamma V^*/V_F) \tag{2.6}$$

where γ is a constant close to unity, and V^* is near to the molecular volume. This equation is similar to the Doolittle's (Eq 2.2), with the difference that U contains the term $T^{1/2}$. U is the velocity of the molecule as predicted by the kinetic theory of gases and is given by

$$U = \sqrt{\frac{8kT}{\pi m}} \tag{2.7}$$

As also V_F is defined slightly differently, because the free volume is considered to be zero at a temperature T_o, that is

$$V_F = \alpha\overline{V_m}(T - T_o) - \beta\overline{V_p}P \tag{2.8}$$

where α is the coefficient of thermal expansion, β the compressibility, $\overline{V_m}$ and $\overline{V_p}$ are the mean molecular volume for the temperature and pressure increment. In the absence of pressure, the Cohen and Turnbull equation reduces to :

$$D = ga^*U \exp[\frac{-\gamma V^*}{\alpha\overline{V_m}(T - T_o)}] \tag{2.9}$$

taking $U \simeq T^{1/2}$, we obtain,

$$D = C_1 T^{1/2} \exp[-B/(T - T_o)] \tag{2.10}$$

where C_1 is a constant and B = $-\gamma V^*/\overline{V_m}\alpha$. Using the Nerst-Einstein equation,

$$\sigma = \frac{nq^2}{kT}D \tag{2.11}$$

the result obtained is

$$\sigma = \sigma_o \exp[-B/(T - T_o)] \tag{2.12}$$

which is the VTF equation with $\sigma\alpha T^{-1/2}$.

2.4.4 Application to polymers and the WLF approach

The preceding arguments and derivations essentially apply to liquids. In the case of polymers it is not possible to measure viscosities at high volumes since degradation occurs before the relative free volume, $(V - V_o)/V$, reaches values above 0.25.The Williams,Landel and Ferry (WLF) Model (Williams, Landel and Ferry, 1955) concerns not only with the viscosity, but also with the relaxation processes which characterize any glass forming material. In this model a quantity, a_T, is introduced to represent the temperature variation of the segmental friction coefficient for any mechanical relaxation, and showed that it could be represented by an equation of the type:

$$\ln a_T = -\frac{C_1(T - T_s)}{C_2 + (T - T_s)} \tag{2.13}$$

where C_1 and C_2 are constants and T_s is a WLF reference temperature defined by $T_s - T_g \simeq 50$K. Empirically, $C_1 \simeq 8.9$, $C_2 \simeq 102$ K. For suitable values of C_1 and C_2 this equation will represent the experimental results for a wide range of polymers, The constants C_1 and C_2 obtained in this way have been compiled by Ferry (1970).

In their original paper, Williams, Landel and Ferry (1955) showed that if , instead of T_s, the glass transition temperature T_g was substituted , the following

universal relation is obtained,

$$\ln a_T = \frac{-17.44(T - T_g)}{51.6 + T - T_g} \tag{2.14}$$

which they claimed to be generally representative of the relaxation or viscosity behavior of polymers and other glasses in the temperature range $T_g < T < (T_g + 100)$.

Starting with the relation :

$$\eta = \ln A + B(V - V_o)/V_o \tag{2.15}$$

Williams et al showed that their parameter a_T (Eq 2.13)could be represented by

$$\ln a_T = B[\frac{1}{f} - \frac{1}{f_g}] \tag{2.16}$$

where $f = V_F/(V_o + V_F) \simeq V_F/V_o$ and f_g is the value of f at T_g,
and $f = f_g + \alpha(T - T_g) + ...$
where α is the thermal expansivity, the WLF equation then becomes:

$$\log a_T = \frac{\frac{-B}{2.303 f_g}(T - T_g)}{f_g/\alpha + T - T_g} \tag{2.17}$$

comparing with Eq 2.13, we get

$$\alpha = 4.8 \times 10^{-4} K^{-1}$$
$$\text{and } f_g = 0.025$$

Thus,

$$V_F = V_g[0.025 + \alpha(T - T_g)] \tag{2.18}$$

Comparing Eq. 2.18 and Eq. 2.7,i.e, the equation derived from the Cohen Turnbull relation, we get,

$$\alpha V_m(T - T_o) = V_g 0.025 + \alpha V_g(T - T_g) \tag{2.19}$$

which leads to $T_o = T_g - 0.025/\alpha$
Using the above value of α obtained from the WLF equation we get

$$T_o = T_g - 50K \tag{2.20}$$

Watanabe, Itoh, *et al.* (1987) have modified the WLF equation to the form:

$$\log \frac{\sigma(T)}{\sigma(T_g)} = \frac{C_1(T - T_g)}{C_2 + (T - T_g)} \tag{2.21}$$

They have further modified it by selecting a temperature $T_o = T_g + 50$, because the conductivity data close to T_g for the network polymer electrolytes could not be measured.

$$\log \frac{\sigma(T)}{\sigma(T_o)} = \frac{C_1'(T - T_o)}{C_2' + (T - T_o)} \tag{2.22}$$

where $C_1 = C_1'C_2'/[C_2' - (T - T_g)]$
$C_2 = C_2' - (T_o - T_g)$
In another work (Killis, LeNest, *et al.*, 1982) C_1 and C_2 were determined from dynamic mechanical measurements and $\log a_T$ was then calculated. A plot of $\log \sigma$ Vs this $\log a_T$ gave a straight line indicating that the form chosen in Eq 2.21 is valid.

2.4.5 Configurational Entropy Model

The prediction of the WLF approach that $T_s - T_g = 50°C$ is often found to be invalid, and large deviations from the values of C_1 and C_2 are observed for experimental results. Thus the "universality" of this approach may be questionable. Furthermore, in the case of polymers, the *free volume* cannot be associated with a real molecular volume but has to be interpreted in terms of inter- and intra molecular interactions as well as topology of molecular packing in the amorphous phase. In order to overcome these discrepancies in the free volume approach, Gibb's and Coworkers (Adam and Gibbs, 1965; Gibbs and DiMarzio, 1958) gave the **Configurational Entropy Model**. They gave

a statistical–mechanical argument to relate the relaxation properties of glass forming liquids to their *quasistatic* properties, characterized by ,the glass transition temperature T_g, and the specific heats of the glass and the equilibrium melt. At the *quasielastic* glass temperature T_g the molecular relaxation times are too long to permit establishment of equilibrium in the duration of even the slowest experiments. This sluggish relaxation behavior governing T_g is due to the very small number of configurations available to the system in this region. Gibbs and coworkers (Gibbs and DiMarzio, 1958) gave the transition probabilities for glass forming liquids in terms of the equilibrium distribution of an isothermal–isobaric ensemble of small systems of the size of the cooperatively rearranging region. The *cooperatively rearranging* region is defined as the smallest region that can undergo a transition to a new configuration without a requisite simultaneous configurational change on and outside its boundary.

Adam and Gibbs (1965) assumed the number of molecules in the cooperative region to be z, out of which n reside in states which allow a cooperative rearrangement and the N–n are in the state not allowing a transition. Then the isothermal–isobaric partition function for the ensemble is given by

$$\Delta(z, P, T) = \Sigma w(z, E, V) \exp(-E_a/kT) \exp(-PV/kT) \tag{2.23}$$

where w is the degeneracy of the energy level, E and volume, V of the subsystem. The Gibb's free energy, G = $z\mu = -kT \ln \Delta$. Summing over values of E and V that permit transition, we get a partition function $\Delta'(z, P, T)$ and corresponding Gibbs free energy, G' = $z\mu' = -kT \ln \Delta'$ for the rearrangeable subsystems. The fraction of subsystems that permits rearrangement is given by

$$N/n = \Delta'/\Delta = \exp[-(G' - G)/kT] \tag{2.24}$$

The cooperative transition probability , W(T), is proportional to n/N and using the relation $z\delta\mu = z(\mu' - \mu) = G' - G$, we get

$$W(T) = A \exp(-z\Delta\mu/kT) \tag{2.25}$$

To arrive at the average transition probability $\overline{W}$ (T), we have to sum all

non-zero values of W(T),

$$\overline{W}(T) = \Sigma A[\exp(-\Delta\mu/kT)]^z \tag{2.26}$$

where z^* is the critical size of cooperative regions that can yeild non-zero transition. The summation of this truncated geometric progression gives

$$\overline{W}(T) = \frac{A}{1-\exp(-\Delta\mu/kT)}\exp(\frac{-z^*\Delta\mu}{kT}) \tag{2.27}$$

$1-\exp(-\Delta\mu/kT) \rightarrow 1$, thus may be absorbed into the preexponential factor, giving

$$\overline{W}(T) = \overline{A}\exp(-z^*\Delta\mu/kT) \tag{2.28}$$

In this equation we need to determine the temperature dependence of z^*. The configurational entropy S_c of the supersystem is given by

$$S_c = k\ln W_c \tag{2.29}$$

If the supersystem consists of N subsystems, and $S_c = Ns_c$ where s_c is configurational entropy of a subsystem of z monomer units. If we consider the supersystem to contain N_A (Avogadro number) segments, then

$$S_c = k\ln(W_c^{z/N_A}) \tag{2.30}$$

This equation shows that for a given temperature and pressure the configurational entropy of a subsystem increases monotonically with the size of the subsystem, z^*,i.e. the lower limit to the size of the representative cooperative rearranging region may be characterized by a critical configurational entropy,

$$s_c^* = k\ln(W_c^{z^*/N_A}) \tag{2.31}$$

giving, $z^* = N_A s_c^*/S_c$. Inserting this relation into Eq 2.28

$$\overline{W}(T) = \overline{A}\exp(\frac{-\Delta\mu s_c^*}{kTS_c}) \tag{2.32}$$

S_c is related to specific heat through a simple thermodynamic relation

$$S_c(T) = \int(\frac{\Delta C_p}{T})dT \tag{2.33}$$

where ΔC_p is the change in the specific heat at temperature T going from the glassy to liquid state. Angell and Sichina (1976) have used the following approximate but fairly accurate relationship obtained from the experimental results on a number of glass forming liquids to calculate S_c.

$$\Delta C_p(T) = \frac{B}{T} \tag{2.34}$$

Eq 2.33then can be rewritten as

$$S_c(T) = \int_{T_o}^{T} (\frac{B}{T^2})dT = B(\frac{1}{T_o} - \frac{1}{T}) \tag{2.35}$$

where B is a constant, T_o, the usual glass-transition temperature at which the configurational entropy tends to zero, $S_c(T_o) \rightarrow 0$. Substitution of Eq 2.35 in Eq 2.32 leads to the empirical V-T-F type form for the transition probability

$$\bar{W}(T) = \bar{A} \exp[\frac{-(E_a/k)}{T - T_o}] \tag{2.36}$$

where

$$E_a = \Delta\mu s_c^* T_o/B \tag{2.37}$$

is the apparent activation energy for the polymer rearrangement. As emphasized by Ratner (1987), Eq 2.36 describes the motion of polymer host in the polymer-salt complex which constitutes the solid electrolyte but not the motion of ions. The jump frequency of the ions which is proportional to the fluidity (or transition probability ,W(T), Eq(2.36) is then used within the dynamic band percolation model (Ratner, 1987; Druger, Nitzan and Ratner, 1983; Druger, Ratner and Nitzan, 1986) to obtain an empirical V-T-F like expression for the conductivity (σ)

$$\sigma = A' T^{-1/2} \exp[\frac{-(E_a/k)}{T - T_o}] \tag{2.38}$$

where A′ is a constant.

2.5 NMR studies on Polymer Electrolytes

NMR studies have been extensively used to probe the structure and dynamics of polymer electrolytes. These studies can be classified as follows:

- Studies leading to determination of concentration of amorphous phase: NMR allows to distinguish nuclei of the crystalline and the amorphous phase. This is based on the determination of the spin-spin relaxation time,T_2,which is a measure of how fast a nuclear magnetization perpendicular to the external magnetic field,M_L, will decay due to interactions between the spins. Quite often this decay can be written as

$$M_L(t) \alpha \exp(-t/T_2) \tag{2.39}$$

This decay arises from fluctuating local magnetic fields at the nuclear site . In the amorphous phase due to the ionic movements, the local fields at the nucleus of the mobile ions are averaged out to a certain extent and thus T_2 is larger than the time constant in the crystalline phase. Thus, the total NMR signal will contain two contributions, one from the crystalline the other from the amorphous phase, both decaying according to Eq 2.39 with different values of T_2. This allows to separate the relative amounts of nucleii belonging to either phase. For $PEO - LiCF_3SO_3$ it could be shown (Berthier, Gorecki, *et al.*, 1983; Minier, Berthier and Gorecki, 1984) that by increasing the temperature, the crystalline phase progressively dissolves in the amorphous phase. For $PEO - LiClO_4$ a similar analysis of the data has been carried out.

- Relaxation and Linewidth Studies:
Relaxation and linewidth studies in polymer electrolytes are difficult to interpret because of the complex structure of the materials. Qualitative conclusions may however be made. Schantz, Kakikhana and Sandberg (1990) have carried out ^{23}Na and ^{19}F linewidth and T_1 measurements in $PPO-NaCF_3SO_3$ in order to detect ion pairs. The authors observed two ^{23}Na components in the NMR spectrum with very different T_1 values indicating the presence of at least two Na sites which differ by their dynamics. On the other hand, Raman studies showed that anions exist either as dissociated or as ion pairs, however, no evidence was found for the presence of clusters. The author therefore concluded that the

narrow NMR line (T_1 = 9μs at 297.5 K) is due to dissociated cations and the broad line (T_1 = 13ms at 297.5 K) due to cation-anion pairs. This assignment is based on the fact that broad lines usually imply (as noted above) a more "rigid" lattice, which means in this case a reduced mobility of the cation-anion pairs. The inverse of the linewidth (measured in Hz) is a measure for the lifetime of the configuration giving rise to NMR line. Thus from the width of the broad line a pair life time of at least 10^{-4}s is estimated. A similar investigation has been performed by Greenbaum (1985) who also observed a narrow ^{23}Na line in $PPO - NaCF_3SO_3$ but attributed the broad line to ionic clusters because of it's similarity to the spectra of uncomplexed sodium salts.

^7Li NMR studies in $(PEO)_8LiClO_4$ + x wt.%$\gamma - LiAlO_2$ (Gang, Roos, *et al.*, 1992) lead to the conclusion that the local dynamics of the Li-ions, in particular the Li mobility, is not changed by adding the $\gamma - LiAlO_2$ filler. The increase in conductivity with the addition of a filler may be caused by stabilizing and increasing the fraction of the amorphous phase.

- Diffusion Coefficient measurement:
  The diffusion coefficient,D may be determined by the pulsed-field gradient (PFG) method which has been applied in many liquid and solid phase studies. The method employs the Hahn $pi/2 - \pi$ spin-echo experiment with two magnetic field gradient pulses applied after the first and the second radio-frequency (rf) pulse. If spins change their spatial position between the application of the gradient pulses, the echo signal will be attenuated. If the spin-echo amplitude A_g and A with and without gradient pulses, respectively, are measured then the diffusion coefficient follows the relation

$$\ln \frac{A_g}{A} = \gamma^2 D\delta^2(\Delta - 1/3)g^2 \tag{2.40}$$

  where δ and g are length and amplitude ,respectively, of a gradient pulse and the πrf pulse. In addition, the steady background gradient is assumed to be very small with respect to g.

Several PFG studies in polymer electrolytes have been made (Bhattacharjee, Smoot and Whitmore, 1986; Gorecki, Andreani, *et al.*, 1986) . The transport number have also been estimated using the Eq

$$t_{Li^+} \alpha \frac{D_{Li^+}}{(D_{Li^+} + D_{X^-})} \tag{2.41}$$

The conclusions obtained were that the anion (for the $(PEO)_8 LiCF_3SO_3$) diffuses faster than the lithium irrespective of its size. The maximum value of cation transport number was $t_{Li^+} = 0.42$ at 412 K. Using the Nerst- Einstein relation, we get

$$\sigma_D = Ne^2(D_{Li^+} + D_{X^-})/kT \tag{2.42}$$

The σ_D value can be compared to the measured σ value. σ_D/σ was found to be close to 1 in the temperature range 350-400 K, which indicates that the interaction between charged particles is negligible.

- NMR Imaging:
  The NMR Imaging technique utilizes the fact that the position of a magnetic nucleus in a magnetic field gradient is encoded onto the NMR frequency. By scanning the various frequencies of a sample one,two or three dimensional NMR images can be obtained(Sonderegger, Roos, *et al.*, 1992).

2.6 Ion association in polymer electrolytes

The earliest measurements of electrical conductivity were made in electrolytic solutions by Kohlrausch, Arrhenius and Ostwald. The electrical measurement data in solution and molten salts is generally analysed in terms of equivalent conductance (Λ), defined as

$$\Lambda = \frac{1000\sigma}{c} \tag{2.43}$$

where c = concentration of the solution in equivalents per litre
From the Arrhenius hypothesis , the ionic concentration of the reactants of a reaction of the type

$$AB \rightleftharpoons A^+ + B^-$$

where AB denotes the neutral molecule of the electrolyte, and A^+ and B^- the ions into which the electrolyte dissociates, may be given as,

$$[A^+] = c\gamma = [B^-]$$

where γ, is the fraction of ions which are free to carry the current. By hypothesis, $\gamma = \Lambda/\Lambda_o$, where Λ_o is the conductivity at infinite dilution. Using the mass action hypothesis we have the Arrhenius equation:

$$\frac{c\gamma^2}{(1-\gamma)} = K \tag{2.44}$$

and $\gamma = \Lambda/\Lambda_o$, we obtain the Ostwald dilution law,

$$1/\Lambda = 1/\Lambda_o + c\Lambda/K\lambda_o^2 \tag{2.45}$$

Thus a plot of $1/\Lambda$ against $c\lambda$ should give a straight line. The Ostwald dilution law explained well the behavior of weak electrolytes. This was followed by the Debye-Huckel-Onsager theory, which assumed complete dissociation.

Bjerrum (1926) was the first to suggest that the ions of strong electrolytes in solution could associate to nonconducting pairs, provided their coulomb potential energy were large compared to the thermal energy, kT. Fuoss and Krauss (1926) used Bjerrum's results and modified it by representing ions as charged spheres rather than point charges to obtain the result

$$\Lambda = (\Lambda_o - Sc^{1/2}\gamma^{1/2} - Ec\gamma \log c\gamma + Jc\gamma \tag{2.46}$$

where ($1 - \gamma$) is the fraction of salt associated into pairs, S is the Onsager coefficient and E is a constant defined by the same variables as S. J is a function of the ionic size. If the higher terms are omitted, we obtain,

$$\Lambda = \gamma(\Lambda_o - Sc^{1/2}\gamma^{1/2}) \tag{2.47}$$

Thus a plot of Λ vs $c^{1/2}$ will start with a negative slope equal to $-s\gamma^{3/2}$ at c = 0, become concave down, goes through an inflexion point at a limiting value of c, and then asymptotically approaches $\Lambda = 0$ at $c = \infty$.

An ion pair, while electrically neutral, still possess a dipole field, and as a dipole is attracted by either anions or cations and becomes conducting. Thus at very low dielectric constants, $10 < \epsilon < 20$, a triple ion cluster is thermally stable. Thus an additional associative equilibria has to be included in the description of electrolytic solutions:

$$A^+ + AB \rightleftharpoons (A_2B)^+B^- + AB \rightleftharpoons (AB_2)^-$$

From this,Fuoss and Krauss (1933), obtained a relation for the equivalent conductance,

$$\Lambda = Ac^{-1/2} + Bc^{1/2} \tag{2.48}$$

which reduces to the following form when the concentration is very small ($c \rightarrow 0$),

$$\Lambda \simeq Ac^{-1/2}$$

Thus a plot of log Λ against log c should approach linearity with slope equal to (-1/2). Eq 2.48 may be rewritten as

$$\Lambda c^{1/2} = A + Bc \tag{2.49}$$

which suggests that a plot of $\Lambda\, c^{1/2}$ vs c should also be linear. These relations Eq 2.48 and 2.49 are obeyed by many solutions, and have been employed, though without much success, to explain the results in polymer–salt complexes as well. However, the concept of formation of neutral ion pairs and triple ion-pairs are frequently invoked to justify the observed structure in the σ vs composition behavior for polymer-salt complexes.

Experiments on polyether-lithium perchlorate complexes Camaron, Ingram and Sorrie (1986), Cameron, Harrie, *et al.* (1988), Gray (1990) have shown that a plot of Λ Vs $c^{1/2}$ goes through a minimum due to ion pairing [$c = 0 - 0.2 moldm^{-3}$], followed by a rise in the conductivity due to the formation of triple ions [$c = 0.2 - 0.4 moldm^{-3}$], followed by a fall which seems to

be due to the steep rise in viscosity at higher concentrations [$c > 0.4$]. Studies on $LiClO_4$ in THF also gives evidence for triple ion formation Gray (1990)

$$LiClO_4 + ClO_4^- \rightleftharpoons Li(ClO_4)_2^-$$
$$LiClO_4 + Li^+ \rightleftharpoons Li_2(ClO_4)^+$$

Thus plots of $\Lambda c^{1/2}$ Vs c for $LiClO_4$ in THF are linear upto 0.1M after which a strong deviation from linearity appears. The results for polyether-$LiClO_4$ complexes indicate that in the concentration range upto 0.1M, the majority of the electrolyte is present as ion pairs with some triple ion formation.

Chapter 3

Experimental Techniques

3.1 Materials Used

Table 3.1 gives a description of all the starting materials used in this work.

3.2 Preparation of Films

The polymer complex films were prepared by simple solvent casting technique. Weighed quantities of the polymer and the inorganic salts were dissolved in appropriate solvents (Table 3.2). The solutions were cast onto teflon sheets (thickness: 1.5mm). As slow solvent evaporation is the primary criteria for complex formation, the solutions cast onto teflon sheets were allowed to dry in an open atmosphere (without vacuum heating) for $\sim$ 6 hrs. and then in a vacuum desiccator fitted with a heater at $\sim 60^{o}C$ for $\sim$ 12 hrs. Subsequently, the heater was switched off and the films were dried under vacuum at room temperature ($25^{o}C$). This produced solvent free self-supporting films of about $\sim$ 0.5 mm thickness, which were then stored in an inert (N_2) gas atmosphere inside

Table 3.1: **List of Chemicals Used**

Chemicals	Manufacturers	Remarks
Polymer:		
PEG	Aldrich Chemical Co., USA	mol. wt.:8000
PEG	"	mol.wt. : 10,000
salts:		
$LiClO_4$	Alfa Products, USA	purity: 99+%
$LiBr$	"	purity: 99+%
$LiCl$	"	purity: 99+%
LiI	Aldrich Chem. Co., USA	purity: 99+%
NaI	"	purity: 99+%
KI	"	purity: 99+%
CsI	"	purity: 99+%
Dispersed phase:		
Al_2O_3	Buehler Products , Germany	particle size: 0.3 μ
Solvents:		
methanol	Sarabhai Chem. Co. India	AR grade
acetonitrile	Sarabhai Chem. Co., India	AR grade

Table 3.2: **The PEG polymer and various salts and the corresponding solvents used in the synthesis of polymer electrolytes**

PEG	acetonitrile [for $PEG - LiClO_4$ system]
PEG	methanol [for other systems]
$LiClO_4$	acetonitrile
$LiBr$	methanol
$LiCl$	"
LiI	"
$CsBr$	"
KBr	"
$NaBr$	"

a glove box. The films were used as such for all the characterizations except the conductivity measurements.

3.3 Experimental Techniques

3.3.1 Conductivity Measurements

PEG-LiX (X = Cl, Br) systems

The self–supporting films of these samples were packed into teflon rings of fixed dimensions (thickness$\simeq$1 mm;dia.$\simeq$8 mm). The teflon ring was then spring loaded into a specifically designed sample holder (Fig 3.1), which in turn was was placed inside a cryostat whose temperature could be varied in the range –20 to 100 ^oC.

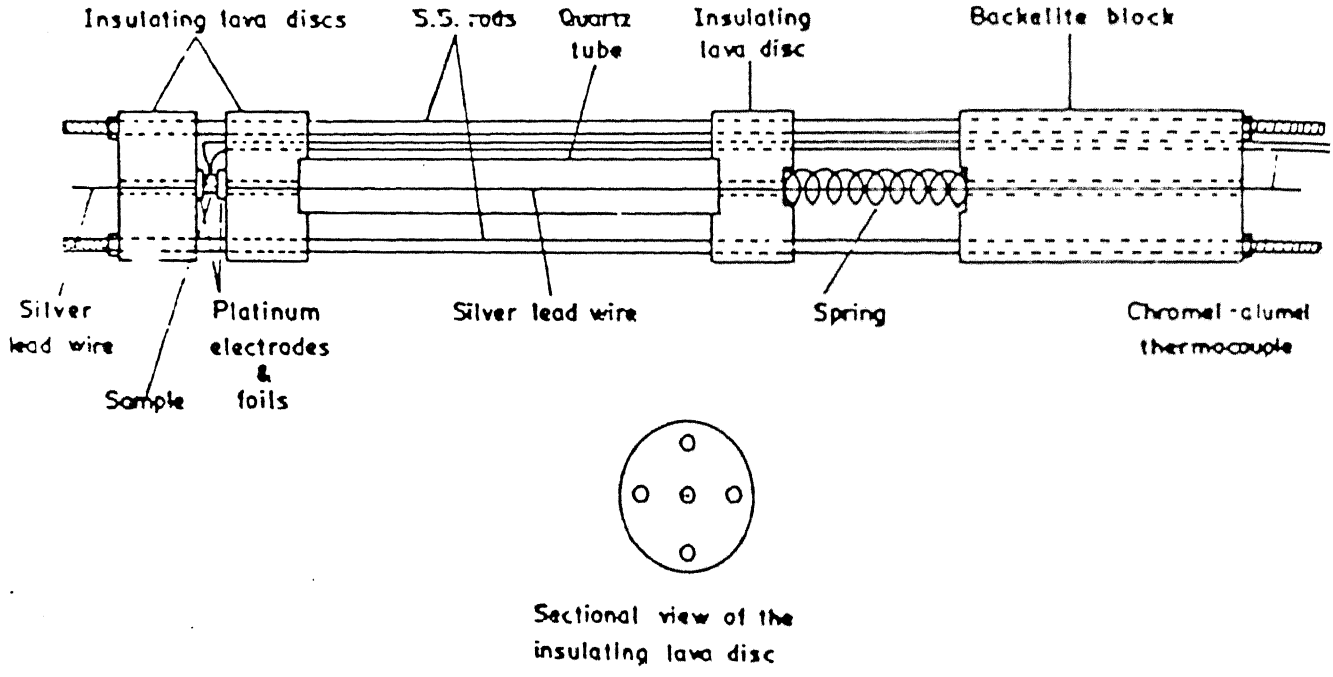

Figure 3.1: Sample Holder for Conductivity Measurement

The Oxford model DN1710 is a compact liquid nitrogen reservoir cryostat designed for variable temperature measurements of solid or liquid samples. The sample temperature is continuously variable from 77 K upto 500 K. The cold region extends approximately 50 mm above the bottom of the sample space and has a diameter of 20 mm. Fig 3.2 gives a schematic diagram of the cryostat. The sample is top loaded and is cooled by a static column of exchange gas which thermally links the sample to a heat exchanger, which in turn is connected to a liquid nitrogen reservoir. A platinum temperature sensor and a heater are fitted to the heat exchanger. An Oxford model ITC4 temperature controller was used for controlling the temperature of the cryostat. The ITC4 can accept a wide range of temperature sensors and can provide upto 80 W power. The heater resistance is 20 Ohm . It employs the proportional, integral, derivative (P,I,D) temperature control method. A copper–constantan thermocouple was used as sensor.

Each samples was heated upto $\sim 80^{o}C$ and cooled to room temperature so as to resolidify it from the melt and form a more homogeneous composition inside the teflon ring. The role of the teflon ring of course was to maintain a definite geometry (cell constant) which is used to calculate the conductivity from the measured value of resistance of various samples. The measurements were generally taken during heating cycle in most cases. In some cases the measurements were taken during the cooling cycle to check the reproducibility as well as any hysterisis effects.

$(PEG)_xLiClO_4$ system

Since self–supporting films of PEG–$LiClO_4$ samples could not be obtained, a special conductivity cell was designed and fabricated (Fig 3.3). The cell consists of a pyrex tube (i.d. = 12 mm) fitted with an air tight cap (a ground glass joint was used). One graphite electrode was fitted to the bottom of the tube (See Fig 3.3) and the other to the cap. A copper–constantan thermocouple was inserted close to the sample to measure the

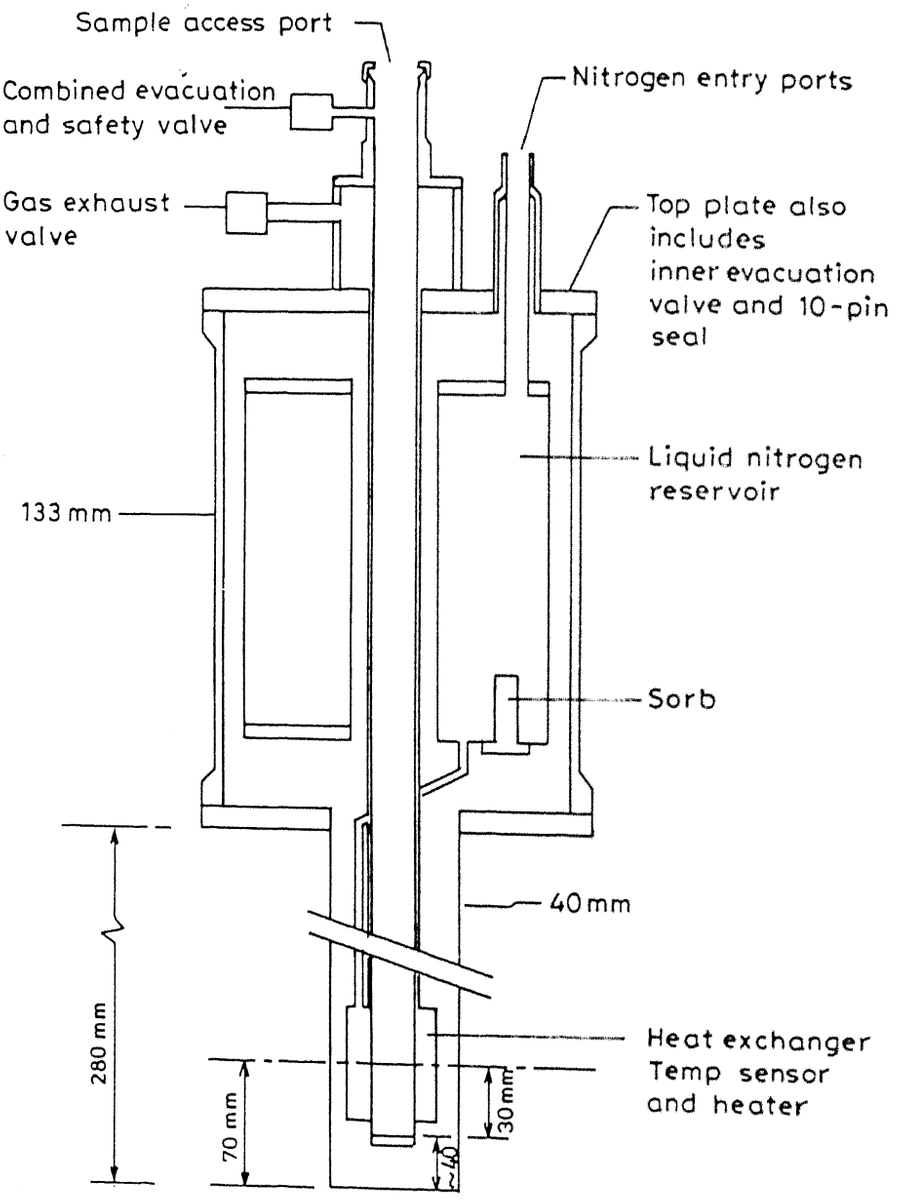

Figure 3.2: **Schematic diagram of the Liquid Nitrogen Cryostat**

sample temperature. The polymer-salt solution in acetonitrile was poured into this cell which was then heated under vacuum at $\sim 90^{o}C$ to remove the solvent. The conductivity measurements were then made during heating or cooling cycle over the temperature range -25 to $100^{o}C$. To obtain temperatures below the ambient, a mixture of ethanol and liquid N_2 was used as a coolant. Ethanol was used to retard the rate of evaporation of liquid N_2 and keep the coolant effective for a longer period.

The cell constant (l/A) of this cell was determined by calibrating with a 3 % KCl solution with a known specific conductance of 43.6×10^{-3} Ohm^{-1} cm^{-1}. We used the relation

$$R_t = R_o + \rho\frac{l}{A} \tag{3.1}$$

where l is the distance between the two electrodes , A the cross sectional area, and R_t the resistance measured at 1 kHz for a particular value of l, ρ the specific resistivity and R_o is the residual resistance comprising largely the contact resistance. By raising or lowering the electrode attached to the cap, the value of l could be varied . From the intercept of the plot of R_t versus l, the quantity R_o was determined. Then the distance between the electrodes was fixed by fixing the upper electrode at a particular position using an adhesive resin. The value of R_t for this configuration was then measured using the same 3 % KCl solution. Using the calculated value of R_o and known value of ρ the value of the cell constant (l/A) was determined using Eq. (3.1).

3.3.2 Complex Impedance Analysis

The d.c. conductivities of the samples were found from the impedance data by complex impedance analysis (CIA). The complex impedance $Z(\omega)$ at an applied frequency (ω) can be expressed as

$$Z(\omega) = Z_R(\omega) + jZ_I(\omega) \tag{3.2}$$

where the magnitude of the complex impedance, $Z = (Z_R^2 + Z_I^2)^{1/2}$, and $\theta = tan^{-1}(Z_I/Z_R)$ is the phase angle, and Z_R and Z_I are the real and imaginary

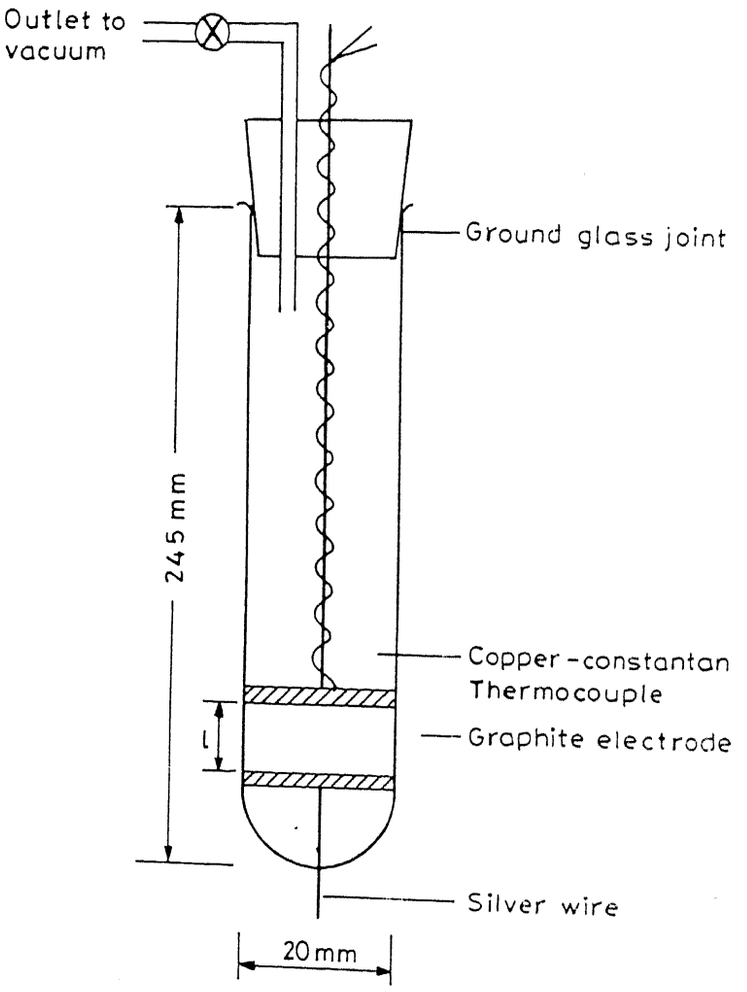

Figure 3.3: **Sample Holder for $(PEG)_xLiClO_4$ system**

parts of the impedance respectively. If one plots the imaginary part of the impedance (Z_I) vs the real part (Z_R) at various frequencies, the resulting locus shows distinct features for certain combinations of circuit elements. The method is best illustrated by a specific example of such a plot shown in Fig. 3.4. In this method a low ac signal is used through the sample, which helps avoid irreversible electrode changes and heating effects. As the measurement is done over a wide frequency range (5 Hz–13 MHz), the various polarization processes occurring in a sample may be resolved.

The impedance was measured using a HP4194A Impedance Analyzer over the frequency range 100Hz-1MHz. The HP 4194 A provides a wide frequency range, from 100 Hz to 40 MHz with a resolution of 1 mHz. It has a four terminal pair configuration and can measure impedances in the range 10 mΩ to 100 MΩ with a maximum resolution of 100 $\mu\Omega$.An oscillation level of 1 V was used for all measurements. The impedance data thus obtained were then analysed using the package– EQUIVALENT CIRCUIT developed by Boukamp et al (Boukamp, 1986). This package uses a Non-Linear-Least-Square (NLLS) fit of the given circuit parameters to the measured data (Macdonald, Schoonman and Lehnen, 1982).

The impedance (Z) or admittance (Y) response of the model or equivalent circuit used to describe the system can be expressed in terms of the complex function:

$$f(\omega; \overline{R}) = f_x(\omega, \overline{R}) + j\ f_y(\omega, \overline{R}) \tag{3.3}$$

where f is a function both of the angular frequency, ω, and the set of model parameters, $\overline{R}$. For the purposes of the fit , the frequency, as is usually the case experimentally, is assumed to have negligible error as compared to the *measured* values of Z (or Y). In this approximation, with measurements made at angular frequencies ω_i (i=1,2 ...k) of the complex Z (or Y) data of the form $x_i + j\ y_i$, the goal of a complex least squares analysis is to find the set of parameters which minimizes the weighted sum

$$S = \sum_{i=1}^{k} \{\omega_i^x\ [x_i - f_x\ (\omega_i, \overline{R})]^2 + \omega_i^y\ [y_i - f_y\ (\omega_i, \overline{R})]^2 \tag{3.4}$$

Table 3.3: **Circuit Elements, corresponding symbols and dispersion relations.**

Element	Symbol	Dispersion relation		
description	CDC	Admittance	Impedance	Parameters
Resistance	R	$1/R$	R	R
Capacitance	C	$j\omega c$	$-j\omega c$	C
Inductance	L	$-j/\omega L$	$j\omega L$	L
Warburg Impedance	W	$Y_o\sqrt{(j\omega)}$	$1/Y_o\sqrt{(j\omega)}$	Y_o
CPE	Q	$Y_o(j\omega)^n$	$(j\omega)^{-1}/Y_o$	Y_o, n

where ω_i^x and ω_i^y are the weights associated with the i^{th} data points. If the standard deviations σ_i^x and σ_i^y of each point are known, then $\omega_i^x = (\sigma_i^x)^{-2}$ and $\omega_i^y = (\sigma_i^y)^{-2}$.

For the case of impedance and/or admittance data, a least square fit puts both real and imaginary components on an equal footing. The results of the analysis are estimated parameter values and their estimated uncertainties, along with an estimate of the overall standard deviation of the fit. Thus , if the data determines some parameter values better than others, this is immediately obvious. In order to obtain a greater accuracy, impedance data from either end of the semicircle should be avoided, only the central part of the semicircle should be included.

The various circuit elements utilized in this particular package are given in Table 3.3. Two of these circuit elements , viz., the Warburg Impedance and the Constant Phase Element are elaborated below.

Warburg Impedance: The Warburg is a well known diffusion element, also known as the semi-infinite transmission line. The dispersion relation follows from Fick's second law for a (one dimensional) semi-infinite diffusion problem.

The general form is

$$Y^*(\omega) = Y_o(j\,\omega)^{1/2} = Y_o[(\omega/2)^{1/2} + j\,(\omega/2)^{1/2}] \tag{3.5}$$

where Y_o is the adjustable parameter containing the diffusion coefficient and other parameters which depend on the characteristics of the electrochemical system.

Constant Phase Element (CPE): The CPE is another diffusion related element. It can be represented as (Macdonald, 1986):

$$Y_c = Y_o(i\omega)^n = Y_o\omega^n[cos(n\pi/2) + isin(n\pi/2)] \tag{3.6}$$

The CPE for n = 0, represents a resistance with $R = Y_o^{-1}$, for n = 1 a capacitance with $C = Y_o$, for n = 0.5 a Warburg Impedance and for n = -1 an inductance with $h = Y_o^{-1}$.

It has been noted that the CPE in series with a capacitor leads to a Cole-Cole distributed response and in parallel with a resistor it leads to a depressed circular arc response often found for solid electrolytes. In fact in most samples used in this work such depressed semicircles, sometimes accompanied with tails, were obtained. The tail could be attributed to an additional Warburg in series. Thus the circuit code chosen was (RQ)W. The simulated and the measured data are shown in Fig 3.4.

3.3.3 X-Ray Diffraction Analysis

X-Ray diffraction (XRD) patterns of the various polymer films have been recorded using a Rich Siefert (Iso-Debyeflex 200 2D) counter diffractometer employing a filtered CuK α radiation (λ = 1.542 o A). The generator was operated at 30kV and 14 mA. The chart speed was fixed at 15mm/min and the scanning speed was 0.3 deg/min in 2θ. All the XRD studies were done at room temperature (25^oC).

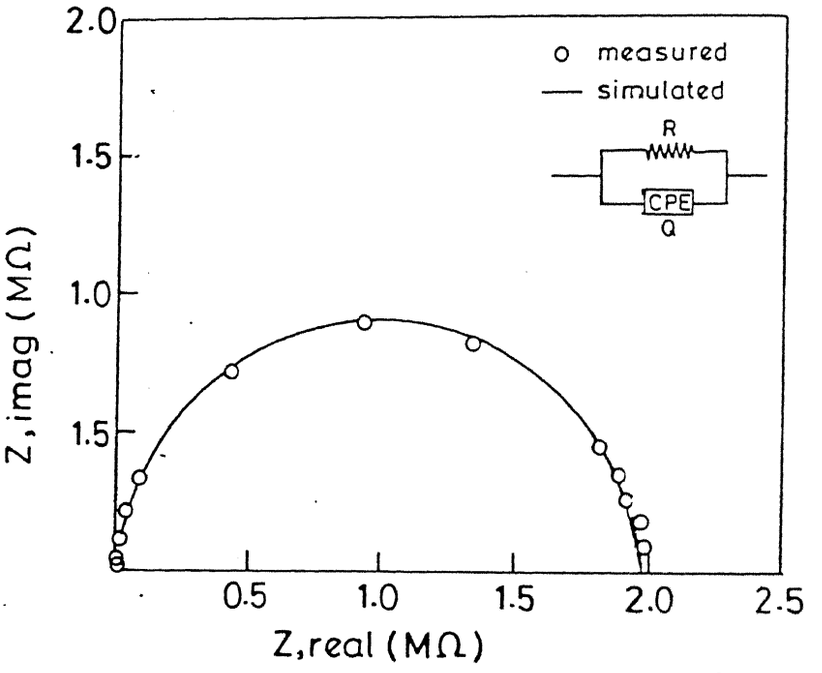

Figure 3.4: **A typical Complex Impedance plot**

For the XRD measurements the sample films were fixed on glass slides with a drop of methanol. However, the $(PEG)_x(LiClO_4)$ samples could not be studied using this technique as self supporting films could not be obtained.

3.3.4 Thermal Analysis

The differential thermal Analysis (DTA) were carried out using a Linsies L-62 Mini Differential Thermal Analyser. This equipment employs a SiC furnace which can go upto 1500^oC. The heating rate employed was $5^oC/min$ in all cases. The DSC measurements were carried out using a DuPont 9000 Differential Scanning Calorimeter over a temperature range -50^o to 250^oC. The unit was standardized using pure Indium metal (m. pt.156.8^oC). Typical sample size used were 3-6 mg. All runs were repeated to check reproducibility.

There were some discrepancies in the DTA and DSC results, which could be partly attributed to the lower sensitivity of the Pt-Pt(Rh) thermocouple especially below 100^oC, employed in the DTA studies. The peak areas were measured using graph papers and used to obtain the enthalpies of various transitions.

3.3.5 Solid State NMR

The solid state NMR measurements were carried out on a Bruker MSL–300 spectrometer at a ^7Li resonance frequency of 116.64 MHz. Spectra were obtained by Fourier transformation of free induction decays averaged over 25–700 scans following $\pi/2$ pulses of 5 μs duration. Temperature variation (to an accuracy of $\pm$ 1 K) was achieved using a Bruker temperature controller. Spin lattice relaxation time (T_1), was determined using a $\pi - \tau - \pi/2$ pulse sequence, with a cycle time of 3s. For NMR measurements the samples were sealed in glass tubes having an o.d. of 5 mm.

3.3.6 FTIR and SEM Analysis

The Fourier Transform Infrared Spectroscopy (FTIR) data was taken on a Perkin–Elmer FTIR 1600 Series spectrometer. Transparent pellets of the polymer–salt complex, the polymer and the pure salt mixed with KBr were used for FTIR studies. The accuracy of the instrument was $\pm$ 1 cm^{-1}.

The Scanning Electron Micrographs were taken with a JEOL Scanning Microscope (JSM - 840 A). The polymer films were cut into 3×3 mm^2 size and coated with silver (International Scientific Instruments PS–2 coating unit) before loading in the system. The photographs were taken at a probe current of 10^{-11} A and 15 kV accelerating voltage. The system has a provision of 10× to 3,00,000× magnification of the images. The magnification was fixed according to the need.

Chapter 4

Structure and Phase Studies

In the past solid electrolytes based on low molecular weight PEG as a plasticizer with polyethylene oxide(PEO) have been studied. The use of plasticizers in polymers is known to increase polymer chain flexibility, increase free volume, and decrease the glass transition temperature,T_g. These changes are also known to increase ionic conductivity in solid electrolytes. Hardy and Shriver (1984) first reported fast ion conduction in poly(diallyldimethyl ammonium chloride) (DDAC) plasticized with PEG (M_w = 300). In another work, Kelly, Owen and Steele (1984) reported that the addition of dimethoxy poly(ethylene glycol) (PEGDME) to PEO results in a large conductivity increase due to partial dissolution of the crystalline phases and plasticization of the amorphous phases. Studies on interactions of homogeneous polyethylene glycol (PEG) (EO_n, n = 1–8) with alkali and magnesium metal cations and the ammonium cation (Yanagida, Takahashi and Okahara, 1978) led to the conclusions that the terminal hydroxyl groups contribute to stable complex formation. More recently complexes of PEG (Mol.wt.400) with $NiBr_2$ (Mendolia and Farrington, 1992) have yielded good results. Studies on electrolytes based on poly(tetra methylene ether)glycol (PTHF) (Cameron, Ingram and Sarmouk, 1990) indicate that the hydroxyl ended polymers have markedly higher conductivities than their acetylated counterparts, which may be ascribed to the superior solvating

Table 4.1: Systems Investigated

Complex	Compositions	Maximum σ	x at σ_{max}
$(PEG)_x(LiCl)$	x= 4,6,8,10,12, 20,40,60.	1.5×10^{-5}	10
$(PEG)_x(LiBr)$	x= 4,6,7,8,10,12,20 30,40,60.	7.9×10^{-4}	10
$(PEG)_x(LiClO_4)$	x= 4,6,8,10,12, 20,40,60.	4.0×10^{-3}	8
$(PEG)\ (LiClO_4)$ $+x\%Al_2O_3$	x = 5,10,20,30	1.2×10^{-5}	20

power of the -OH group over internal ether links, leading to less ion-pairing. Even though the high molecular weight PEG can be predicted to have a behavior almost identical to PEO, so far no systematic studies have been reported on electrolytes based only on high molecular weight PEG. In view of this fact, it was considered worthwhile to study the complexes of PEG with some Li–salts, as they are the most promising from the battery point of view. Table 4.1 gives a summary of the polymer-salt complexes studied. The other complexes studied in this work include $(PEG)_{10}MI$ where M = Li, Na, K and Cs and $(PEG)_{10}MBr$ where M = Na,K and Cs.

This chapter reports the structure and phase behavior of these complexes investigated by means of X-ray diffraction (XRD), Differential Scanning calorimetry (DSC), Scanning Electron Microscopy (SEM) and Fourier Transform Infrared Spectroscopy (FTIR). The electrical conductivity results along with Solid State NMR and dielectric studies are discussed in Chapter 5, and the effect of ion size and dispersion of alumina particles on the electrical conductivity are reported in Chapter 6.

4.1 Infrared Spectroscopy

The infrared spectroscopy studies on polymer–salt complexes are expected to give mainly two kinds of information; firstly about the conformation of the polymer chain and secondly, about the position of the metal ions in the polymer chain. The conformation of the $O-(CH_2)_2-O$ portion in the polymer chain is of particular interest. This branch can exist in two conformations : trans and gauche. Previous studies have lead to varying conclusions : Davidson (1955) suggested a gauche structure; White and Lovell (1962) suggested a gauche structure but with the two terminal hydroxyl groups in the trans conformation; Kuroda and Kubo (1955, 1959) suggested a gauche structure and Rossi and Magnasco, 1962 obtained a structure of the form TGGTGG... from statistical calculations. There is no FTIR data available on PEG based salt–polymer complexes. However, FTIR studies on pure PEO (Matsui, Kubota, *et al.*, 1965; Liu and Parson, 1969; Takahashi and Tadokoro, 1973) lead to the conclusion that it has a helical structure in the crystalline state. The polymer chain has seven CH_2CH_2O units in two turns of the helix with a crystallographic repeat distance of 19.3 A. The structure of PEO–salt complexes has been put forward by Papke et al (Papke, Ratner and Shriver, 1981) to be $T_2GT_2\bar{G}$. This conformation may be described as a compressed helix, with a repeat distance of 9–11 $\mathring{A}$, the smaller cations (Li, Na) are expected to be within the helix having four nearest neighbours oxygens with lone pairs oriented towards the cation.

Our results on PEG–LiX (X = Cl and Br) are summarized below.

4.1.1 PEG–LiCl system

The FTIR plots of pure PEG and $(PEG)_{10}LiCl$ in the range 400–1500 cm^{-1} are shown in Fig 4.1. Table 4.2 lists the exact location of the peaks. Extensive vibrational spectroscopy data on PEO–salt complexes are available (Papke,

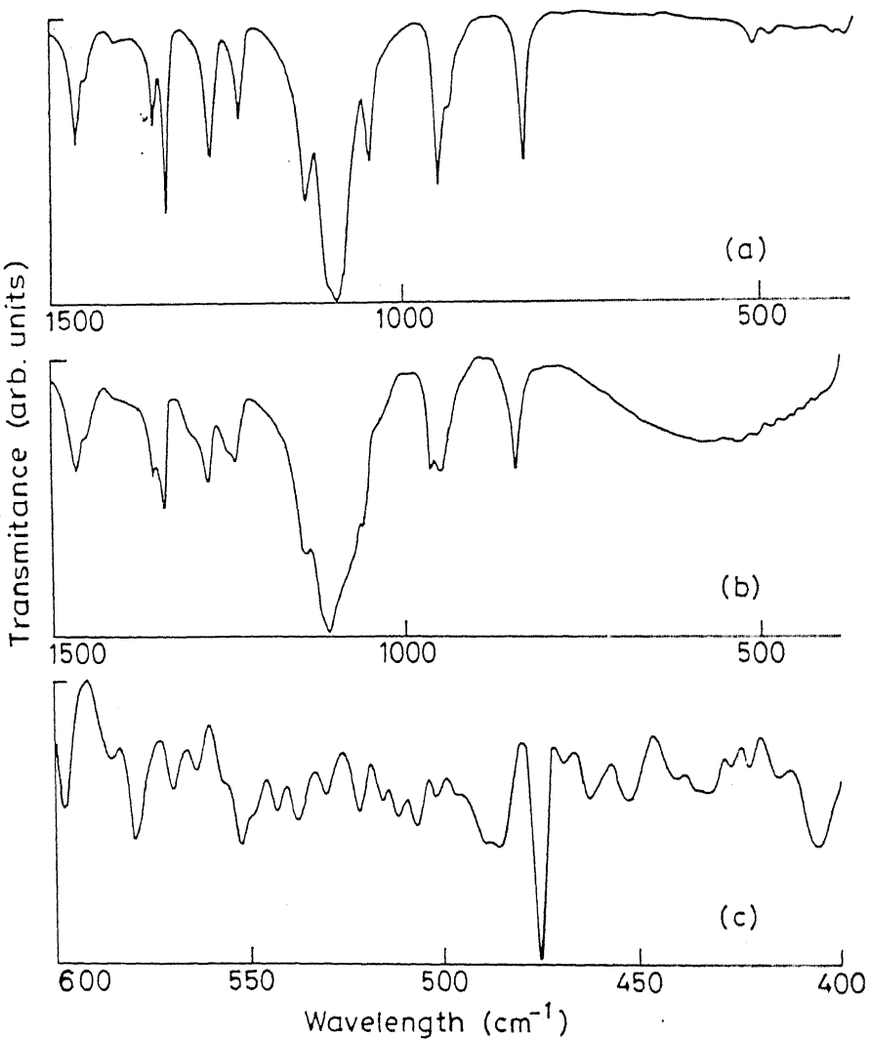

Figure 4.1: FTIR plots for (a) PEG (b) $(PEG)_{10}LiCl$ (c) LiCl

Ratner and Shriver, 1982b, 1981). The studies on PEG–LiX systems have been found to be similar to these results. The two peaks in the 800–1000 cm^{-1} region are assigned to $-CH_2$ rocking vibrations, and may be attributed to the gauche form. The region from 1060–1150 cm^{-1} has been assigned to contributions from C–C stretching and C–O stretching modes in the mutual couplings. If the alkali metal cations were coordinated to the ether oxygens, one would expect to see largest changes in this region. This is observed; the broad peak at 1149 cm^{-1} in the pure PEG shifts to 1143 cm^{-1} in the $(PEG)_{10}LiCl$ complex. The peaks at 1061 cm^{-1} and 1107 cm^{-1} in pure PEG have shifted and merged into one peak at 1112 cm^{-1} in the complex. The new peak at 949 cm^{-1} in $(PEG)_{10}LiCl$ could be assigned to a combination of symmetric $-CH_2$ rocking and -C-O-C- stretching vibrations. The FTIR plot of pure LiCl is also shown. The peaks at 572 and 535 cm^{-1} may be due to Li–Cl stretching. Infrared studies on complexes of $LiNO_3$ with PEO (Papke, Ratner and Shriver, 1982b) indicate the formation of ion pairs, which was reflected in the appearance of two different i.r. active bands in the PEO complexes, in place of one for NO_3 ions in other environment. Thus if we take the band at 554 cm^{-1} for pure LiCl, it may be assumed to have been replaced by the two bands at 571 and 535 cm^{-1} in the complex indicating the presence of two kinds of environment for the Cl ion in the PEG–LiCl complex. This may lead to the conclusion that some ion pairs may be present in these complexes as well.

In Table 4.2 the data for pure PEO obtained from literature (Papke, Ratner and Shriver, 1981) have been compared with those for pure PEG obtained in this work. Some new peaks appear in the 400–600 cm^{-1} region in the case of pure PEG, otherwise the data for pure PEO and pure PEG are very similar. The differences may be brought about by the presence of the -OH group at the end of PEG. The role of terminal hydroxyl groups in stabilizing the complexes of low molecular weight PEG with alkali metal salts have been reported in the past (Yanagida, Takahashi and Okahara, 1978). This is particularly valid for Li cations. The shift in the -C-O-C- stretching band due to the association with Li has also been reported in the past. This confirms the fact that the Li is located at the ether oxygen. The shift in the Li–Cl stretching bands from the

Table 4.2: **FTIR data for the $(PEG)_{10}LiCl$ complex**

Pure PEO[1]	Pure PEG	Pure LiCl	$(PEG)_{10}(LiCl)$	Assignment
1473 sh[2]				
1466 m	1467 m		1467 m	a-CH_2 b
1461 m				
1453 m				
1358 m	1360 s		1359 s	a-CH_2 w
1342 s	1342 s		1343 s	a-CH_2 w
1283 m	1280 m		1281 m	a-CH_2 t
1244 m	1241 s		1243 s	a-CH_2 t
1147 s	1149 s		1143 s	C-C and a-C-O-C st
1103 vs	1107 vs		1112 vs	a- C-O-C st
	1060 m			
958 s	962 s		964 s	-CH_2 r
948 m				-CH_2 r
844 s	842 s		843 s	a- -CH_2 r
	529 m	591 s	572 m	
		581 s		Li–Cl s
		554 m	535 s	
	406 w	475 m		

1 Data from Papke, Ratner and Shriver (1981)

2 sh = shoulder, m = medium , s = strong, vs = very strong, b = bending, w = wagging, tw = twisting, stret. = stretching

values for pure LiCl may be due to the difference of the local environment of the Cl within the PEG complex.

4.1.2 PEG-LiBr System

The FTIR data on $(PEG)_{10}LiBr$ complex is shown in Table 4.3. Fig 4.2 shows the FTIR plots for pure PEG, $(PEG)_{10}LiBr$ and LiBr in the 400–1500 cm^{-1} range. There is a peak at 1119 cm^{-1} which is attributed to asymmetric -C-O-C- stretching. Also there is a shift from the value of 1107 cm^{-1} and 1060 cm^{-1} for the pure PEG to the value 1119 cm^{-1} for the complex, indicating that the Li ion may be located on the ether oxygen of the polymer chain, $-(CH_2CH_2-O)_n$. The peak at 1149 cm^{-1} for pure PEG, that had shifted to 1143 cm^{-1} for the $(PEG)_{10}LiCl$ complex, is totally absent in the $(PEG)_{10}LiBr$. The peaks at 949 cm^{-1} and 843 cm^{-1} may be assigned to $-CH_2$ rocking vibrations as in the case of $(PEG)_{10}$LiCl. The peaks in the 400–600 cm_1 may be assigned to Li–Br stretching vibrations. Unlike in the case of $(PEG)_{10}$LiCl, there are a number of peaks in this region. They are comparable to those obtained for the pure LiBr salt. The disappearance of some of the peaks seen for pure LiBr in the case of $(PEG)_{10}LiBr$, may be due to the fact that the Br^- ion is in different surroundings in the polymer complex as compared to that in the pure LiBr salt. This kind of shift has been seen in the case of $(PEG)_{10}LiCl$ and pure LiCl.

4.2 X-Ray diffraction (XRD)

It has been pointed out that obtaining structural information about the crystalline polymer–salt complexes from XRD analysis is difficult due to the presence of multiple phases. The various phases present are : the crystalline polymer phase, the amorphous polymer phase and more than one crystalline

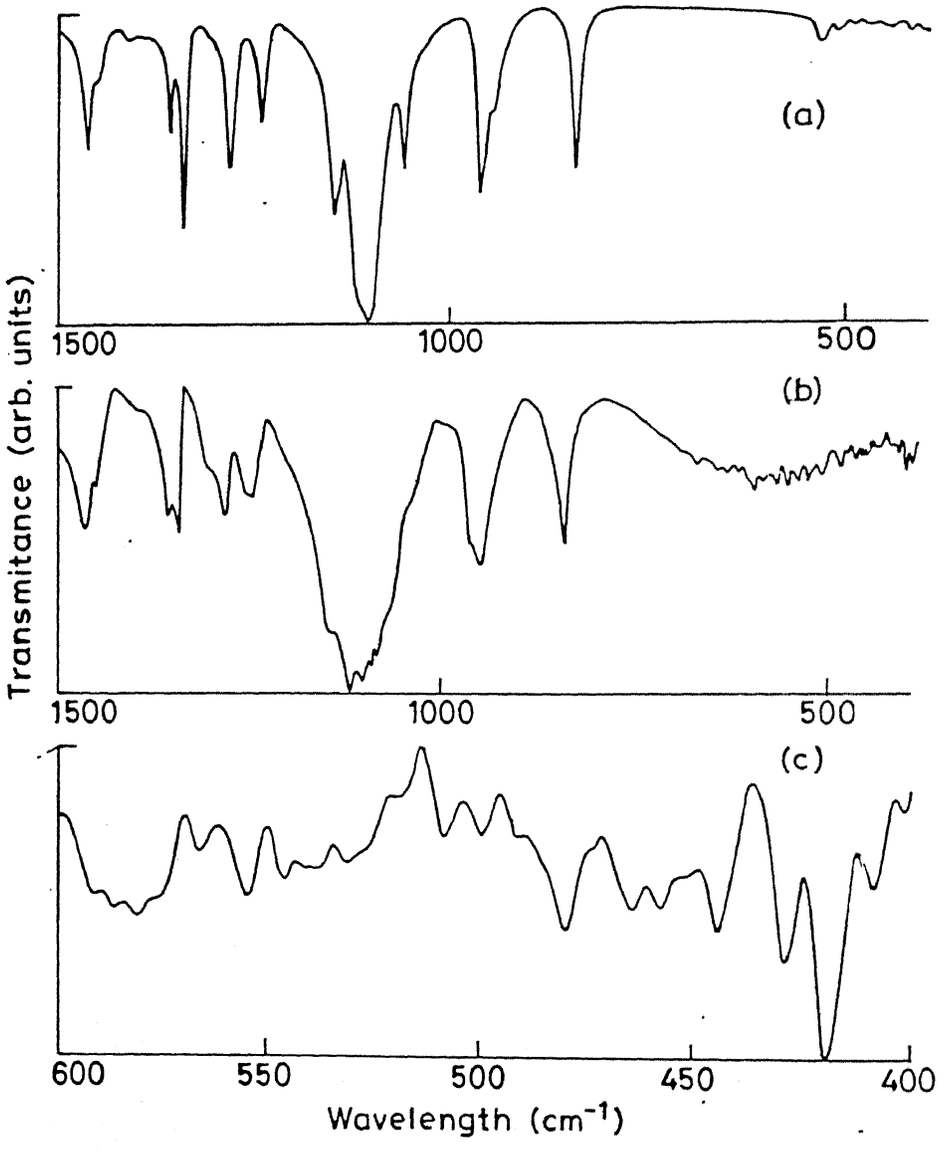

Figure 4.2: **FTIR plots for (a) PEG (b) $(PEG)_{10}LiBr$ (c) LiBr**

Table 4.3: **FTIR data for the $(PEG)_{10}LiBr$ complex**

Pure PEO[1]	Pure PEG	Pure LiBr	$(PEG)_{10}(LiBr)$	Assignment
1473 sh[2]				
1466 m	1467 m		1468 m	a-CH_2 b
1461 m				
1453 m				
1358 m	1360 s			a-CH_2 w
1342 s	1342 s		1344 s	a-CH_2 w
1283 m	1280 m		1281 m	a-CH_2 t
1244 m	1241 s		1244 s	a-CH_2 t
1147 s	1149 s			C-C and a-C-O-C st
1103 vs	1107 vs		1119 vs	a- C-O-C st
	1060 m			
958 s	962 s			-CH_2 r
948 m			949 s	-CH_2 r
844 s	842 s		843 s	a- -CH_2 r
	529 m	581 s	596 w	
		555 s	552 w	
			528 w	
		546 m	509 w	
		508 m		
		499 m		Li-Br st
		480 m	486 w	
		464 s	467 w	
		444 m		
		428 m	420 w	
		418 vs	410 w	
	406 w	408 m	403 w	

1 Data from Papke, Ratner and Shriver (1981)

polymer–salt complex phases. As the crystalline PEO–salt complex phases generally possess low symmetry and a large unit cell containing many atoms, the accurate determination of atomic positions is very difficult. Studies on oriented fibers (Hibma, 1983) of PEO– NaX complexes drawn from 2–3 percent solutions of PEO in methanol, indicate a monoclinic unit cell with average values of lattice parameters as a $\simeq$ 17.1 Å, b $\simeq$ 8.00 Å, c $\simeq$ 16.0 Å.

Our results on PEG–LiX (X = Cl and Br) are briefly discussed below.

4.2.1 PEG–LiCl system

The X-Ray powder diffraction patterns of PEG–LiCl complexes of different salt concentrations are shown in Fig.4.3. The observed X-ray intensities have been corrected for absorption and polarization according to the following expressions (Klug and Alexander, 1974)

$$\text{Absorption correction} = \frac{\mu T(1-\sec 2\theta)}{\exp[\mu T(1-\sec 2\theta)]-1} \tag{4.1}$$

where μ is the refractive index and T the thickness of the sample and μT is the optimum value of the absorption exponent of the specimen which may be obtained from the weight of the sample and its surface area.

$$\mu T = (\mu/\rho)\rho T = \omega/A.\mu/\rho \tag{4.2}$$

the factor ω/A for typical samples was taken to be 0.024 and for CuK-α radiation μ/ρ = 5.50. Thus

$$\mu T = 0.024 \times 5.50 = 0.132$$

, and

$$\text{Polarization correction} = \frac{1+cos^2 2\theta' cos^2 2\theta}{1+cos^2 2\theta'} \tag{4.3}$$

where θ' is the bragg angle for the reflecting planes of the monochromatizing crystal. Thus, for the (200) planes of sodium chloride, $\cos^2 2\theta'$ for CuK-α radiation is 0.723. θ is the usual Bragg angle for the sample.

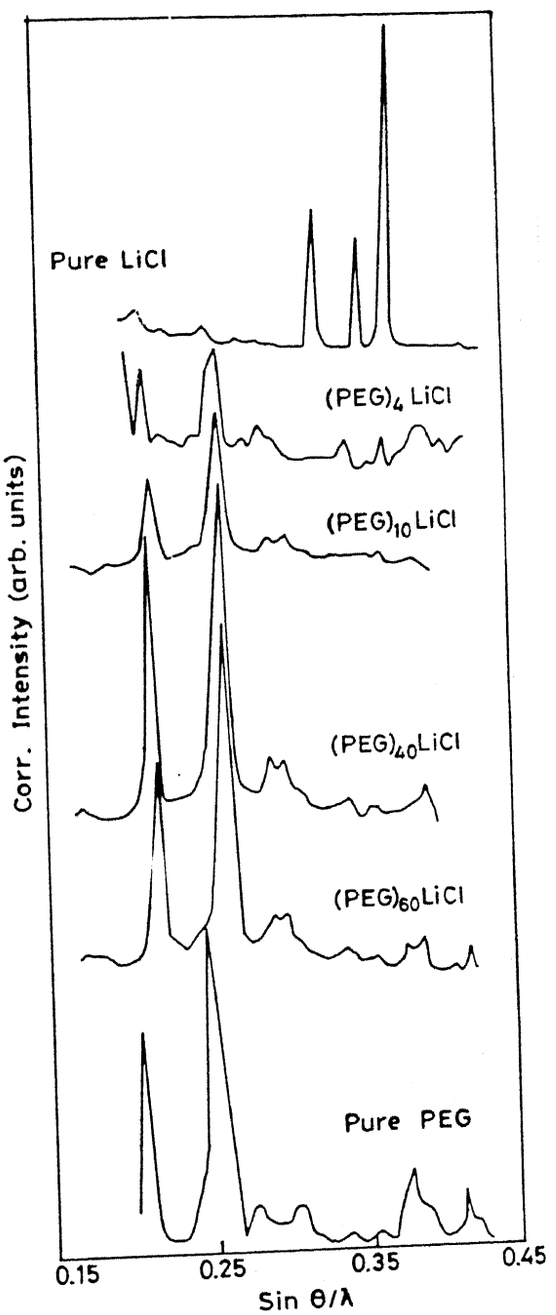

Figure 4.3: **XRD patterns for the $(PEG)_xLiCl$ system (x = 60, 40, 12, 7), and pure PEG and LiCl**

The XRD patterns for the $(PEG)_xLiCl$ complexes with x > 12 are very similar to those of pure PEG. With the increasing salt concentration the intensity of the pure PEG peaks diminish. This indicates that in the complexes with low salt concentrations, the salt tends to stay either in the amorphous phase of PEG or appears in the crystalline region as impurity. With increasing salt concentration more of the crystalline PEG phase is destroyed to accomodate the salt. Similar results have been reported for complexes of PEO with $NiBr_2$ (Cai, Hu, *et al*, 1992). However, in certain other PEO complexes some new peaks appear due to compound formation (Fauteux and Robitaille, 1986). No such peaks are in evidence in the PEG–LiCl system. No peak corresponding to pure LiCl are found indicating that no unreacted LiCl was present.

4.2.2 PEG–LiBr system

As pointed out earlier (sec. 4.1.3) that the polymer–salt complexes generally have low symmetry and a large unit cell containing many atoms. Fig. 4.4 shows the X-ray diffraction patterns corrected for absorption and polarization (using Eq. 4.1 and 4.2). The XRD patterns for the complexes with x >> 12 are very similar to that for pure PEG. With increasing salt concentration the intensity of the pure PEG peaks diminish. This has also been observed for the $(PEG)_xLiCl$ system. The peaks of pure LiCl are slightly removed from the pure PEG peaks and hence may be identified in the complexes with high salt concentration. However, in the case of $(PEG)_xLiBr$ the single peak of high intensity for pure LiBr that may be identified in this particular range, overlaps with the pure polymer peaks and is difficult to distinguish even in the high salt concentration complexes. There is not much variation in the XRD pattern with the salt concentration. This leads us to conclude that the complexes formed are not crystalline, and the x-ray peaks appear due to the presence of the pure crystalline polymer phase. This result is different from the $(PEG)_xLiCl$ system where the complexes for concentrations x < 12 were crystalline. This difference in behavior is also reflected in the salt–polymer

phase diagram, as discussed in the next section.

4.3 DSC Analysis

4.3.1 PEG–LiCl system

DSC traces over a temperature range of 223–523 K of the various compositions of the $(PEG)_xLiCl$ system are shown in Fig 4.5 . The peak corresponding to the melting of LiCl is missing in the DSC traces of salt–polymer complexes indicating that there is no uncomplexed salt phases present. The complexes in the concentration range x < 12 show two thermal events – one at about 62°C and the other at around 190 °C. This behavior is similar to that of the $(PEO)_xNaI$ system (Chiang, Davis, *et al.*, 1983; Minier, Berthier and Gorecki, 1984) and indicates the coexistence at room temperature of the two crystalline phases : a pure polymer phase which melts at $\sim$ 62°C and a crystalline polymer–salt complex phase which gradually dissolves into the amorphous phase. We are not aware of any DSC/DTA studies on PEG–LiX system. However, the $(PEO)_xLiCF_3SO_3$ system has been investigated (Berthier, Gorecki, *et al.*, 1983) and is found to exhibit a similar behavior. For lower salt concentrations, viz., x > 12, only the melting of the polymer at $\sim$ 62°C is observed. This is because in this temperature range the elastomeric phase is too dilute to allow any formation of crystalline salt–polymer complex.

Fig 4.6 is a summary of the phase analysis of $(PEG)_xLiCl$. These results are essentially similar to those reported previously on the PEO–NaI and PEO–LiCl systems (Chabagno, 1980; Chiang, Davis, *et al.*, 1983). Chabagno (1980) has reported that in the complexes of PEO with NaI and LiCl, several crystalline phases coexist. Below 55°C the crystalline phases are : NaI and $(PEO)_4NaI$ in the composition range x < 4; $(PEO)_4NaI$ at x = 4 and $(PEO)_4NaI$ and pure PEO in the range x > 4. It was assumed that these complexes did

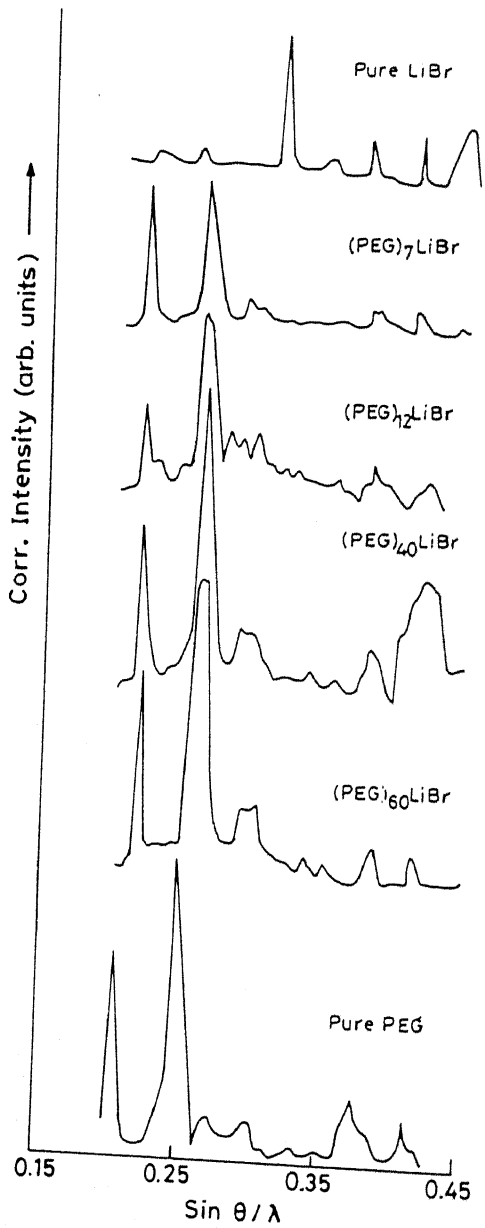

Figure 4.4: **XRD pattern for pure PEG, pure LiBr and the complexes** $(PEG)_xLiBr$ **(x= 60, 40, 10,8)**

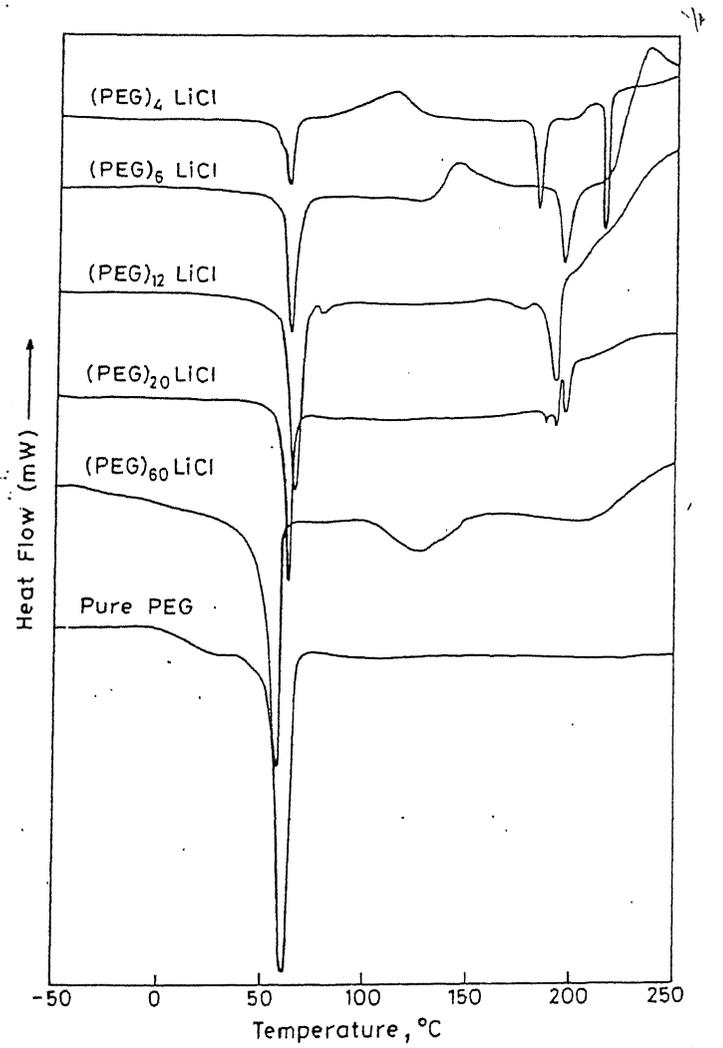

Figure 4.5: **DSC results on the $(PEG)_xLiCl$ system**

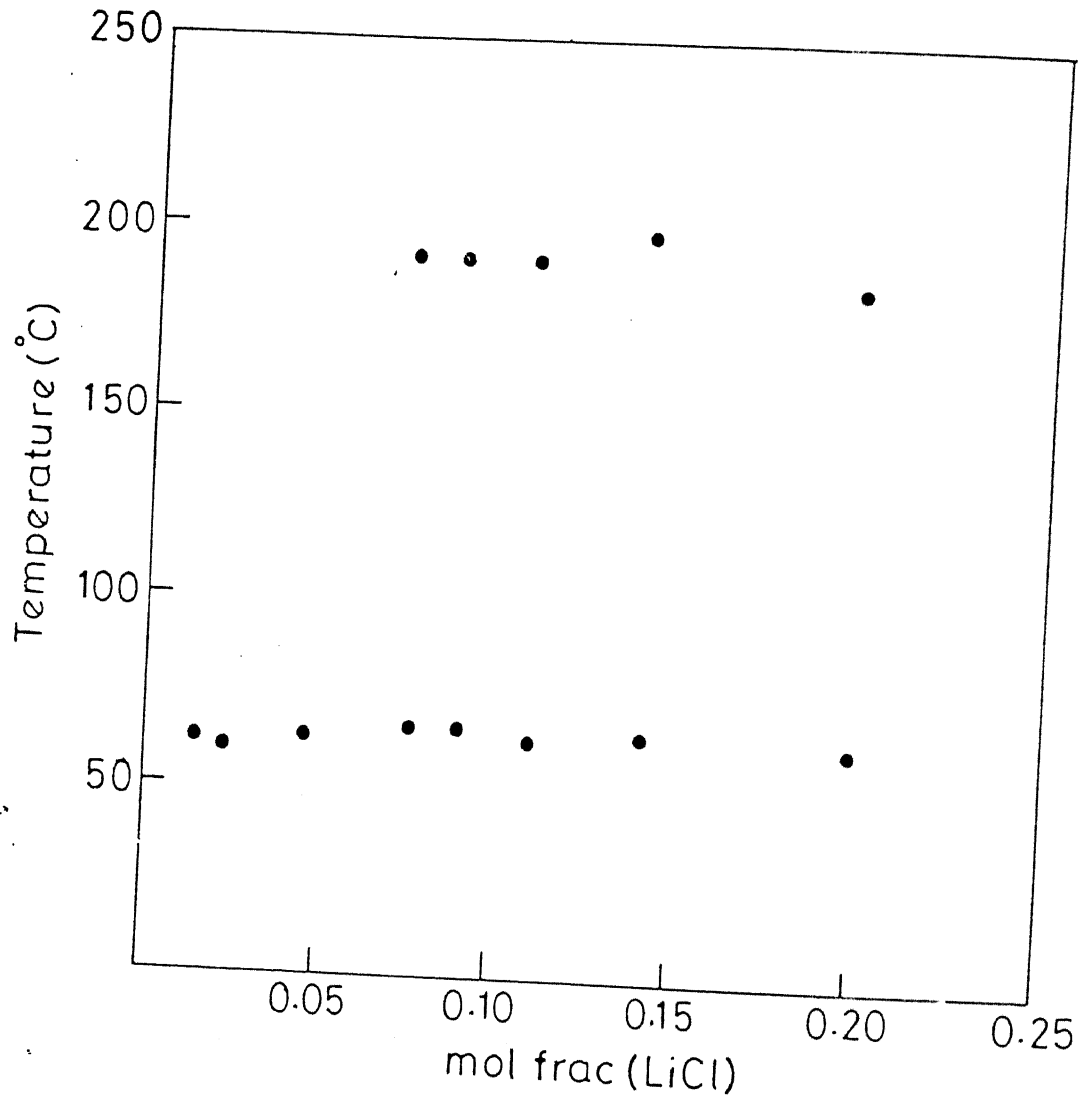

Figure 4.6: **Parts of the PEG–LiCl phase diagram inferred from DSC studies**

not possess a non-stoichiometric domain as in the case of the $(PEO)_xLiClO_4$ system. Following this the $(PEO)_{4.5}LiCl$ composition for several ions was reported by Reitman, Kaplan and Cava (1985). The $(PEO)_{4.5}LiCl$ complex was found to be fully crystalline. Minier, Berthier and Gorecki (1983) studied the recrystallization of both, the salt rich complex phase and the pure PEO phase for the $(PEO)_xNaI$ system and concluded that $(PEO)_{10}NaI$ was an intermediate compound that could be maintained fully elastomeric at room temperature for several hours. The salt rich complex could be recrystallized easily upto x < 10, at x = 10 it was drastically reduced and at x > 10 it was hindered due to the low salt concentration. The recrystallization of pure PEO followed an opposite pattern and thus at x = 10 an amorphous/elastomeric phase could be maintained even near room temperature. In another work (Chiang, Davis, *et al.*, 1983) the melting point of the crystalline salt–polymer complex, which was about 468 K (195 °C), shifted to higher temperatures with increasing NaI concentration.

Our DSC results (Fig 4.6) indicate the existence of crystalline salt polymer complex upto a concentration $X_{LiCl} \leq 0.07$ or O/Li > 12. The melting point of this complex which is $\simeq$ 463 K (190 °C) is observed to shift to higher values for higher salt concentrations; 197 °C for $(PEG)_6LiCl$ and 214 °C for $(PEG)_4LiCl$. The pure polymer melting temperature does not shift to lower temperatures with the increase in the salt concentration upto x = 8, which is attributed to the presence of some dissolved salt ions which behave as impurities. The high temperature peak at 190–200 °C in the $(PEO)_x(NiBr_2)$ complexes in the concentration range x < 8 has been attributed to the precipitation of the uncomplexed salt (Mendolia and Farrington, 1992). There is no evidence of any glass transition temperature (T_g) over the studied temperature range for the compositions x < 10. This result is similar to that obtained for the $(PEO)_xNaI$ system (Minier, Berthier and Gorecki, 1983) indicating that the amorphous phase is highly inhomogeneous. The heats of transition were determined from the area of the crystalline polymer melting peaks. A plot of heat of transition, H_f, with the stoichiometry of the complex is shown in Fig. 4.7. The value of H_f increases initially as the salt concentration decreases,

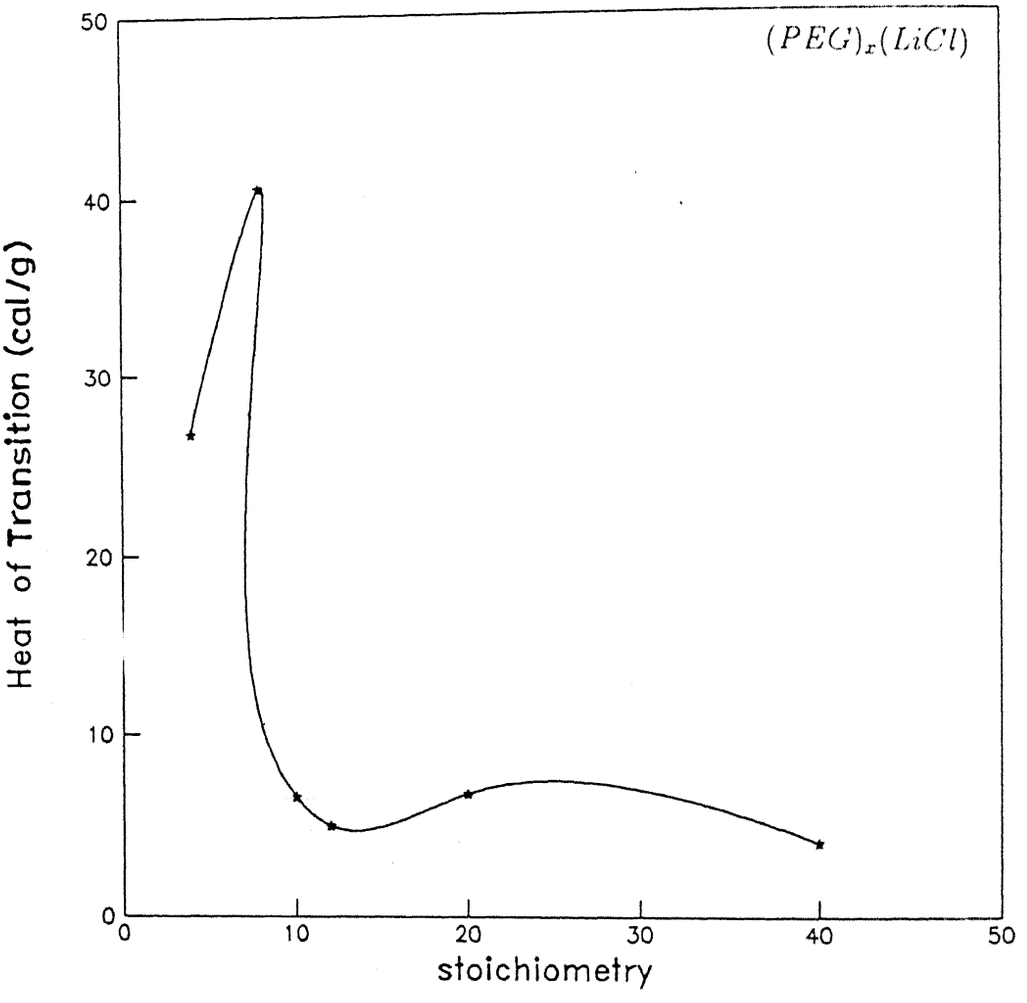

Figure 4.7: **A plot of Heat of Transition, H_f versus the stoichiometry of the complex (x)**

attains a maximum value of about $\sim$ 40 cal/g, and then drops sharply between x = 8 and x = 10. This may be due to the fact that most of the excess PEG is amorphous in this composition range. This is consistent with the conductivity results (Chapter 5), where the x = 10 composition was found to exhibit the highest conductivity.

4.3.2 PEG–LiBr system

The phase analysis diagrams of salt–polymer systems like, the PEO– $LiClO_4$, PEO–$LiCF_3SO_3$ and PEO–$LiAsF_6$ have been determined (Fauteux and Robitaille, 1986). In the PEO–$LiClO_4$ system, a eutectic was detected at around x = 10 with a melting temperature of $\simeq 50°C$. There were also two crystalline complexes of the composition $(PEO)_6LiClO_4$ and $(PEO)_3LiClO_4$. In the case of PEO–$LiAsF_6$ the eutectic composition is approximately $(PEO)_{22}LiAsF_6$. In the case of the PEO–$LiCF_3SO_3$ system an intermediate compound at x = 3, viz., $(PEO)_{3.5}LiCF_3SO_3$ was detected and an eutectic at x = 100, viz., $(PEO)_{100}LiCF_3SO_3$ was reported. (Fauteux and Robitaille, 1986). In all these cases the eutectic composition has been found to exhibit higher conductivity and the compositions at which intermediate compounds were formed show lower conductivities. The DSC results on the PEG–LiBr system are consistent with the above studies.

Fig 4.8 shows some of the DSC plots for the $(PEG)_xLiBr$ system. For most of the compositions there are two peaks, one at $\simeq$ 60 $°C$ and one at higher temperatures. In the case of the complex $(PEG)_4LiBr$ there are endothermic peaks at 116, 167 and 239 $°C$ in addition to the one at 60 $°C$. The peak at 116 $°C$ was not reproducible and may be due to the vaporization of solvent remaining from the casting process. This has been reported for the $(PEO)_8NiBr_2$ complex (Huq, Saltzberg and Farrington, 1989). The peak at 167 $°C$ may be due to the melting of some crystalline salt–polymer complex formed at this composition. The peak at $\simeq$ 230 $°C$ that is observed for the x = 4 and also x = 6 complexes is due to salt precipitation. This is analogous to

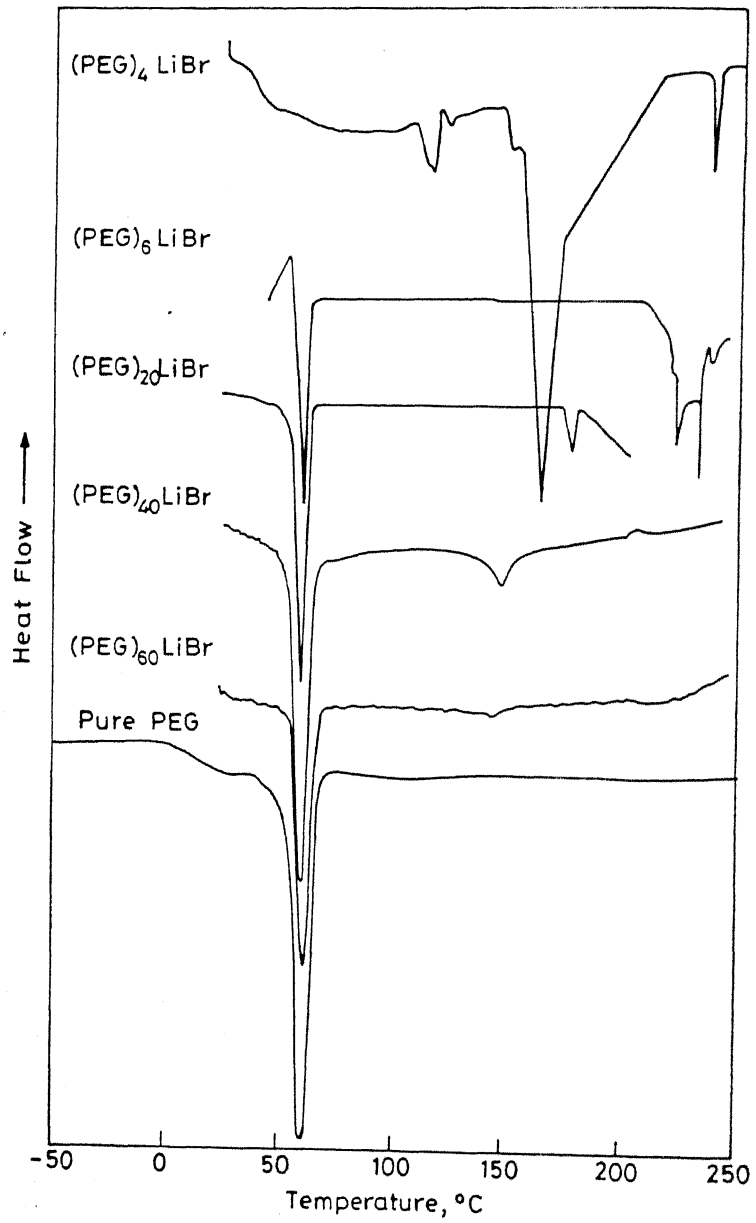

Figure 4.8: Summary of DSC results for the $(PEG)_xLiBr$ complex (x = 4,6,20,40,60) and that of pure PEG.

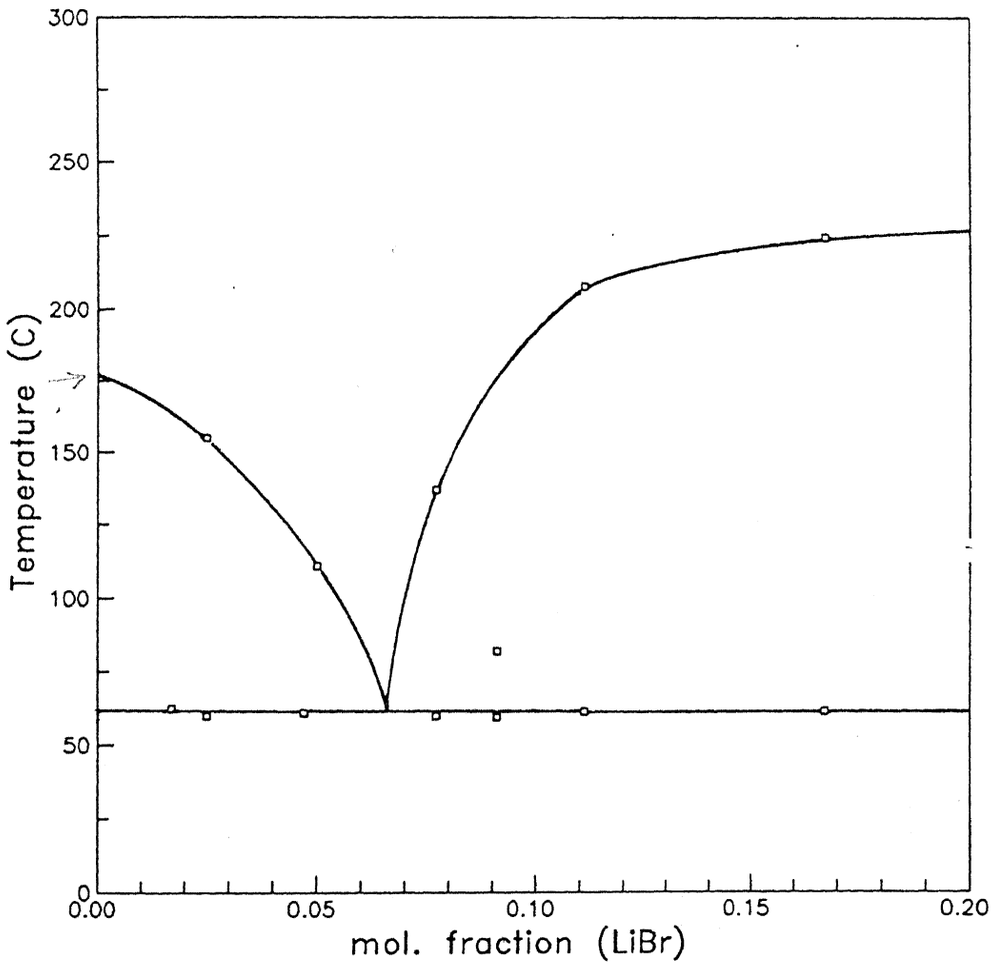

Figure 4.9: **Parts of phase diagram for the $(PEG)_xLiBr$ system**

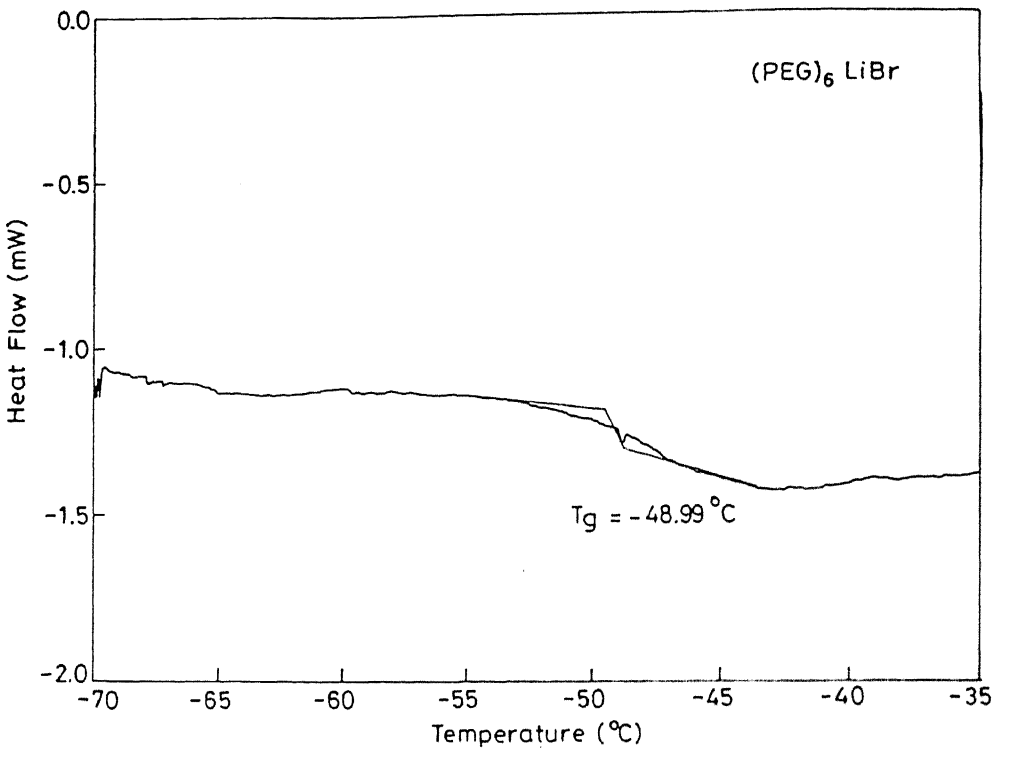

Figure 4.10: **Glass transition temperature, T_g, for the $(PEG)_6LiBr$ complex**

the behavior reported for $(PEO)_8NiBr_2$ (Huq, Saltzberg and Farrington (1989), Cai, Hu, *et al.* (1992)),. In the case of $(PEG)_8LiBr$ complex two peaks at 61 $°C$ and 208 $°C$ is observed which may be attributed to pure polymer melting and crystalline salt–polymer complex melting temperatures. It is observed that the melting point of the crystalline salt–polymer complex reduces to 82 $°C$ for the $(PEG)_{10}LiBr$ complex, and for the $(PEG)_{12}LiBr$ composition there is a possibility of a eutectic composition between x = 10 and x = 12. A summary of the DSC results showing the transition temperatures with the corresponding compositions are shown in Fig. 4.9. Fig 4.10 shows the DSC plot for the $(PEG)_6LiBr$ complex in the low temperature region (-80 to 15 $°C$). The T_g is seen at -49 $°C$.

The phase analysis diagrams of salt–polymer systems like, the PEO– $LiClO_4$, PEO–$LiCF_3SO_3$ and PEO–$LiAsF_6$ have been determined (Fauteux and Robitaille, 1986). In the PEO–$LiClO_4$ system, a eutectic was detected at around

x = 10 with a melting temperature of $\simeq 50^{o}C$. There were also two crystalline complexes of the composition $(PEO)_6LiClO_4$ and $(PEO)_3LiClO_4$. In the case of PEO–$LiAsF_6$ the eutectic composition is approximately $(PEO)_{22}LiAsF_6$. In the case of the PEO–$LiCF_3SO_3$ system an intermediate compound at x = 3, viz., $(PEO)_{3.5}LiCF_3SO_3$ was detected and an eutectic at x = 100, viz., $(PEO)_{100}LiCF_3SO_3$ was reported. (Fauteux and Robitaille, 1986). In all these cases the eutectic composition has been found to exhibit higher conductivity and the compositions at which intermediate compounds were formed show lower conductivities. The DSC results on the PEG–LiBr system are consistent with the above studies.

4.4 SEM Analysis

The crystalline regions, even in polymers of highly regular chemical structure, extend over distances of only a few hundred angstroms. The dimension along the chain axis is limited by chain folding and the wandering of molecules into the amorphous regions to arrive at other crystalline regions. In lateral directions continuity is maintained over longer distances, because crystal growth from the melt occurs predominantly by accretion of molecular segments side by side and distortion and branching during growth lead to a radial structure, known as a *spherulitic structure*. Optical microscopy has been used in the past (Fauteux and Robitaille, 1986) for PEO-LiX systems to detect the phase transitions by noting the disappearance of the spherulitic morphology as temperature increases. It was observed that the progressive dissolution of the polymer-salt complex can be better detected by microscopy than DSC in the case of the more dilute compositions. In the case of the PEG–MX complexes spherulitic structures were observed in the SEM micrographs. Fig 4.11 shows the electron micrograph for the $(PEG)_{10}CsI$ complex showing maltese cross like structures which are characteristic of such complexes (Ferloni, Chiodelli, *et al.*, 1986; Wright, 1975)

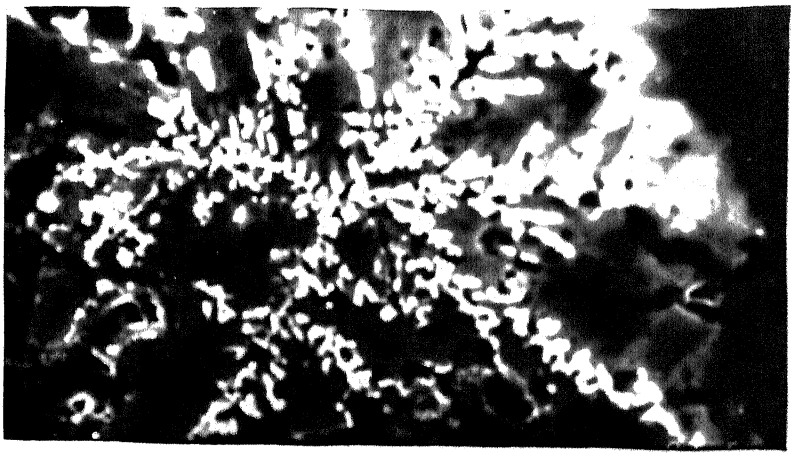

Figure 4.11: SEM micrograph for the $(PEG)_{10}CsI$ complex showing spherulitic structure

Transmission electron microscopy (TEM) studies on PEO–NaSCN and PEO–NaI complexes indicate that the thermal history of the sample affects the morphology as seen under the microscope (Lee and Wright, 1982a) PEO–NaSCN and PEO– NaI complexes deposited from polymer–salt solutions were found to form crystalline lamellae, 150–200 Å in thickness. The electron micrographs in such cases would show close striations. However, complexes that are annealed for a long time near the melting point, have lamellar thickness of as high as 600 A, which is visible in the micrograph. When the complex is heated to above its melting point, and crystallized from the melt, there is no evidence of spherulites, but the thickened lamellar fragments appear to be threaded together and appear as concentrated blobs or *shish-kebab* like structures. The complexes with high salt concentration were found to show less lamellar thickening due to the reduced concentration of vacancies in the ionic lattice of the salt, which is generally present in excess in these compositions. The studies by Lee and Wright (1982a), lead to the conclusion that the PEO–NaI and PEO–NaSCN complexes contain at least two distinct complex phases, phase I (the higher melting phase) and phase II the (lower melting phase). The complexes exist in the layer sandwiched between the crystalline lamellae.

The SEM micrographs for the $(PEG)_{20}LiBr$ complex , at room temperature and quenched from $55°C$ and $70°C$ are shown in Fig 4.12 (a), (b) and (c) respectively. DSC studies on this sample indicate a melting temperature of $\simeq 60°C$ (Fig. 4.8). In Fig 4.12 (a) we observe close striations and lamellar growth. In Fig 4.12 (b), where the sample has been annealed at a temperature below the melting point, we see thicker lamellae. When the complex is heated above its melting point (i.e. at $70°C$) and crystallized from the melt, there is total absence of spherulitic structure, Fig. 4.12 (c). A comparison of Fig. 4.12 (a) and (d) shows that in the case of $(PEG)_{20}LiBr$ the spherulitic lamellae are thicker than those in the case of the complex with a higher salt concentration, $(PEG)_8LiBr$.

The role of larger anions instabilizing complexes is also reflected in the

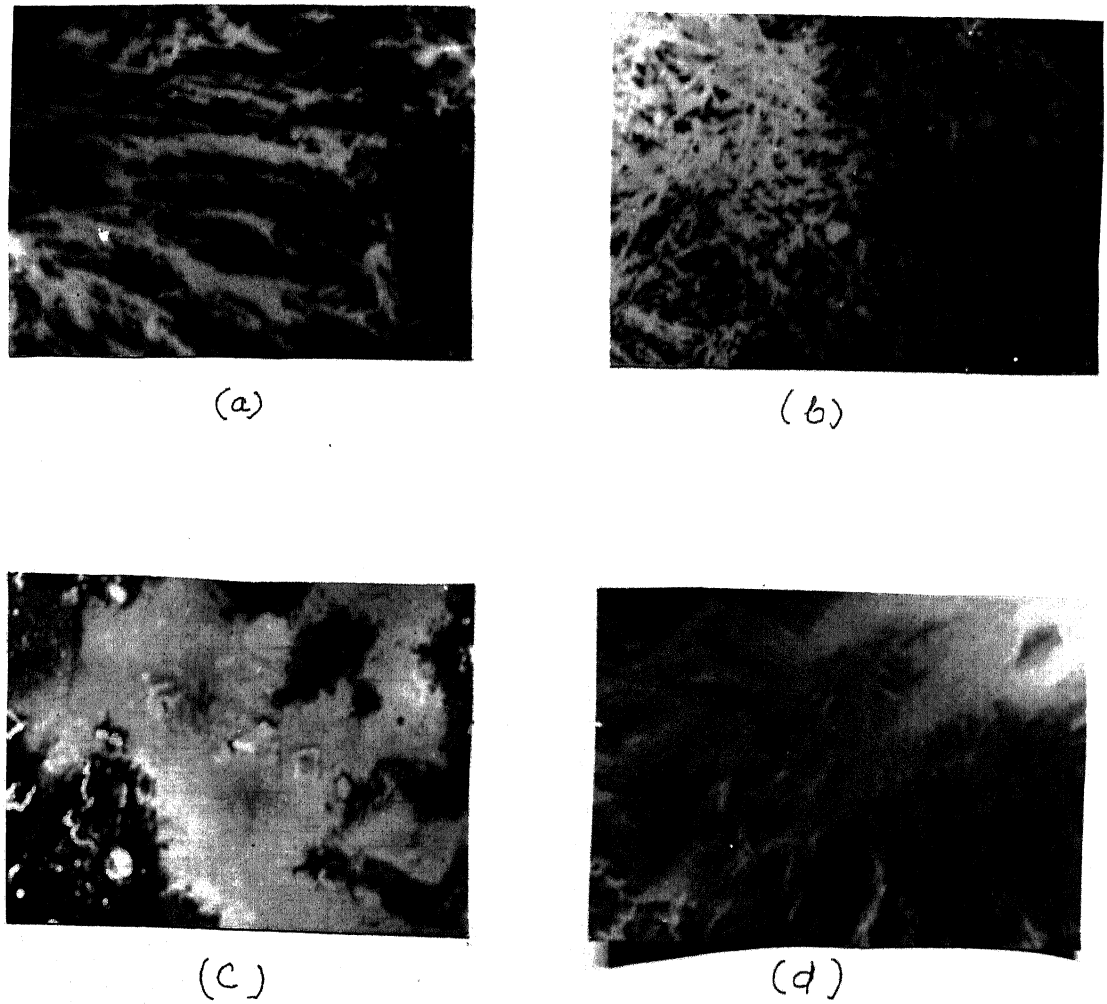

Figure 4.12: SEM micrographs for $(PEG)_{20}LiBr$; a, at room temperature ($30^{o}C$) ;b, quenched from $55^{o}C$, and c, quenched from $70^{o}C$. The micrograph of $(PEG)_{8}LiBr$ is also shown ,(d).

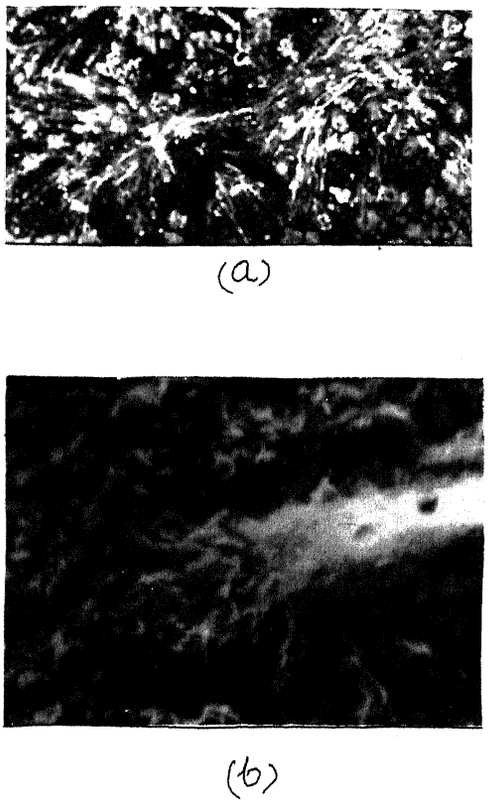

Figure 4.13: SEM micrographs for , (a) $(PEG)_{10}LiI$ and (b) $(PEG)_{10}LiBr$

electron micrographs (Lee and Wright, 1982b). It has been reported that the PEO–NaSCN complex (with a larger anion) has a more stable structure than the PEO–NaI complex and this is reflected in the well defined lamellar structure of the former (Lee and Wright, 1982a). Fig 4.13 (a) and (b) show the SEM micrographs of $(PEG)_{10}LiI$ and $(PEG)_{10}LiBr$ respectively. The $(PEG)_{10}LiI$ appears to have well defined lamellar growth as compared to the (PEG)10LiBr complex.

4.5 PEG–$LiClO_4$ system

In this work, the $(PEG)_xLiClO_4$ complexes were found to be viscous in nature and hence could not be obtained in the form of self supporting films. Thus the DSC, NMR, XRD and SEM studies could not be made. Debye– Scherrer patterns of this viscous material pasted on thin glass capillaries showed a diffused halo.

4.6 Conclusions

The FTIR studies suggest that the alkali metal cations are coordinated to the ether oxygens of the polymer repeat unit CH_2-CH_2-O. The presence of two kinds of environment for the anion was predicted, leading to the possibility of existence of ion–pairs. XRD studies indicate that with increasing salt concentration more of the crystalline PEG phase is destroyed to accomodate the salt, hence the pure polymer peaks are absent in the high salt concentration region. DSC studies lead to the conclusion that the $(PEG)_xLiX$ complexes are essentially a mixture of at least two phases. The SEM studies show that the morphology of the complexes is affected by their thermal history. Complexes annealed near (but below) the melting point show lamellar thickening.

Chapter 5

Ionic Transport Studies

Polymeric solid electrolytes have emerged as promising materials for high energy density batteries in the past two decades. The properties that make these electrolytes particularly useful are : easy processability, high flexibility leading to favorable electrode-electrolyte contact, a wide potential window and high conductivity at moderate temperatures. It is well recognised (Minier, Berthier and Gorecki, 1984; Stainer, Hardy, *et al.*, 1985) that these electrolytes, which are also called polymer–salt complexes, consist of several phases– the crystalline polymer phase, the amorphous polymer phase and the crystalline salt– polymer complex phase. The ionic transport in the various phases has been reported to be governed by different mechanisms (Armand, Chabagno and Duclot, 1979). This is reflected in the conductivity-composition and conductivity-temperature variations of these complexes.

During the past two decades, the polymer-salt complexes have been extensively studied (MacCallum and Vincent, 1987; Armand and Gandini, June 1991; Chawdari, Chandra, *et al.*, 1992). There are many studies especially on poly(ethylene) oxide (PEO)-based polymer-salt systems. Of all the properties, the thrust has naturally been on the electrical conductivity and, in particular, its variations with temperature(T) and the composition (concentration, X, of

the salt in the system). The former, viz., σ Vs T behaviour is by and large understood but the latter is not.

Considerable advancement at the theoretical level has also been made. The various transport properties like viscosity, electrical conductivity, diffusion etc. are explained in terms of free volume theory (Cohen and Turnbull, 1959; Williams, Landel and Ferry, 1955) or the configurational entropy model (Gibbs and DiMarzio, 1958; Adam and Gibbs, 1965). However, the latter is found to be more appropriate for polymeric solid electrolytes where the ionic interactions are not insignificant. Both the free volume and the configurational entropy models lead to VTF type of σ Vs T relation and thus explain the observed behaviour reasonably well in the polymeric electrolytes. In certain polymer-salt complexes, an Arrhenius type of behaviour is observed which is attributed to the presence of sizable amounts of crystalline phases in the polymer complexes.

The conductivity (σ) vs composition (X) behaviour, on the other hand, is poorly understood at present. Even the broad features such as the existence of optimum salt concentration(s) for maximum enhancement in the conductivity, etc. are not duly recognized, let alone their theoretical justifications.

Besides electrical conductivity, a number of other techniques have been used to elucidate the ion–transport mechanisms in general. For instance, NMR studies have been used to probe the structure and dynamics in polymer electrolytes (Sandahl, Schantz, *et al.*, 1989; Schantz, Kakikhana and Sandberg, 1990; Panero, Scrosati and Greenbaum, 1992). Linewidth and spin -lattice relaxation time (T_1) studies on ^{23}Na nuclei have indicated the presence of two kinds of Na sites, leading to broad and narrow lines. The narrow lines are assigned to dissociated cations and the broad ones to ion–pairs (Schantz, Kakikhana and Sandberg, 1990). The variation of T_1 with temperature reveals that there are two relaxation processes operative in the polymer–salt complexes (Panero, Scrosati and Greenbaum, 1992). The frequency dependent conductivity and dielectric constant measurements also show the presence of

two distinct relaxation mechanisms (Fontanella, Wilson, *et al.*, 1992; Fontanella, Wintersgill and Calame, 1985).

This chapter reports the electrical conductivity (obtained from complex impedance analysis) as a function of the composition (mole fraction of salt in the polymer) and temperature, results of NMR, the dielectric loss (ϵ'') and electric modulus (M″) vs frequency and temperature measurements for the PEG–LiX (X = Cl, Br, ClO_4) system. Besides, the configurational entropy (CE) model has been extended to include the effect of the salt. This extended CE model explains some of the salient features observed in the σ–X behavior of polymer–salt complexes in general including the PEG–LiX systems.

5.1 Ionic Conductivity versus Composition

5.1.1 Experimental results on PEG–LiX (X = Cl, Br, ClO_4) systems

PEG–LiCl system

Fig. 5.1 shows the log σ vs mole fraction of LiCl (X_{LiCl}) in the PEG–LiCl system at two different temperatures (30° and 75°C). The conductivity (σ) increases initially as the salt concentration increases which is as expected because the ion concentration which is negligible in the pure polymer (PEG) increases when the salt is added. As the salt concentration increases further, the conductivity attains a maximum value at $X_{LiCl} \sim 0.03$, starts decreasing and passes through a minimum at $X_{LiCl} \sim 0.05$, then increases again and goes through another (larger) maximum at $X_{LiCl} \sim 0.10$. A maximum enhancement in the conductivity by a factor of $\sim$ 32 at 30°C and 2000 at 75°C is attained at $X_{LiCl} \sim 0.10$ and 0.11 respectively, corresponding to the larger maximum in the σ(X) isotherms. Thus the larger maximum appears to shift to higher

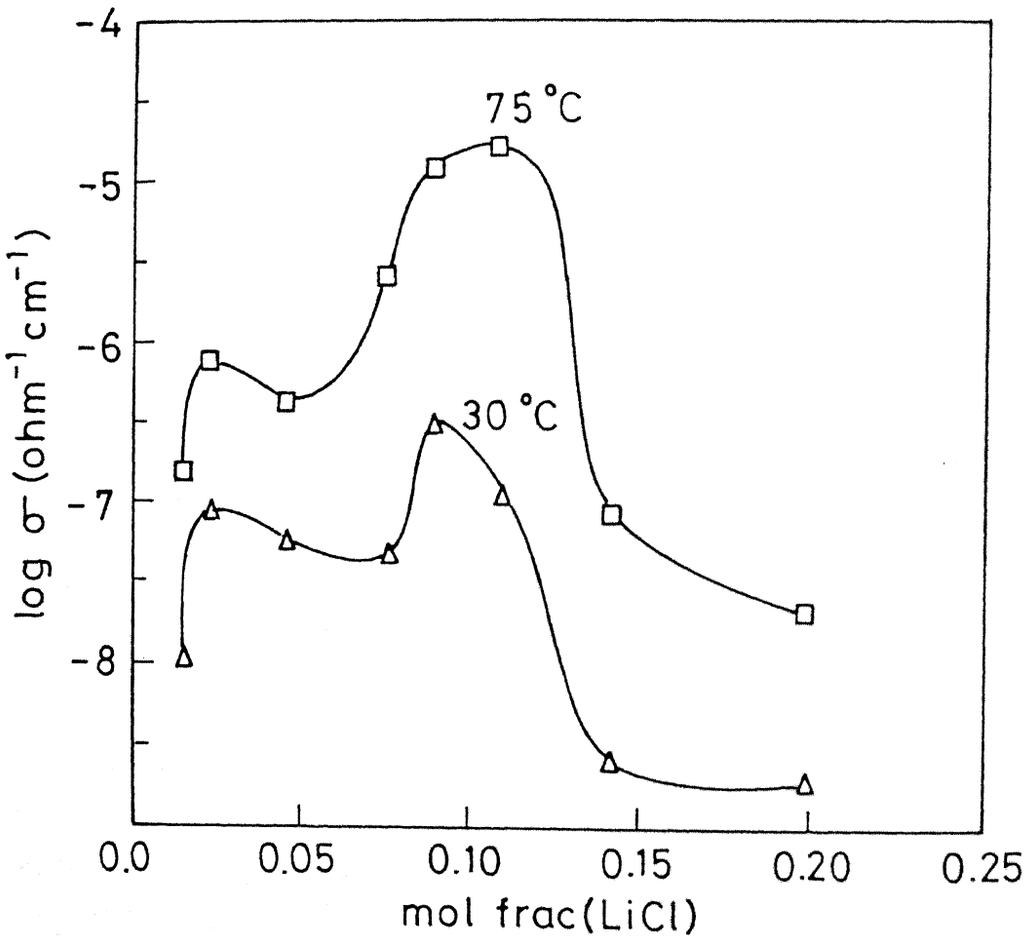

Figure 5.1: The plot of log σ vs composition (mole fraction of LiCl, X) for the PEG-LiCl complex

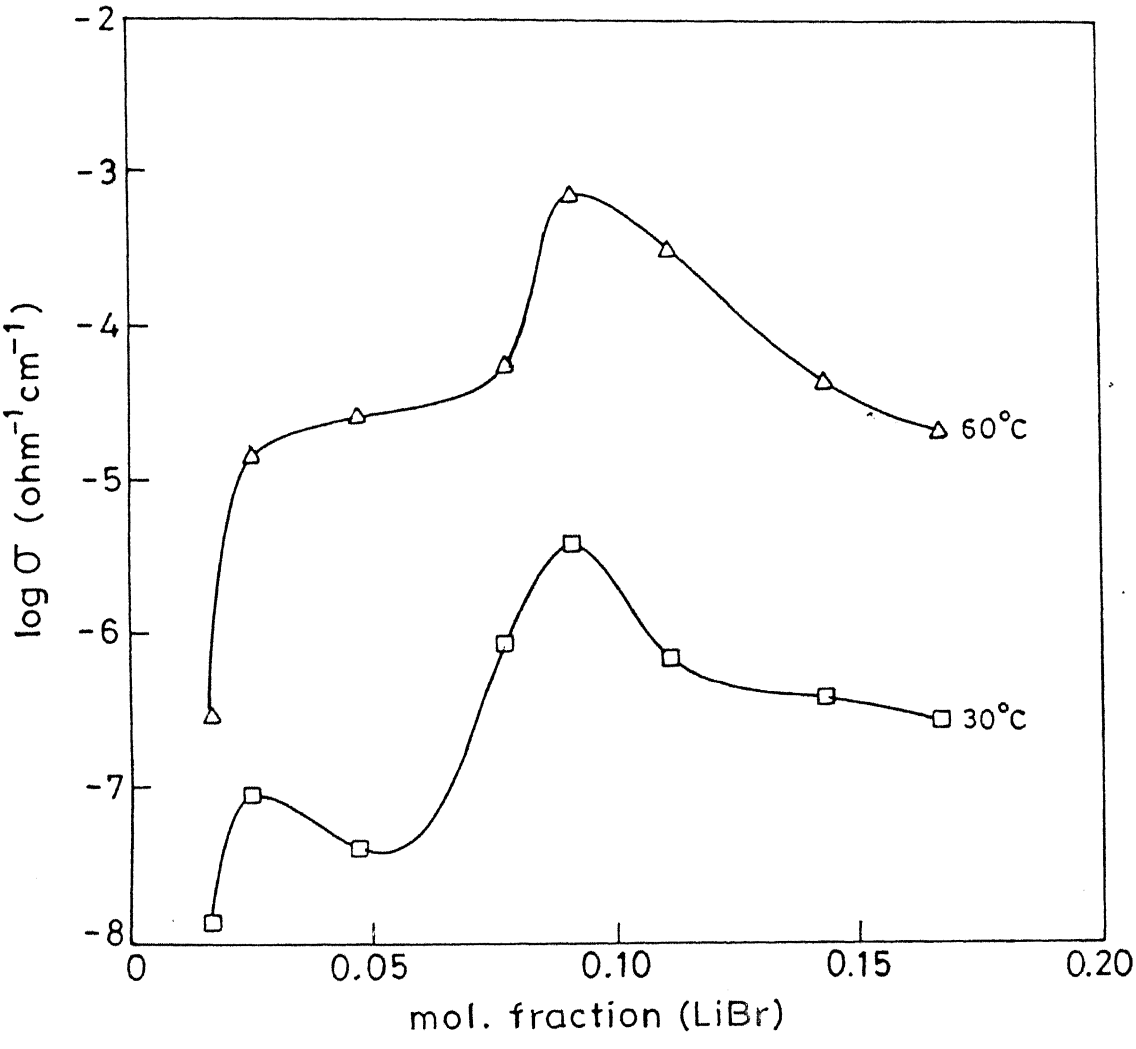

Figure 5.2: **The plot of log σ vs composition (mole fraction of LiBr, X) for the PEG-LiBr complex**

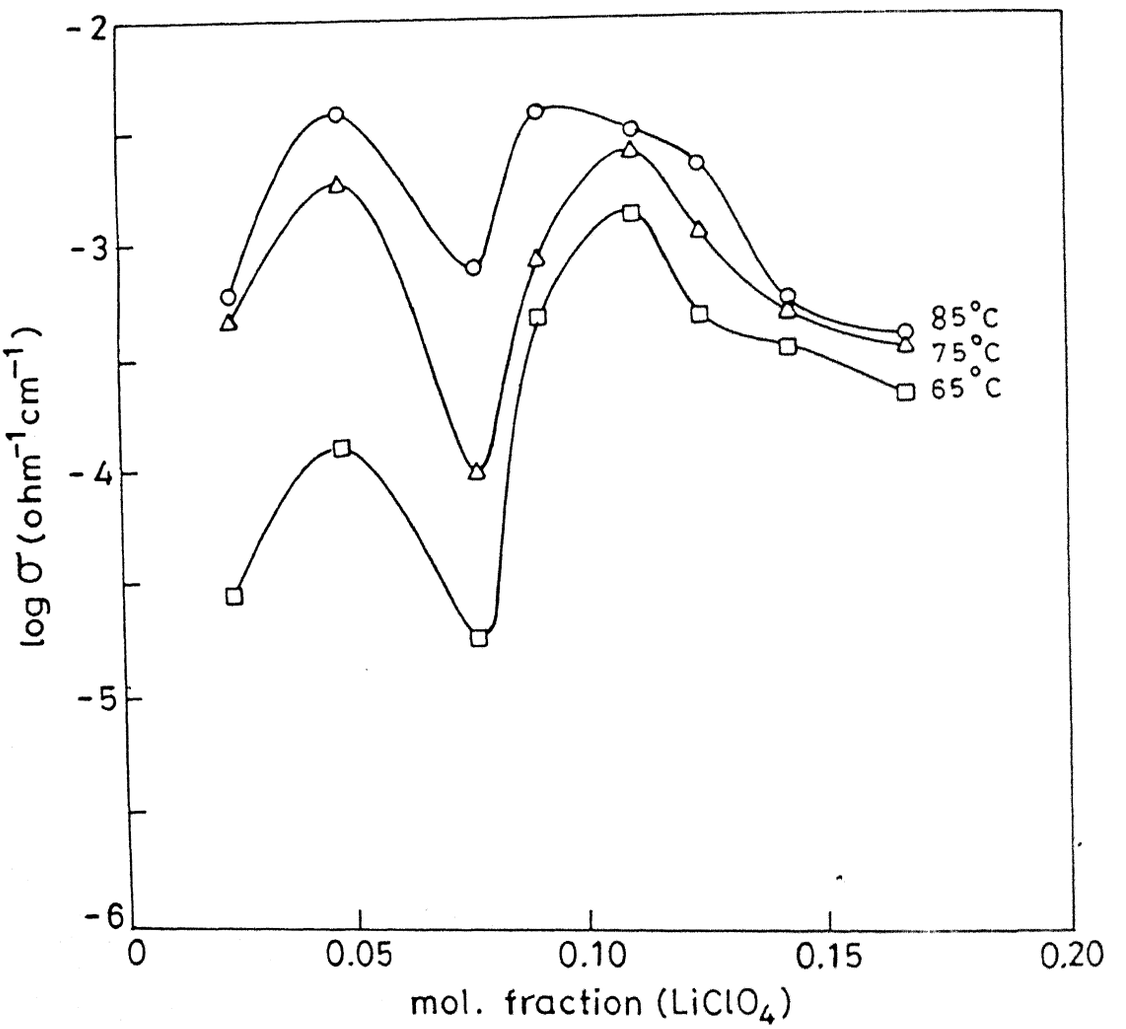

Figure 5.3: The plot of log σ vs composition (mole fraction of $LiClO_4$, X) for the PEG-$LiClO_4$ complex

salt concentration as temperature increases. A similar but less perceptible shift seems to occur in the first maximum (at $X_{LiCl} \sim 0.025$) as well. Table 5.3 lists the conductivity values corresponding to the two maxima in the σ(X) isotherm, along with the relevant data on PEO–LiX systems for comparison.

PEG–LiBr system

Fig. 5.2 shows the log σ vs composition (mole fraction of LiBr, X_{LiBr}) behavior for the PEG–LiBr system at 30°C and 60°C. These conductivity–composition, σ(X), isotherms are qualitatively similar to those for PEG–LiCl system (Fig. 5.1). The behaviour is characterised by a pair of maxima separated by a minimum in the σ(X) isotherms. A maximum conductivity of $\sim 3.9\times10^{-5}$ Ohm^{-1} cm^{-1} is observed at 30°C at $X_{LiBr} \sim 0.09$ (or x = O/Li $\simeq$ 10). PEG–LiBr system was also examined by DSC measurements, and a peak in the DSC curves is observed at around the same composition ($X_{LiBr} \sim 0.09$) corresponding to the eutectic of the system. Another (minor) maximum in the σ(X) isotherm is observed at $X_{LiBr} \sim 0.025$. No thermal event could be detected for this composition by DSC measurements. In this case also, the extrema, especially the larger maximum, in the σ(X) curves appear to shift towards higher salt concentrations. The σ values corresponding to two maxima in the σ(X) curves (Fig. 5.2) are listed in Table 5.3.

PEG–$LiClO_4$ system

Fig. 5.3 shows the variation of log σ as a function of the salt concentration (X_{LiClO_4}) for the PEG–$LiClO_4$ system at 65°C and 85°C. Like the other two systems (Figs. 5.1 and 5.2), here also the σ(X) isotherms exhibit two maxima at $X_{LiClO_4} \sim 0.05$ and ~ 0.09, (O/Li = 20 and 10 respectively) and a minimum in between them at X $\sim$ 0.07. A maximum conductivity of $\sim 3.8\times10^{-3}$ Ohm^{-1} cm^{-1} at 85°C is obtained for $(PEG)_{10}LiClO_4$ complex which is 5 orders of magnitude higher than that of either parent phase. These results may be

compared with those on PEO–$LiClO_4$ system (Table 5.3) in which a conductivity maximum is reported at $X_{LiClO_4} \sim 0.09$ (O/Li = 12). There is some evidence that the conductivity extrema, especially the maximum around $X_{LiClO_4} \sim 0.09$, shift to higher salt concentrations as temperature is increased. Besides, it does not seem that there is a good correlation between the σ–composition (Fig. 5.3) and the phase diagram (temperature– composition) behavior, though the conductivity maximum occurring at $X_{LiClO_4} \sim 0.09$–0.11 is fairly close to the eutectic of the system (Fauteux and Robitaille, 1986).

One of the most important features of these results (Figs. 5.1, 5.2 and 5.3) is evidently the existence of a pair of maxima separated by a minimum. A brief literature survey reveals that the above features are not uncommon and that a large number of polymer salt complexes exhibit similar features. On the basis of the available electrical conductivity–composition (σ-X) data, the various polymer-salt complexes may be grouped into three categories (see section 2.3) - Category I includes those systems which exhibit no maximum or minimum but a monotonically increasing conductivity with the salt concentration, (Table 5.1). Category II consists of systems which show a single maximum in the log σ - X isotherms (Table 5.2). And the third variety, i.e., Category III, comprises systems which show a pair of maxima separated by a minimum (Table 5.3). The available theories of transport in polymer electrolytes do not explain even these broad features. The configurational entropy (CE) model which leads to the well known V-T-F form of σ vs T behaviour as observed experimentally,was extended to include the effect of the salt on the transport properties. The extended CE model, which is presented in the next section, predicts not only the broad structures but also several other features observed in the σ - X isotherms of Category I and III systems.

5.1.2 Extension of Configurational Entropy Model

Even though sufficient experimental and theoretical advances in the area of polymeric solid electrolytes have been made, the distinct features in the

Table 5.1: **Polymer-salt systems of category I in which the conductivity vs composition plots exhibit no maxima/minima**

System	Concentration range (X) (m/f salt)	Form of σ-X	Remarks	References
PESc–$LiClO_4$	0 - 0.12	σ - X	linear increase	(i)
Network PEO- –$NaB(C_6H_5)_4$	0 - 0.05	log σ Vs log X	linear behaviour	(ii)
Network PEO (3000) –$LiClO_4$	0 - 0.1	log σ Vs log X	linear behaviour	(iii)
Network PEO (1050) –$LiClO_4$	0 - 0.18	log σ Vs log X	linear behaviour	(iv)

(i)Watanabe et al (1984); (ii)Killis et al (1984); (iii)Watanabe et al (1987); (iv) LeNest et al (1988)

Table 5.2: **Polymer-salt systems of category II in which the conductivity-composition plots exhibit a single maximum**

System	Concentration range (X) (m/f salt)	Form of σ - X	Remarks	References
PEO-$LiCF_3SO_3$ PEO-$LiClO_4$	0.08 - 0.2	σ - X	maximum at X $\sim$ 0.1	(i)
PEO-NaSCN	0 - 0.2	logσ - X	maximum at X $\sim$ 0.01	(ii)
MEEP-$AgCF_3SO_3$	0 - 2	σ-X	maximum at X $\sim$ 0.17	(iii)
PEO-$LiClO_4$	0 - 0.3	log σ-X	broad maximum from X = 0.03-0.1	(iv)
DMS-nEO -$LiClO_4$	0 - 0.1	log σ-X	broad maximum at X $\sim$ 0.03	(v)
PEO-PDMS 4000 Copolymer-$LiCF_3SO_3$	0 - 0.1	σ - X	maximum at X $\sim$ 0.04	(vi)
PEG-MBr_2 (M = Ca,Co,Cd,Zn)	0 - 1	σ - X	maximum at X $\sim$ 0.5	(vii)
PEO-$NiBr_2$	0 - 0.10	σ - X	maximum at X $\sim$ 0.06	(viii)

(i)Chabagno (1980); (ii)Lee and Crist (1986); (iii)Blonsky et al (1986); (iv)Ferloni et al (1986); (v)Cowie and Martin (1986); (vi)Albensson et al (1992); (vii)Mendolia and Farrington (1992); (viii)Cai et al (1992).

Table 5.3: **Polymer-salt systems of category III in which σ-X isotherms feature pair of maxima (at salt concentrations X_1 and X_3) separated by a minimum (at salt concentration X_2^*)**

System	Temp.	Composition		σ_{max}		Ref.
	^oC	(m/f salt)	(m/f salt)	(Ω^{-1}cm^{-1})	(Ω^{-1}cm^{-1})	
		X_1	X_3	σ_{X_1}	σ_{X_3}	
PEG-LiCl	30	0.024	0.10	8×10^{-8}	3.0×10^{-7}	
	75	0.025	0.11	8×10^{-7}	1.5×10^{-5}	(a)
PEG-LiBr	30	0.025	0.091	1×10^{-7}	3.16×10^{-6}	(a)
	60	0.027	0.091	1.78×10^{-5}	7.9×10^{-4}	(a)
PEG–$LiClO_4$	65	0.048	0.113	1.58×10^{-4}	1.58×10^{-3}	
	85	0.049	0.113	1.19×10^{-4}	4.0×10^{-3}	(a)
PEO–$LiClO_4$	85	0.029	0.078	8.9×10^{-3}	1.12×10^{-2}	
	105	0.029	0.083	1.4×10^{-2}	2.5×10^{-2}	(b)
PEO–$LiCF_3SO_3$	65	0.008	0.057	1×10^{-5}	5.6×10^{-4}	
	85	0.009	0.059	3.16×10^{-3}	3.16×10^{-3}	(b)
PEO–$LiAsF_6$	65	0.039	0.169	5.12×10^{-3}	3.67×10^{-3}	
	85	0.048	0.174	1×10^{-2}	1.25×10^{-2}	(b)
PEO–$LiBF_4$	25	0.025	0.188	1×10^{-7}	1.25×10^{-2}	
	100	0.041	0.181	5.6×10^{-4}	5.6×10^{-4}	(c)
EO–PO Copolymer –$LiBF_4$	15	0.049	0.198	6.10×10^{-5}	5.18×10^{-6}	
	30	0.056	0.261	1.70×10^{-4}	1.38×10^{-5}	(d)
$(ME)_m$ –$LiClO_4$	27	0.02	0.048	5.28×10^{-5}	5.3×10^{-5}	(e)
PEO–NH_4ClO_4	30	0.02	0.086	6×10^{-7}	8×10^{-7}	(f)

* For X_2 values, see Table 5.6

(a)present work; (b)Robitaille and Fauteux (1986); (c)Chiodelli et al (1988); (d)Przyluski and Weiczorek (1992); (e)Nagae et al (1992); (f)Chandra et al (1990).

conductivity-composition behaviour pointed out above have not been explained in any detail. Of the existing two models, viz., the free volume model and the configurational entropy model, often used to explain the ion transport phenomenon in polymeric solid electrolytes, the latter has been found to be more appropriate (Papke, Ratner and Shriver, 1982a; Angell and Sichina, 1976) for polymer-salt complexes where strong interactive forces exist. This model which is breifly outlined in Chapter 2 (Section 2.4.5), leads to the well known V-T-F equation, rewritten below for ready reference,

$$\sigma = A'T^{-1/2} \exp\left(\frac{-E_a/k}{T - T_o}\right) \tag{5.1}$$

Eq 5.1, strictly speaking, applies to pure polymer hosts. In order to account for the effect of pressure, the presence of salt in the polymer etc., Eq 5.1 has been modified variously (Angell, 1967; Angell, Pollard and Strauss, 1969; Ratner, 1987 . For instance when a salt (MX) is added to a polymer (PM), (i) the concentration of the mobile ions in the complex and hence its conductivity (σ) changes by and large proportionately, and moreover (ii) the glass transition temperature (T_{ox}) also increases. The former is accounted for if the preexponential factor of Eq 5.1, $A'/\sqrt{T}$, is modified to

$$A''X/\sqrt{T} \simeq A(T)X, \tag{5.2}$$

where A″ is a pure constant and A(T) is a new (temperature dependent) constant. To account for the latter, the composition (X)- dependent glass transition temperature T_{ox} given by the observed empirical relation

$$T_{ox} = T_o + T_\sigma X \tag{5.3}$$

where T_o is the glass transition temperature of pure polymer and T_σ a characteristic constant for a given polymer - salt system, , may be introduced in place of T_o in the exponent of Eq 5.1. Thus the modified V-T-F equation for polymer–salt complexes may be written as

$$\sigma(X,T) = AX \exp[-\frac{K_\sigma}{T_r - T_\sigma X}] \tag{5.4}$$

where $K_\sigma = E_a/k$ can be termed the *apparent activation temperature* for the polymer rearrangement which has a characteristic value for each polymer

host and is independent of the salt added to the polymer (Papke, Ratner and Shriver, 1982a; Angell and Sichina, 1976) , and $T_r = T - T_o$ the reduced temperature. Eq 5.4 not only describes the conductivity - temperature, σ-T, dependence but also the conductivity - composition, σ-X, dependence. Here we concentrate on the latter aspect. Apparently the importance of Eq 5.4 has hitherto not been fully realized inasmuch as it not only predicts an increase in the conductivity as the salt concentration (X) increases initially but also suggests that the $\sigma(X)$ isotherms exhibit three extrema (maxima/minima) at the salt concentrations (X) given by the solutions of the following equation

$$\frac{\delta\sigma}{\delta X} = A\exp(\frac{-K_\sigma}{T_r - T_\sigma X})[1 - \frac{K_\sigma T_\sigma X}{(T_r - T_\sigma X)^2}] = 0 \tag{5.5}$$

which are

$$X_2 = T_r/T_\sigma = (T - T_o)/T_\sigma = (T + 50 - T_g)/T_\sigma \tag{5.6}$$

and the two roots (X_1 and X_3) of the following quadratic equation

$$T_\sigma X^2 - T_\sigma[K_\sigma + 2T_r]X + T_r^2 = 0 \tag{5.7}$$

The solution of Eq 5.7 yields X_1 and X_3 as given below,

$$X_1 = \frac{1}{2T_\sigma}[(K_\sigma + 2T_r) - \sqrt{K_\sigma^2 + 4K_\sigma T_r}] \tag{5.8}$$

and

$$X_3 = \frac{1}{2T_\sigma}[(K_\sigma + 2T_r) + \sqrt{K_\sigma^2 + 4K_\sigma T_r}] \tag{5.9}$$

Since T_σ is the slope of $T_{o\sigma}$ Vs X plot (Eq 5.4) , it is supposed to be positive, i.e. $T_\sigma > 0$, and if the reduced temperature $T_r = T - T_o = (T + 50 - T_g) > 0$, i.e. if $T > (T_g - 50)$ K the root X_2 (Eq 5.6) will be positive and hence physically meaningful. The two other roots,X_1 and X_3 (Eqs. 5.8 and 5.9), will be real and distinct if the discriminant of Eq 5.7 is positive, that is if

$$T_\sigma^2(K_\sigma + 2T_r)^2 - 4T_\sigma^2 T_r^2 > 0$$

$$\text{or } K_\sigma > 0 \tag{5.10}$$

which has to be satisfied as K_σ, the *activation temperature* is positive by definition. Besides, X_1 and X_3 will also be physically meaningful if they both are positive. Evidently X_3 will be positive if

$$(K_\sigma + 2T_r) - \sqrt{K_\sigma^2 + 4K_\sigma T_r} > 0$$

$$\text{or } T_r > 0 \tag{5.11}$$

which holds good at temperature above (T_g - 50) K. Thus, in summary, all the three roots , Eqs. 5.6, 5.8 and 5.9 , are real, distinct and positive (hence physically meaningful) at temperatures above T_o, the glass transition temperature of the polymer host, or above (T_g - 50)K where T_g is the experimental glass transition temperature of the polymer-salt complex. This essentially *implies* that the above results will hold good for the polymer-salt complexes at temperatures above their glass transition temperatures, that is when the complexes are *necessarily amorphous* in nature.

Interestingly, the second derivative of σ (Eq 5.4 and 5.5) with respect to X (the salt concentration) given below

$$\frac{\delta^2\sigma}{\delta X^2} = A\beta\left(\frac{1}{\alpha - \beta X^4}\right)\exp\left(\frac{-1}{(\alpha - \beta X)}\right)[(2\alpha + 1)\beta X - 2\alpha^2] \tag{5.12}$$

where $\alpha = T_r/K_\sigma$ and $\beta = T_o/K_\sigma$, is positive at $X_2 = T_r/T_\sigma = \alpha/\beta$ (from Eq 5.6). That is

$$\frac{\delta^2\sigma}{\delta X^2}|_{X_2=\alpha/\beta} > 0 \tag{5.13}$$

and hence $X = X_2 = T_r/T_\sigma$ is a point of *minimum*. It can be shown further that, since $T_r/K_\sigma = \alpha > 0$ and $T_o/K_\sigma = \beta > 0$, X_2 lies between X_1 and X_3, that is $X_1 < X_2 < X_3$. Since X_2 is a point of minimum, the extrema at X_1 and X_3 (Eqs 5.8 and 5.9) must necessarily be points of maxima. The second derivative test, Eq 5.12, indeed confirms this, viz.,

$$\frac{\delta^2\sigma}{\delta X^2}|_{X_1} < 0 \; ; \frac{\delta^2\sigma}{\delta X^2}|_{X_3} < 0 \tag{5.14}$$

5.1.3 Predictions of the Extended Model

At very low salt concentrations, i.e. if $X \rightarrow 0$ or more realistically , $X << T_r/T_\sigma$ [1] the model (Eq 5.4) predicts that the conductivity is simply proportional to the salt concentration (X) at a fixed temperature (T) or fixed reduced temperature $(T - T_o)$ K. Thus, in the limit X→0 , Eq 5.4 reduces to

$$\sigma \simeq AX \exp(-K_\sigma/T_r) \tag{5.15}$$

Thus in the very low salt concentration regime, the $\log\sigma$ vs log X isotherms should be linear with a constant, temperature independent slope of unity. It is indeed interesting to note that the polymer–salt systems listed in Table 5.1 (category I) are in compliance with the above prediction. However, it should be pointed out that there are fewer careful measurements of σ at low concentrations, and the data shown in Fig 5.4 is one such result which lends a strong support to the extended CE model (Eqs. 5.4 and 5.15). The slopes of the linear plots are indeed very close to unity, though it is apparent that the value of slope increases slightly as temperature increases.

Alternatively, Eq 5.15 suggests that a plot of σ vs X should also be linear, of course in the low salt concentration regime, with a slope of

$$\frac{\delta\sigma}{\delta X} = A\exp(\frac{-K_\sigma}{T_r}) \tag{5.16}$$

that increases as the temperature (T) or reduced temperature $T_r(= T - T_o)$ increases because the exponential term on the right hand side of Eq. 5.16 increases much more rapidly than the preexponential factor A(T) α $1/\sqrt{T}$ decreases, see Eq. 5.2. For instance, the value of the slope $\delta\sigma/\delta X \rightarrow 0$ as $T_r \rightarrow 0$ (or T→ T_o), and is of course greater than zero (positive) at $T > T_o$ or

[1]Assuming $T_o \sim 200$ K and $T_\sigma \sim 300$ K per mole fraction (m/f) for a typical polymer–salt complex,at room temperature (300K), one finds the ratio $T_r/T_\sigma \sim 0.33$, so that the salt concentrations in the range 0 – 0.03 (m/f) can be considered to satisfy the above approximation. However, as T or T_r decreases, the width of the domain of the low salt concentration also decreases. For instance at T = 210 K or T_r = 10 K, $T_r/T_\sigma \sim 0.03$ so that a salt concentration of much less than 0.03 (m/f) could be justified to be in the dilute domain

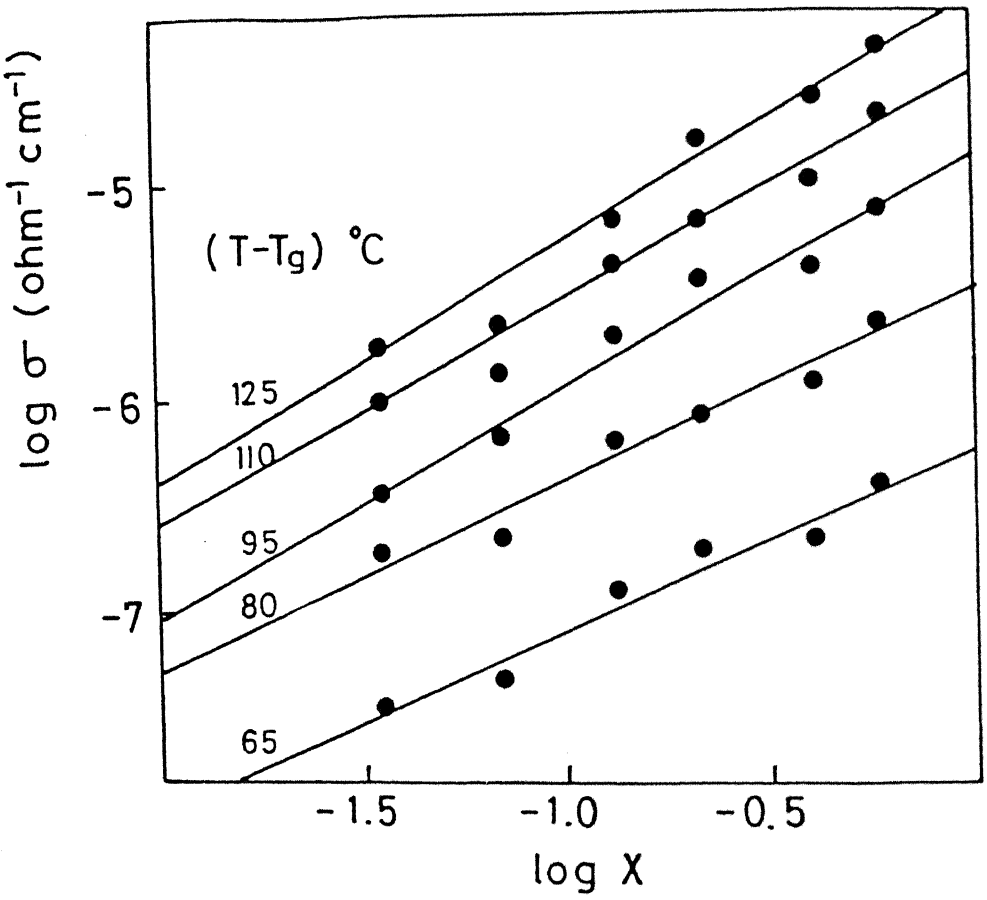

Figure 5.4: The variation of log σ as a function of log X (X = mole fraction of salt) at different temperatures for PEO-$NaB(C_6H_5)_4$ networks (from Killis et al (1984).

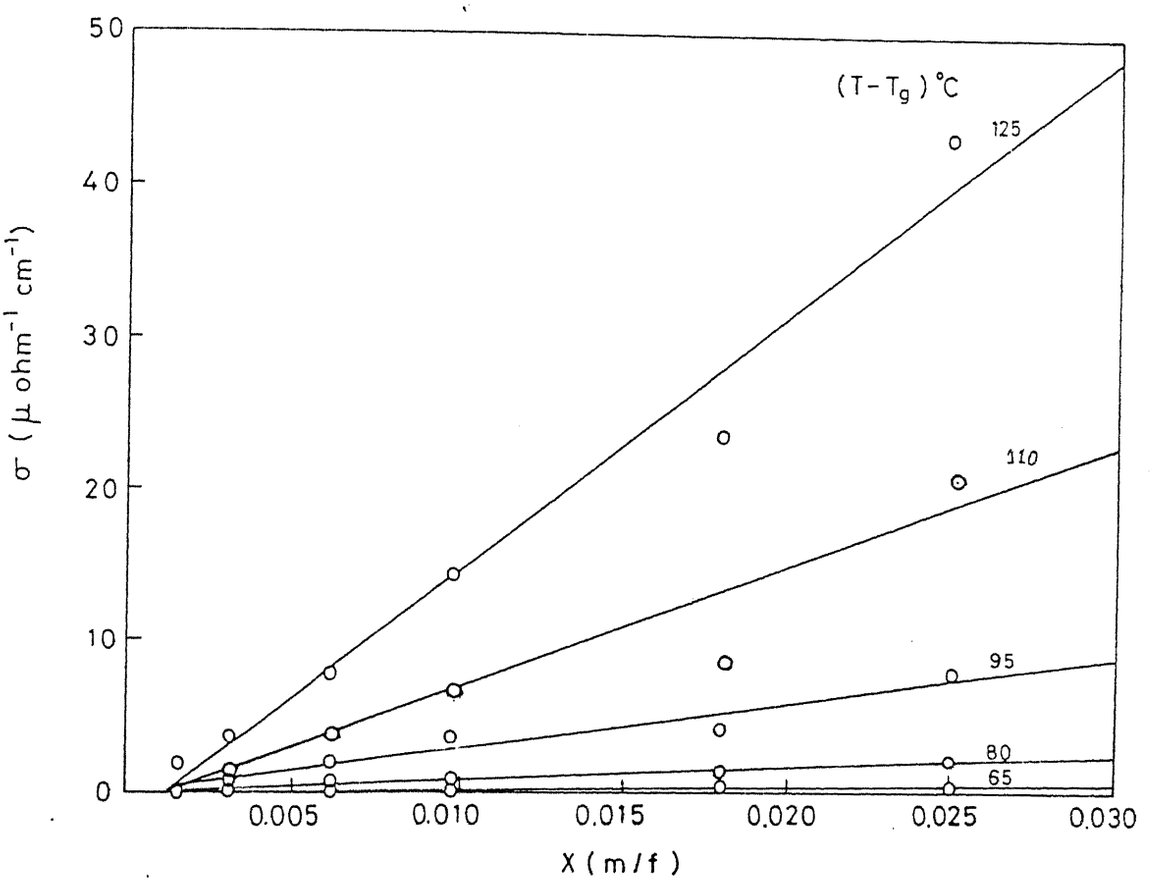

Figure 5.5: The variation of σ as a function of the salt concentration (X, mole fraction) for PEO–$NaB(C_6H_5)_4$ at different reduced temperatures ($T - T_g$ = 65, 80, 95 ,110 and 125 K). The linearity of the plots and the rapid change in their slopes as the reduced temperature increases are noteworthy (see Eq 5.16). (Data taken from Fig. 5.4)

Table 5.4: Some transport parameters for PEO(400)–$NaB(C_6H_5)_4$ system extracted from Fig. 5.5

$(T-T_g)$ (K)	$(T-T_o)$ (K)	$\delta\sigma/\delta X$ (Ohm^{-1} cm^{-1}/m/f)	$10^3/(T-T_o)$ (K^{-1})	$\log(\delta\sigma/\delta X)$
65	115	1.34×10^{-5}	8.70	–4.87
80	130	7.76×10^{-5}	7.69	–4.11
95	145	2.95×10^{-4}	6.90	–3.53
110	160	7.92×10^{-4}	6.25	–3.10
125	175	1.68×10^{-3}	5.71	–2.78

$T_r > 0$. The fact that the slope $\delta\sigma/\delta X \rightarrow 0$ as $T \rightarrow T_o$ implies that σ does not change due to the addition of salt. In other words, the σ of the polymer–salt complex practically remains the same as that of the host polymer regardless of the *nature* and *quantity* of the salt added, as long as, of course, $X << T_r/T_\sigma$ is satisfied. However, this prediction cannot be really tested because the glass transition temperature, $T_g = (T_o + 50)$ K, for most polymer hosts lies below the room temperature where, unfortunately, the conductivity data is not available, perhaps because σ is *too* low to be measured.

However, the earlier prediction, viz., that σ vs X plot should be linear whose slope (Eq 5.16) increases exponentially, can be tested. The conductivity and the composition data for PEO (400) network–$NaB(C_6H_5)_4$ system extracted from Fig. 5.4 are replotted in the form of σ vs X in Fig. 5.5. It is evident that the plots are indeed linear within the experimental error involved in the σ measurement. Moreover, the slope of the linear plot increases rapidly as the temperature (or $T - T_g$) increases. Table 5.4 lists the slopes ($\delta\sigma/\delta X$ values) at different reduced temperatures. It may be pointed out further that, according to Eq. 5.16, a plot of $\log(\delta\sigma/\delta X)$ versus $1/(T-T_o)$ should also be a straight line and that the slope should yield the apparent activation temperature K_σ and hence $E_a(= kK_\sigma)$. Table 5.4 also lists the log $(\delta\sigma/\delta X)$ as well as $10^3/(T - T_o)$

Table 5.5: **The calculated values of the salt concentration X_1,X_2 and X_3 (mole fraction, m/f) at which the σ exhibits extremum for a polymer-salt complex with typical values of $T_o = (T_g - 50) = 160K$,and two different values of $kK_\sigma = 0.08$ and 0.1 eV, and $T_\sigma = \delta T_{\sigma X}/\delta X = 500$ and 250 K per mole fraction of salt.**

kK_σ (eV)	T (K)	$T_r = (T - T_o)$ (K)	$T_\sigma = 500K$			$T_\sigma = 250K$		
			X_1	X_2	X_3	X_1	X_2	X_3
0.08	300	140	0.03	0.28	>1	0.07	0.56	>1
	350	190	0.06	0.38	>1	0.11	0.76	>1
	400	240	0.08	0.48	>1	0.17	0.96	>1
0.10	300	140	0.03	0.48	>1	0.05	0.56	>1
	350	190	0.05	0.38	>1	0.09	0.76	>1
	400	240	0.07	0.48	>1	0.14	0.96	>1

values, and Fig. 5.6 shows their behaviour graphically. The curve is not only a straight line but also the apparent activation energy obtained from its slope ($E_a \sim 0.06$ eV) is very close to the E_a values (0.05–0.08 eV) reported for a number of polymer hosts including PEO, obtained directly from the V-T-F fit of the conductivity data (Minier, Berthier and Gorecki, 1984; Chabagno, 1980; Bouridah, Dalard, *et al.*, 1985).

Perhaps the most important feature of the extended CE model is its prediction that the conductivity-composition, σ(X), isotherms would exhibit a pair of maxima separated by a minimum. The experimental results on a fairly large number of systems (Table 5.3) including the three systems, PEG–LiX (X = Cl, Br, ClO_4), investigated in this work, are consistent with this prediction of the model. The salt concentration (X) at which the σ(X) isotherms exhibit extrema, two maxima at concentrations X_1 and X_3 given by Eqs 5.8 and 5.9 , and a

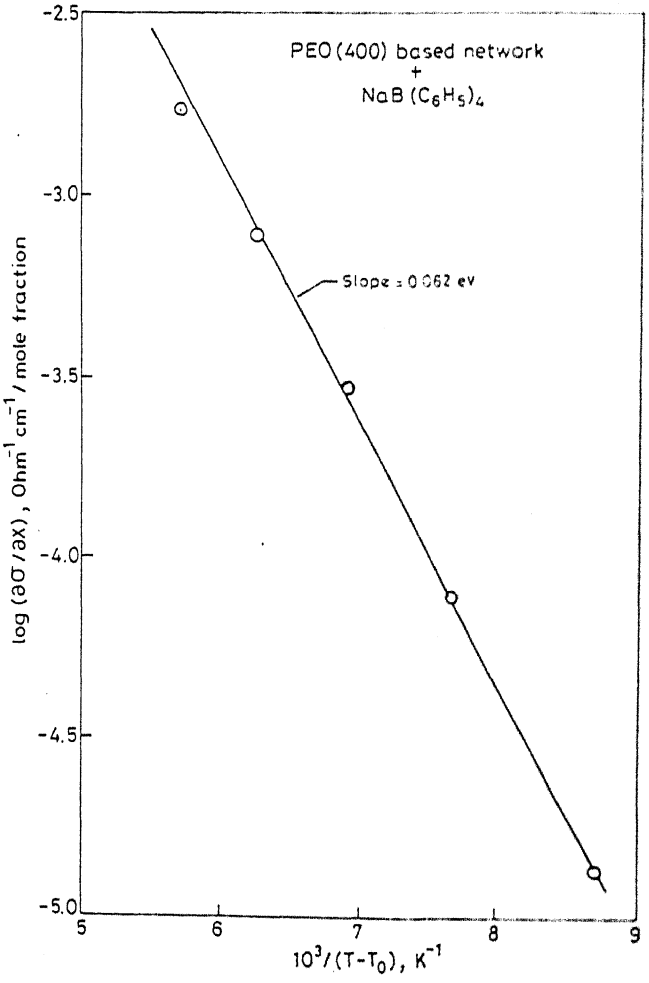

Figure 5.6: The variation of logarithm of the slope of σ vs X linear plot, viz., log $(\delta\sigma/\delta X)$, as a function of reciprocal of reduced temperature, $10^3/(T - T_o)$, for PEO-NaB$(C_6H_5)_4$ system (see Table 5.4).

minimum at $X_2 = T_r/T_\sigma$ (Eq 5.6), depend significantly on three *temperature like* parameters; (i) K_σ ($=E_a/k$), the apparent activation temperature which lies in the range 0.06-0.10 eV/k for a number of polymer hosts (Minier, Berthier and Gorecki, 1984; Chabagno, 1980; Bouridah, Dalard, *et al.*, 1985) and, is assumed to be nearly independent of the salt concentration; (ii) $T_\sigma(=\delta T_{o\sigma}/\delta X)$, the slope of the $T_{o\sigma}$ Vs X linear plot and (iii) $T_r(= T - T_o)$, the reduced temperature. Thus for a given polymer-salt complex both K_σ and T_σ have constant values and only T_r is a variable parameter.

Table 5.5 lists the calculated values of the salt concentrations X_1,X_2 and X_3 (in mole fraction, m/f) at which the σ(X) isotherms exhibit extrema for a typical polymer-salt complex with assumed values of T_g = –63°C or T_o = (T_g – 50)K = 160 K, and two different values of kK_σ = 0.08 and 0.10 eV and T_σ = 250 and 500 K/mole fraction. The T_σ ($=\delta T_{o\sigma}/\delta X$) values chosen for the calculation are quite realistic in view of its reported value of 280 K/mole fraction for PEO-$LiCF_3SO_3$ (Minier, Berthier and Gorecki, 1984) and 480 K/mole fraction for PEO-NaI (M.Minier and Berthier, 1983). The calculated values of X_1 and X_2 corresponding to the first maximum and the minimum respectively are reasonably close to the typical values observed experimentally (Table 5.3). However,the calculated X_3 values corresponding to the second (larger) maximum in the σ(X) isotherms are absurdly high (more than a mole fraction). Arguably, the extended model which relies on some rather crude approximations may fail in the region of high salt concentrations, especially so in view of the assumption that $T_{o\sigma}$ Vs X curve is linear for all values of X which may not hold good for high salt concentrations. Also the apparent activation temperature $K_\sigma = E_a$/k may not remain constant for all values of X (Chabagno, 1980; Ito, Syakushiro, *et al.*, 1986).

The model further suggests that as the temperature (T) or the reduced temperature T_r (=T-T_o) increases, the extrema, i.e., both the maxima and the minimum, shift towards higher salt concentrations. The observed results on various systems do provide a sort of qualitative support to the above prediction. For instance, in PEG-LiCl system (Fig. 5.1) the second maximum

(corresponding to X_3) seems to have shifted from 0.10 (at 30°C) to 0.11 (at 75°C), i.e. by $\sim$ 10%. However, the quantitative agreement is not very good, as elaborated later.

Thus, the extended configurational entropy model predicts the salient features observed in the conductivity-composition behaviour such as (i) the increase in the σ by the addition of salt (ii) the appearance of a pair of maxima separated by a minimum, and(iii) the shift in the conductivity extrema to lower values of salt concentrations as temperature decreases. There are however, some serious discrepancies between the predictions of the model and the experimental results which requires closer considerations.

5.1.4 Comparison with Experimental Results

A genuine test of the extended CE model seems difficult for various reasons. Since the glass transition temperature generally lies below room temperature while the commonly available DTA/DSC machines are limited to measurements above room temperature, the T_σ ($=\delta T_{o\sigma}/\delta X$) data in most cases, are unavailable. In the few cases where these are available , either a complete and carefully studied σ(X) isotherms are not available or quite simply the pair of maxima separated by a minimum in the σ(X) isotherm is non-existent. Under these circumstances, only a pseudo-test can be attempted. In Table 5.6 are listed those polymer-salt complexes which exhibit two maxima (at X_1,X_3) and a minimum in between (at X_2) in their σ(X) isotherms, but their T_σ values (the slopes of $T_{o\sigma}$ Vs X plots) are not known. The experimental value of the salt concentration (X_2) corresponding to the lone minimum is then used to estimate the constant T_σ for that particular system and subsequently the values of X_1 and X_3 (Eqs. 5.8 and 5.9). It should be pointed out here that the T_σ values so estimated are seemingly an order of magnitude higher than the typical experimental values (200 - 500 K/mole fraction). The values of X_1 and X_3, calculated from Eqs. 5.8 and 5.9, using the T_σ values estimated in the above manner are however not unreasonable, though the X_3 values are

much larger than the experimental values which are listed in Table 5.6. This discrepancy reinforces the fact that the extended model does not hold in the region of high salt concentration.

According to the extended model the percent shift in the location of minimum i.e. $X_2 = T_r/T_o = (T - T_o)/T_o$, for PEG based polymers ($T_g = -63°C$ or $T_o = 160$ K) is

$$\frac{\Delta X_2}{X_2} \times 100 = \frac{100\Delta T_r}{T_r} = 0.7\% \text{ per degree} \qquad (5.17)$$

at 303K or a reduced temperature $T_r = T - T_o = 143$ K. Thus a 35°C change in temperature (say from 30°C to 75°C) should, according to the extended model, produce a shift of $\sim 25\%$, while the observed shift in PEG-LiCl system (Fig 5.1, Table 5.3) is only $\sim$ (0.11 - 0.10)100/0.1 $\simeq$ 10% in the minimum in σ(X) isotherms . It should be stressed however that the shift in the location of the extrema in the σ (X) isotherms will be more pronounced at low temperatures or low reduced temperatures. At T_r=50K, the percent shift in X_2 will be $\sim$ 2% per degree K for instance.

Finally, perhaps the most glaring discrepancy, between the predictions of the extended model and the experimental (σ Vs X) results on polymeric electrolytes is that a fairly large number of polymer-salt complexes apparently do not exhibit a pair of maxima and a minimum; but they show just one maximum (Table 5.2). However, a closer inspection of the model and the experimental results on this category of polymer-salt systems suggests that more careful measurements on these systems would probably be required to establish whether there are two or just one maximum in the σ(X) isotherms. As the model suggests, the first maximum appears at a fairly low level of salt concentration (1–2 mol %) and shifts further down as the temperature is lowered, at a rate of $\sim$ 1 - 2 % per degree (Eq 5.17). Thus it is entirely possible that the first maximum in the σ - X isotherms is naturally missed out in certain systems. Secondly, and equally plausibly, since the thrust of experimentalists has been to obtain the maximum conducting polymer - salt composition, and hence in their over enthusiastic pursuit of this goal the smaller maximum at

Table 5.6: Comparison of calculated and experimental values of the salt concentrations (X_1 and X_3) at which σ - X isotherms exhibit maxima at various reduced temperatures and for two different values of kK_σ.

System	T_r	kK_σ	X_2	X_1 (m/f)		X_3 (m/f)		Ref.
	$(T-T_o)$ K	(eV)	(m/f)	calc.	obs.	calc.	obs.	
PEG-LiCl	140	0.1	0.06	0.005	0.024	0.061	0.10	
	140	0.06	0.06	0.009	0.024	0.410	0.10	
	185	0.10	0.06	0.007	0.025	0.489	0.11	
	185	0.06	0.06	0.011	0.025	0.335	0.11	(a)
PEG-LiBr	140	.10	.051	.005	.025	.520	.091	
	140	.06	.051	.007	.025	.309	.091	
	170	.10	.054	.006	.027	.47	.091	
	170	.06	.054	.009	.027	.320	.091	(a)
PEG-$LiClO_4$	175	.10	.078	.009	.048	.664	.113	
	175	.06	.078	.013	.048	.453	.113	
	195	.10	.078	.01	.049	.61	.113	
	195	.06	.078	.014	.049	.420	.113	(a)
PEO-$LiCF_3SO_3$	175	.10	.027	.003	.008	.231	.057	
	175	.06	.027	.005	.008	.157	.057	
	195	.10	.024	.003	.009	.186	.059	
	195	.06	.024	.004	.009	.128	.059	(b)
PEO-$LiClO_4$	195	.10	.05	.006	.029	.391	.078	
	195	.06	.05	.009	.029	.269	.078	
	215	.10	.047	.006	.029	.341	.083	
	215	.06	.047	.009	.029	.237	.083	(b)
EO-PO Copolymer $LiBF_4$	138	.10	.148	.014	.049	1.53	.198	
	138	.06	.148	.021	.049	1.02	.198	
	153	.10	.155	.016	.056	1.47	.261	
	153	.06	.155	.024	.056	.990	.261	(c)
$(ME)_m$ Polymer $-LiClO_4$	91	.10	.04	.003	.02	.587	.048	
	91	.06	.04	.004	.02	.382	.048	(d)

(a)present work ; (b)Robitaille and Fauteux (1986); (c)Przyluski and Weiczorek (1992); (d) Nagae et al. (1992).

the lower salt concentration (X_1) is either missed out or, occasionally, ignored. For instance, the σ - X isotherms on PEO - NH_4ClO_4 (Chandra, Hashmi and Prasad, 1990) and $(ME)_m$- $LiClO_4$i (Nagae, Nekoomanesh, *et al.*, 1992) clearly show the existence of a pair of maxima even though the authors recognize only one at the higher salt concentration with the highest conductivity. Thus it may be highly desirable to reinvestigate some of the systems more carefully.

5.1.5 Microscopic Mechanism(s)

The extended model predicts that the conductivity increases linearly initially as the salt concentration (X) in the polymer increases. As X increases further, the model also predicts the appearance of a pair of maxima separated by a minimum in the σ-X isotherms. The above behaviour is readily observed in a number of polymer-salt systems (Tables 5.1 and 5.3). It would be of interest to discuss the physical mechanism responsible for this kind of behaviour. The host polymers are usually devoid of mobile (ionic) charge carriers and thus have negligible electrical conductivity. As the salt is added to the polymer, the concentration of the mobile ions increases and hence the conductivity is expected to increase linearly with the salt concentration (X) for low values of X (X $\rightarrow$ 0). However, when the salt is added to the polymer to increase the concentration of mobile ions , the glass transition temperature, T_{ox} = (T_{og} - 50) K, also increases which tends to decrease the conductivity for, at any fixed thermodynamic temperature T, smaller the $(T - T_o)$ smaller is the fluidity, and hence smaller is the conductivity. In the limit $(T - T_o) \rightarrow 0$, i.e. T $\rightarrow$ T_o, the fluidity, conductivity, etc. will approach zero. Thus there are two factors competing against each other, and as a result a maximum appears in the σ vs X isotherms at a critical salt concentration when the latter starts dominating the former.

Alternatively, as the salt concentration in the complex increases, the ion pair formation may take place which will reduce the number of mobile ions available for conduction and hence the conductivity. Thus, once again there

are two competing processes, the addition of salt that increses the concentration of mobile ions, while the ion pair formation tends to reduce that number. At some (critical) concentration of the salt, the effect of the latter (ion - pairing) begins to dominate that due the former, leading to a maximum in the σ - X isotherm.

As the salt concentration increases further, the conductivity decreases and passes through a minimum and subsequently starts increasing again. This subsequent increase in the conductivity could be attributed to the formation of triple ion-pairs (Gray, 1990),

$$LiClO_4 + ClO_4^- \rightleftharpoons Li(ClO_4)_2^-$$

$$LiClO_4 + Li^+ \rightleftharpoons Li_2(ClO_4)^+ \tag{5.18}$$

which carry a net charge are relatively mobile and hence contribute to the conductivity. Thus a minimum in the σ-X isotherm appears as a result of two competing processes, viz. the fraction of non-conducting neutral ion-pairs that tend to decrease the σ and the formation of triple ion-pairs which increase the σ. Thus at a critical salt concentration (X_2) the latter (the triple ion-formation) begins to dominate the former. As X increases further, i.e. $X \geq X_2$, the σ increases and passses through yet another maximum and then starts decreasing again for $X > X_3$. This decrease in the σ in the $X > X_3$ regime may be attributed to the reversal of the triple ion-pair formation reactions (Eq 5.18) which regenerate the nonconducting neutral ion-pairs. These triple ion-pair formations are equilibrium processes, and it may be expected that beyond a certain (critical) salt concentration the reverse reactions may be more favorable. This decrease in the σ in the $X > X_3$ region may also be due to the formation of crystalline phases which hinder the ion–transport, as is evident from the fact that activation energies are usually higher at higher salt concentrations (Chabagno, 1980; Ito, Syakushiro, *et al.*, 1986).

Vibrational spectroscopic studies on PEO based electrolytes (Papke, Ratner and Shriver, 1981) reveal that the polymer - salt complex has a helical structure with a T_2GT_2G conformation containing a tunnel which will readily accomodate

ions with radii of upto $\sim$ 1Å. Cations with ionic radii greater than this value may be expected to be found out side the tunnel and hence lead to amorphous complexes. Na^+ ion with an ionic radius of 0.78 Å can be expected to be present within the tunnel and hence form crystalline complexes. The divalent cations like Ca^{2+}, Co^{2+}, Cd^{2+}, Zn^{2+}, Ni^{2+} etc., all of which have cationic radii less than 1 Å are thus expected to form crystalline complexes with PEO or PEG. A closer look at Table 5.2 shows that these complexes show a single maximum in the σ - X plots. Other studies on crystalline- PEO based salt - polymer complexes (Fauteux, Prud'homme and Harvey, 1988) also show a single maximum in the σ - X plots. As the prime assumption of the extended model is the amorphous nature of the complex, it is not surpising that the crystalline complexes do not conform to the pattern of two maxima and and one minimum in the σ - X plots. It may be pointed out that lithium seems to be an exception to the above trend because even though its radius is less than an angstrom, its salts are known to form essentially amorphous phases (Chabagno, 1980).

5.2 Conductivity vs Temperature

The electrical conductivity versus temperature behavior in polymer–salt complexes is generally described either by an Arrhenius equation

$$\sigma = \sigma_o \exp(-E/kT) \tag{5.19}$$

where σ_o is a constant and E the activation energy for ion–hopping, or by a V-T-F equation (5.1), rewritten below for ready reference,

$$\sigma = A' T^{-1/2} \exp(\frac{-E_a/k}{T - T_o})$$

where E_a is the apparent activation energy, and seemingly there is no direct relationship between E (Eq. 5.19) and E_a (Eq. 5.1). The Arrhenius behavior is typical of crystalline salts whereas the V-T-F behavior is more appropriate for

amorphous materials. However, it should be pointed out that a conductivity data over a limited temperature range may fit the two equations equally well, and hence discrimination between the two types of behavior may become difficult. This is true for many of the polymer-salt complexes because their conudctivity data is limited on the high temperature side owing to low melting points, and on the low temperature side due to their too low conductivity values to be measured.

The conductivity-temperature data for the three systems studied in this work , viz., PEG-LiX (X = Cl, Br, ClO_4) are presented below.

5.2.1 PEG–LiCl System

Figs. 5.7 and 5.8 show the Arrhenius (log σ versus 10^3/T) plots for $(PEG)_xLiCl$ complexes with x = 4, 6, 8, 10, 12, 40 and 60. Evidently, there are two distinct regions; one below 60°C and the other above 60°C. The low temperature, low conductivity region is characterized by a relatively high activation energy (E_1), while the high temperature, high conductivity region has lower activation energy (E_2). The activation energies (E_1 and E_2) corresponding to both the regions are listed in Table 5.7. In the low temperature region (T < 60°C), the average value of the activation energy (E_{1av}) is $\sim$ 0.87 eV, while in the high temperature region (T > 60°C) it is $\sim$ 0.37 eV. It should be noticed from Table 5.7, that E_1 has a lowest value of 0.46 eV for $(PEG)_{10}LiCl$ sample which also exhibits the highest ionic conductivity (Fig. 5.7). These results are consistent with each other. The activation energies for ion-transport in PEG-LiCl system may be compared with those in PEO-based systems; for $(PEO)_{4.5}LiCl$, E_1 = 0.43 eV (Reitman, Kaplan and Cava, 1985), for PEO-NaI system $E_{1av} \sim$ 1.40 eV and $E_{2av} \sim$ 0.34 eV (Chiang, Davis, *et al.*, 1983). The lower activation energy in the high temperature region may be due to the fact that the amorphous phase is dominant in this region, hence the energy barrier to ion transport is low. Below the melting temperatures ($\sim$ 60°C) of the polymer, the amorphous phase is no longer the dominant phase, and a

Table 5.7: **The Arrhenius activation energies (E_1 below 60^oC and E_2 above 60^oC) for the $(PEG)_xLiCl$ system**

Composition	E_1	E_2
(O/Li)	(eV)	(eV)
4	0.99	0.29
6	0.85	0.24
8	1.03	0.50
10	0.46	0.46
12	1.41	0.33
20	0.65	0.37
40	0.63	0.36
60	0.94	0.42

part of the sample may be in crystalline form that hinders the ion transport and hence the activation energy is higher.

The discontinuity in the log σ vs $10^3/T$ plots (Figs. 5.7 and 5.8) is associated with the melting temperature of the pure polymer host (PEG), which has been observed around 62 ± 2^oC in the DSC measurements (Chapter 4). At temperatures above $\sim 60^oC$, the crystalline phase would melt. The discontinuous jump in the conductivity near 60^oC is larger for the sample with larger polymer content. This is to be expected in view of the fact that the samples containing larger fraction of polymer (PEG) host will produce larger concentration of amorphous phase on melting ($\sim 60^oC$). The absence of any discontinuity in the log σ vs 1/T plot for the sample with highest salt concentration , viz., $(PEG)_4LiCl$, is also consistent with the above view.

The conductivity–temperature behavior observed for the PEG–LiCl system may be compared with PEO–based polymeric electrolytes. In highly crystalline electrolytes such as PEO–NaSCN the log σ–1/T plots are linear (Chabagno,

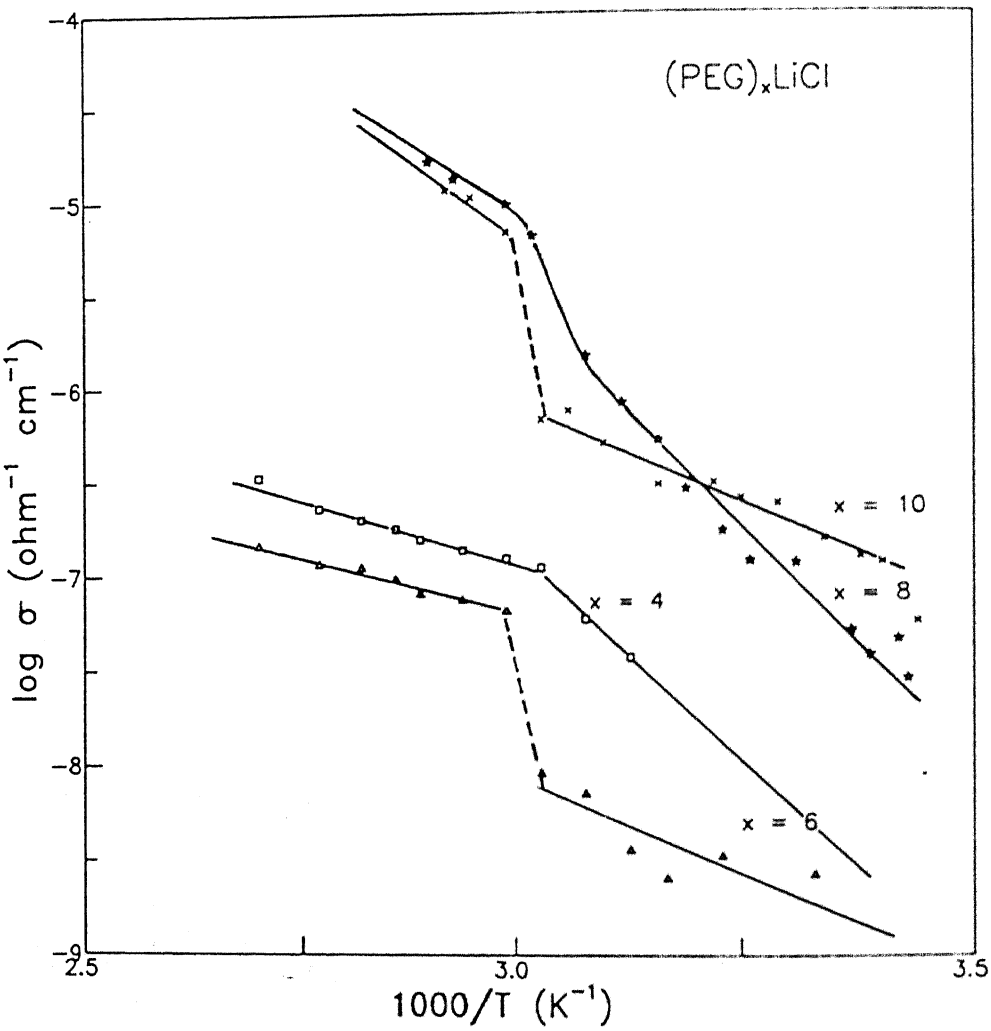

Figure 5.7: The logσ versus $10^3/T$ plots for various $(PEG)_xLiCl$ compositions, x = 4, 6, 8, 10.

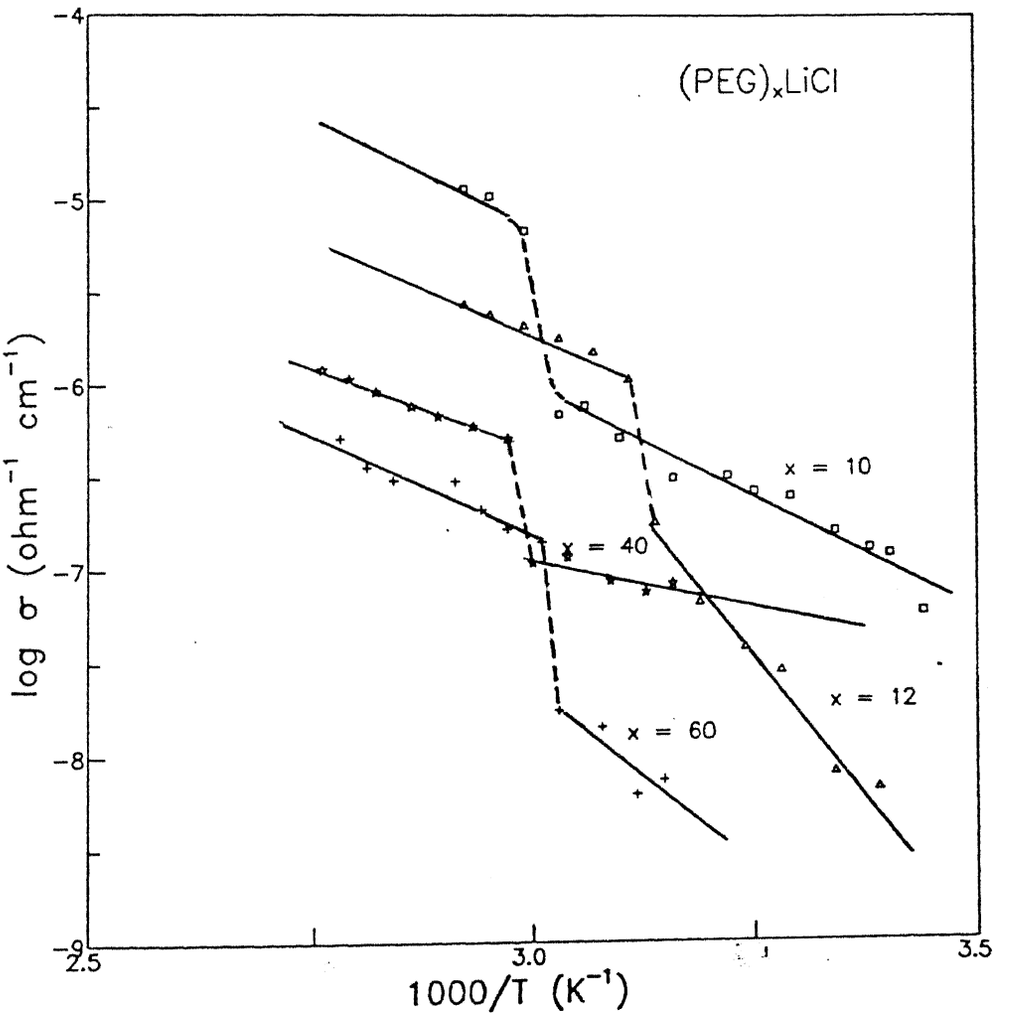

Figure 5.8: The logσ versus $10^3/T$ plots for various $(PEG)_xLiCl$ compositions, x = 10, 12, 40, 60.

1980) while for amorphous complexes like PEO–$LiNO_3$ they are generally curved (Reitman, Kaplan and Cava, 1985). The partially crystalline complexes such as PEO–$LiClO_4$ exhibit knees or breaks in the log σ vs 1/T plots.

The conductivity–temperature data for $(PEG)_x$LiCl complexes were also fitted to the V-T-F equation (Eq.5.1) mainly to extract the values of the glass transition temperature, ($T_{o\infty}$), the apparent activation energy (E_a) . However, it should be mentioned that these, i.e., $[\ln (\sigma\sqrt{T}\ /A')]^{-1}$ vs T, plots for the complexes with compositions x > 12 were found to be reasonably linear, while for x < 12 the linearity of the V-T-F plot was clearly unsatisfactory, which may be due to the presence of appreciable quantity of crystalline phase at higher salt (lower value of x) concentrations. As before, the above plots for x > 12 samples are shown separately for T < 60°C and T > 60°C in Figs. 5.9 and 5.10 respectively. The best fit parameters and the error involved therein are given in Table 5.8.

In order to ascertain whether V-T-F or Arrhenius relation provides a better fit, the conductivity-temperature data for the same complexes (x > 12) have also been fitted to the latter form, i.e. log σ vs $10^3/T$, and the results are displayed in Figs. 5.11 (for T < 60°C) and 5.12 (for T > 60°C) and the best–fit Arrhenius parameters are listed in in the same Table (5.8) for comparison. Evidently, the data fit the VTF and the Arrhenius relation almost as well, the deviation (or error in fit) in both cases being $\sim$ 0.7 %. This observation is not very surprising after all because a σ–T data over a limited range may fit more than one relation as also pointed out by Ratner (1987).

From the various best–fit V-T-F parameters listed in Table 5.9, it is noted that the glass transition temperature increases, as the salt concentration (X) increases (or x decreases) which is as expected. However, the variation of apparent activation energy E_a with the composition (x) is rather too drastic (from 0.04 eV for x = 12 to 0.14 eV for x = 60), though the increasing trend with x is normal.

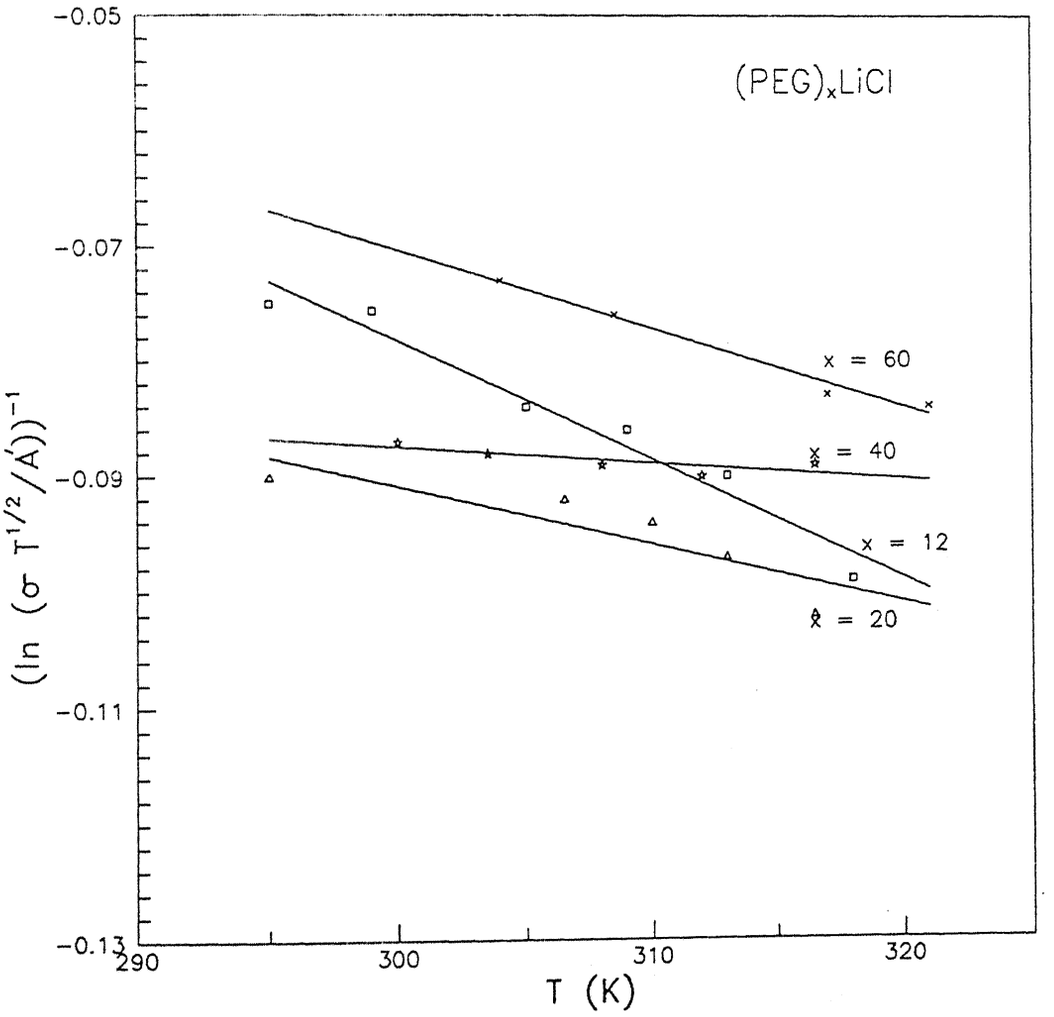

Figure 5.9: The $[\ln(\sigma T^{1/2}/A')]^{-1}$ versus T plots for various $(PEG)_xLiCl$ compositions in the low temperature region (T < 60°C).

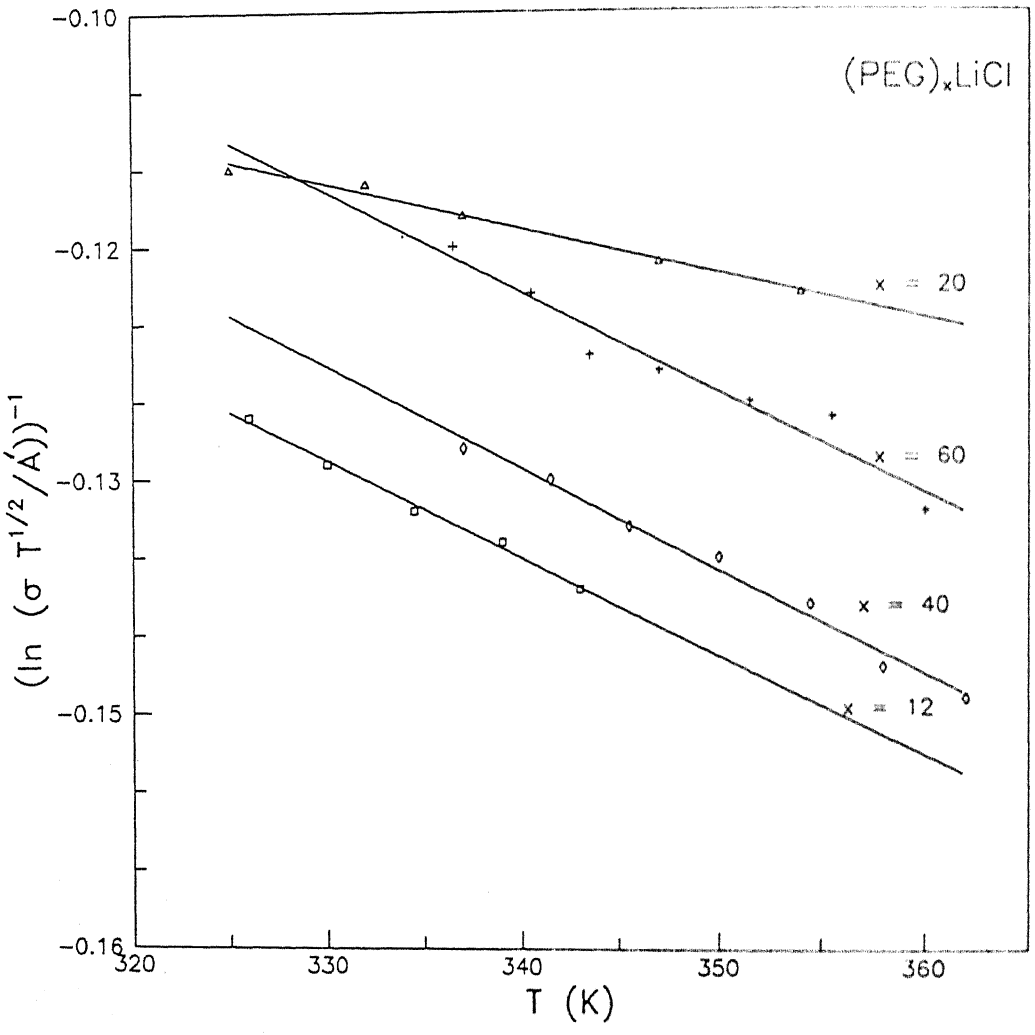

Figure 5.10: The $[\ln (\sigma T^{1/2}/A')]^{-1}$ versus T plots for various $(PEG)_xLiCl$ compositions in the high temperature region (T > 60°C).

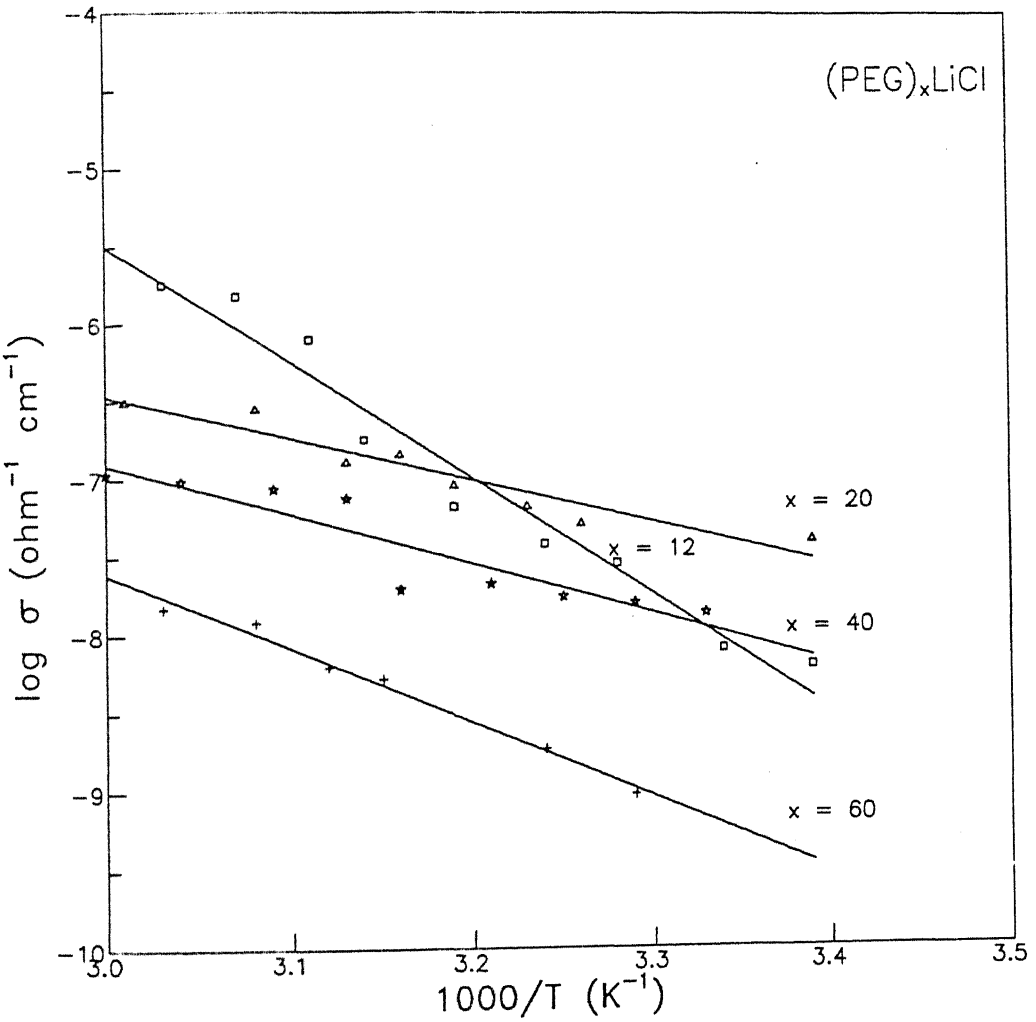

Figure 5.11: The $\log\sigma$ versus $10^3/T$ plots for various $(PEG)_xLiCl$ compositions in the low temperature region ($T < 60^oC$).

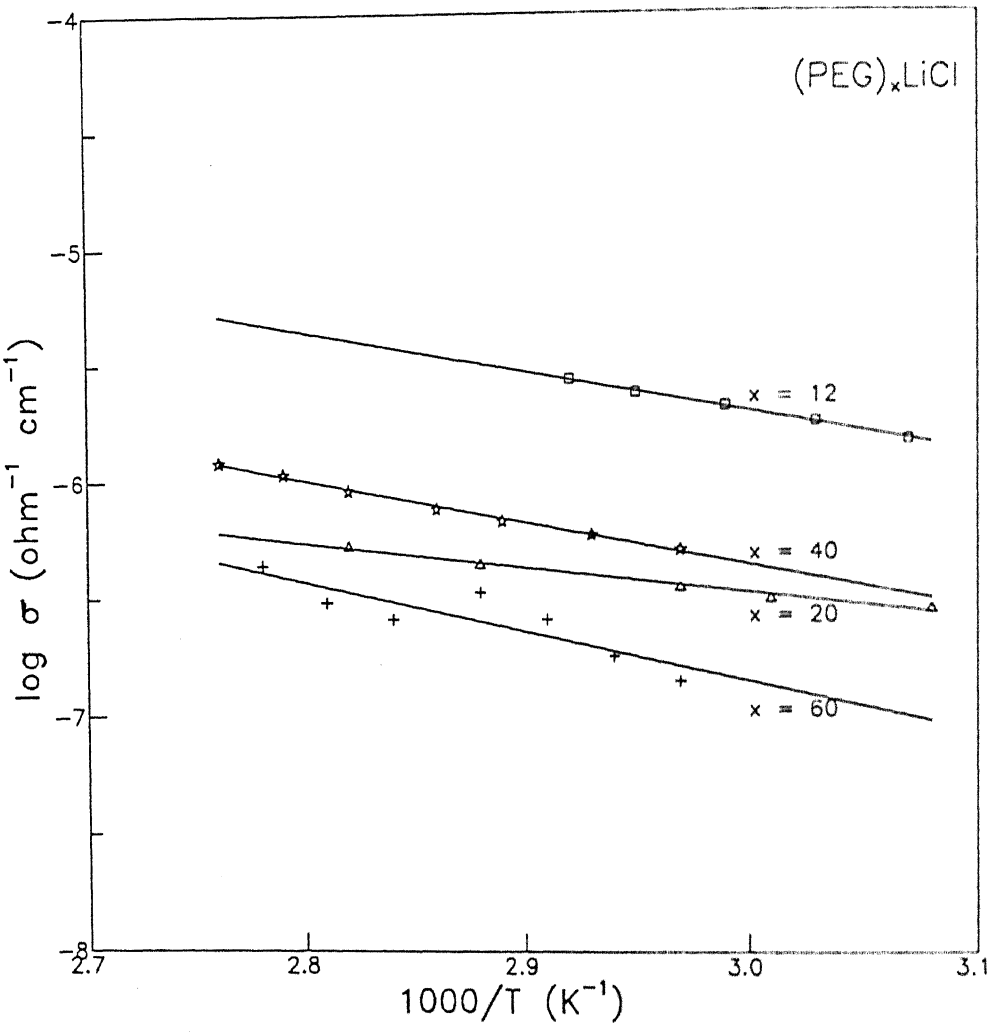

Figure 5.12: The $\log\sigma$ versus $10^3/T$ plots for various $(PEG)_xLiCl$ compositions in the high temperature region (T > 60°C).

Table 5.8: Comparison of Arrhenius and V-T-F best fit parameters* and the errors involved therein for PEG–LiCl system

At T < 60°C

Composition	Arrhenius			V-T-F		
(O/Li)	-m	c	error%	-m×10^3	c	error%
12	7.2	17	0.6	0.5	-0.07	1.0
20	3.3	3.8	0.8	0.7	-0.12	0.8
40	3.2	2.6	0.6	0.7	0.12	0.7
60	4.7	6.6	0.8	1.0	3.1	0.9

At T > 60°C

Composition	Arrhenius			V-T-F		
(O/Li)	-m	c	error%	-m×10^3	c	error%
12	3.3	0.8	0.7	0.39	0.58	0.6
20	3.2	2.6	0.7	1.0	0.36	0.7
40	1.8	0.5	0.6	0.7	0.13	0.5
60	2.1	-0.5	0.7	0.6	0.09	0.7

* For the Arrhenius (log σ vs $10^3/T$) fit m = -E/2303k and c = log σ_o; For the V-T-F ($\ln(\sigma T^{1/2}/A')]^{-1}$ vs T) fit, m = -k/E_a and c = kT_o/E_a.

Table 5.9: V-T-F parameters for the $(PEG)_xLiCl$ system in the temperature range above 60°C.

Composition	A'	E_a	T_o
(O/Li)	$(\Omega^{-1}\ cm^{-1}\ K^{1/2})$	(eV)	K
12	0.077	0.04	278
20	0.047	0.06	254
40	0.024	0.13	202
60	0.016	0.14	143

5.2.2 PEG-LiBr system

It should be remarked at the outset that even though LiBr is expected to behave not very differently from LiCl, the $(PEG)_xLiBr$ complexes were found to be quite different from the PEG–LiCl system. The most striking difference was that the PEG-LiBr samples were found to almost flow out at temperatures above ~ 65°C, hence rendering the electrical conductivity measurements irreproducible and unacceptable at T > 65 °C, and thus these studies are limited to the range –20 to 65°C.

The variation of log σ as a function of $10^3/T$ for $(PEG)_xLiBr$ (x = 6, 7, 8, 10, 20, 40, 60), is shown in Figs. 5.13 and 5.14. It is observed that there is considerable scattering of the data from the straight line behavior. Moreover, the conductivity –temperature data were found not to fit the V-T-F equation either. Thus LiBr certainly seems to behave differently from the rest of the alkali halides. It should be mentioned that Reitman, Kaplan and Cava (1985) have also reported an anomalous behavior in PEO-LiBr complexes. In any case, the Arrhenius transport parameters, viz., σ_o and E, obtained from the intercept and slope, respectively, of the log σ vs $10^3/T$ plots (Figs. 5.13 and 5.14) are given in Table 5.10. The fact that the x = 10 composition, viz., $(PEG)_{10}LiBr$, exhibits the lowest activation energy (1.09 eV) as well as the

Table 5.10: **The Arrhenius activation energy E, for PEG-LiBr system in the temperature range −20 to 65°C.**

Composition	E
(O/Li)	(eV)
6	1.91
7	1.24
8	0.89
10	1.09
20	1.50
40	1.03
60	0.84

highest conductivity ($\sim 8 \times 10^{-4}\ \Omega^{-1}\ cm^{-1}$) is self consistent. Moreover, the fact that the activation energy decreases as the salt concentration decreases is also consistent with the general overall trend reported in literature. It is argued that the increased salt concentration may increase the crystalline phase in the polymer–salt complexes, which hinders the motion of ions and hence a higher activation energy.

5.2.3 PEG–$LiClO_4$ System

The $(PEG)_xLiClO_4$ complexes, as pointed out in the preceding chapter,could not be prepared in form of self supporting films. Hence, the conductivity measurements were made during the first heating cycle in the range 25 to 85°C, in a sample holder designed to hold viscous fluid.

The variation of log σ as a function of $10^3/T$ for the $(PEG)_xLiClO_4$ complexes is shown in Fig. 5.15 for x = 5, 6, 7 and 8, and Fig 5.16 for x = 20, 40 and 60 compositions. It is observed that the conductivity data are not

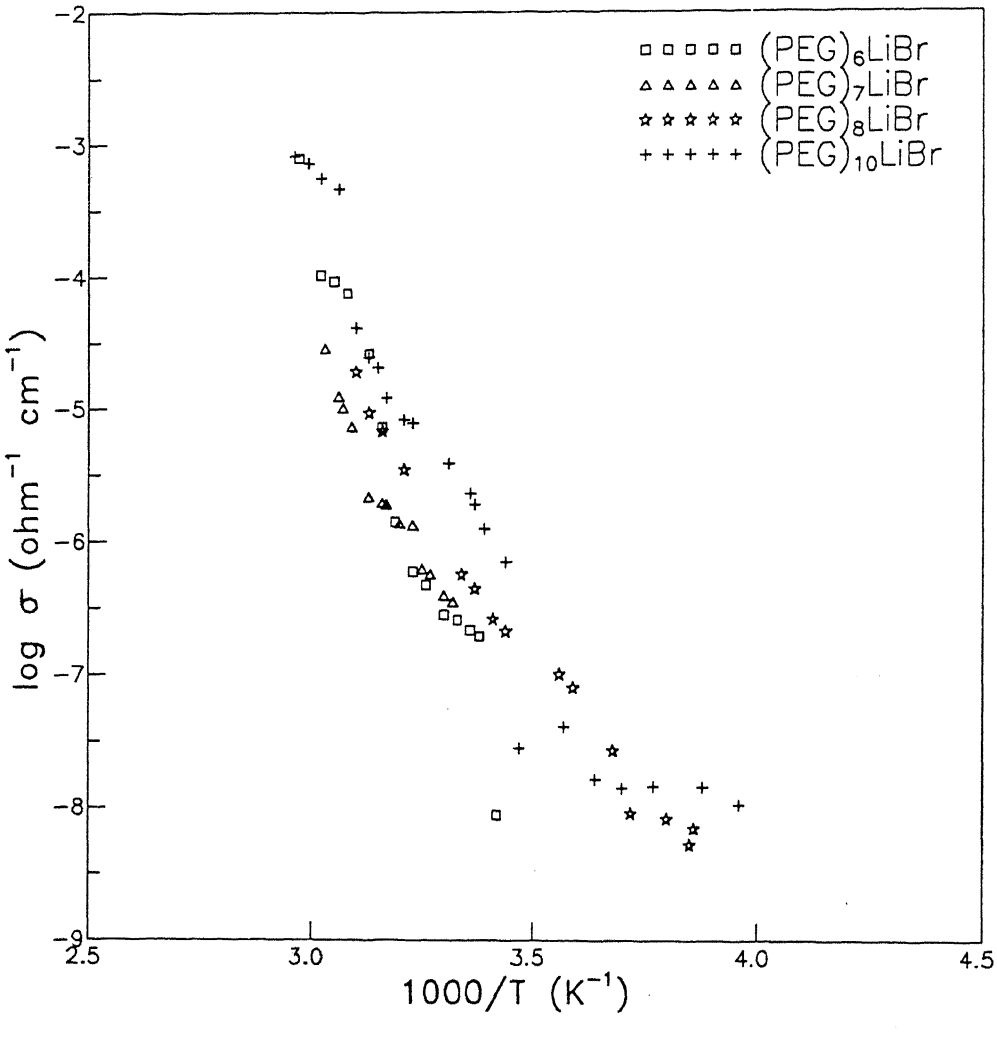

Figure 5.13: The $\log\sigma$ versus $10^3/T$ plots for various $(PEG)_xLiBr$ complexes x = 6, 7, 8 and 10.

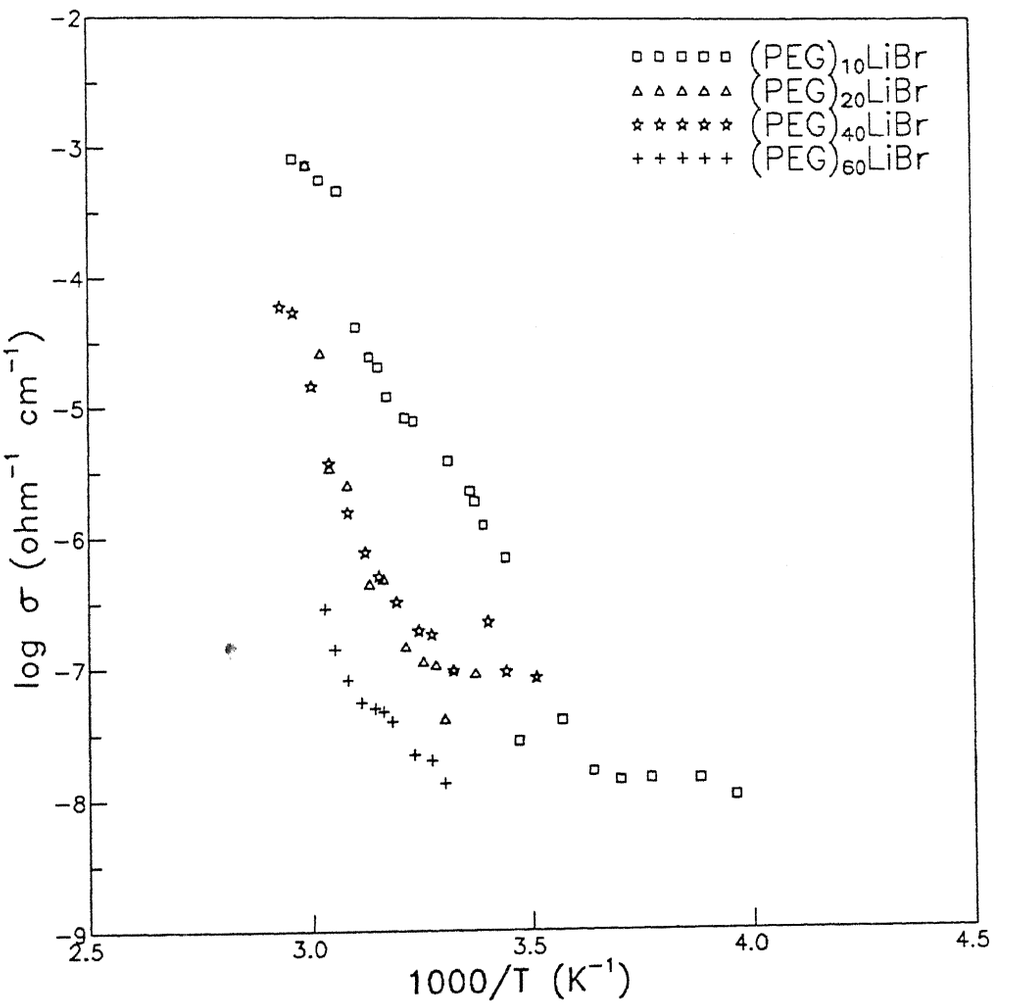

Figure 5.14: The $\log\sigma$ versus $10^3/T$ plots for various $(PEG)_xLiBr$ complexes, x = 10, 20, 40 and 60 .

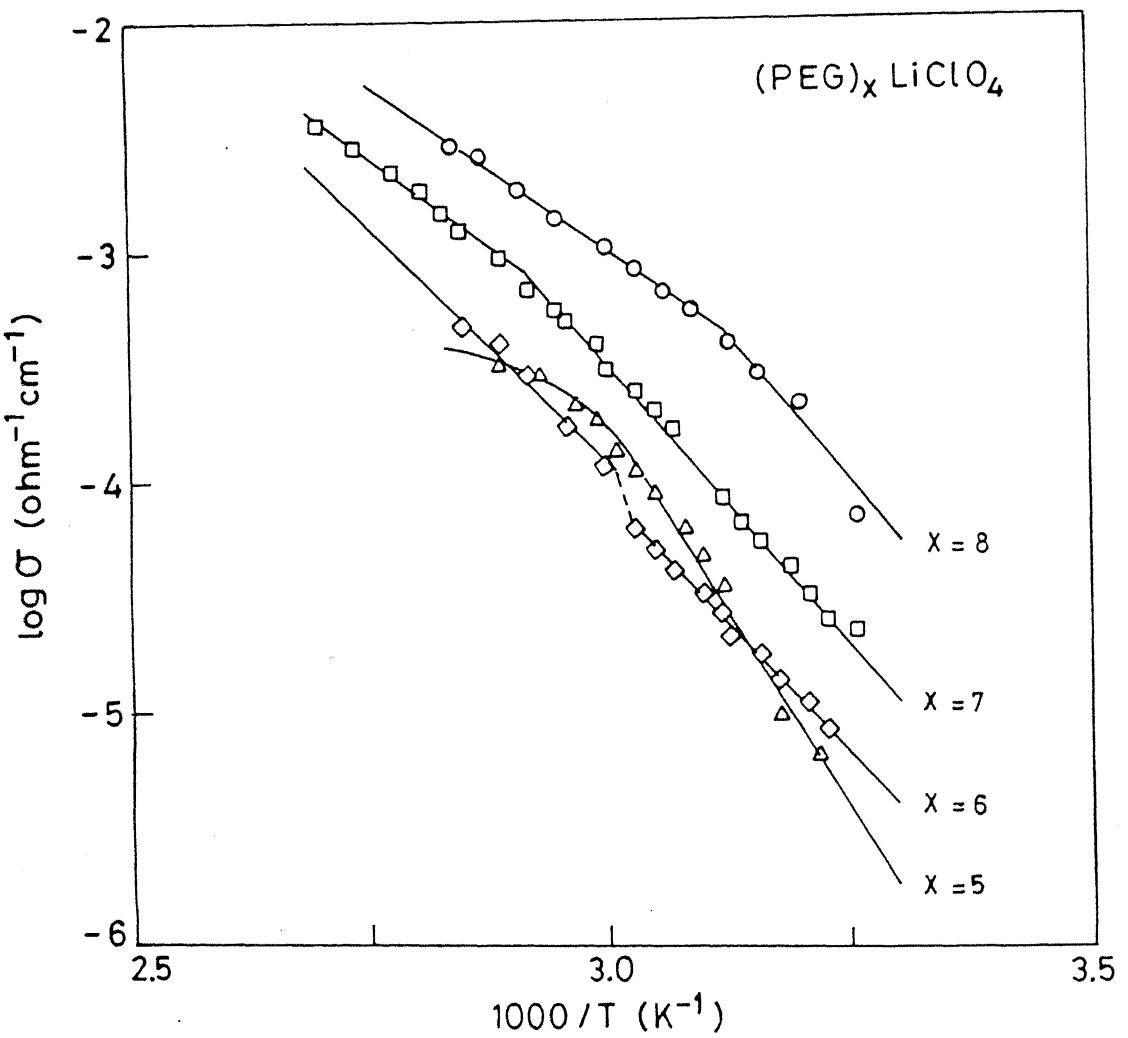

Figure 5.15: The $\log\sigma$ versus $10^3/T$ plots for various $(PEG)_xLiClO_4$ complexes x = 5, 6, 7 and 8.

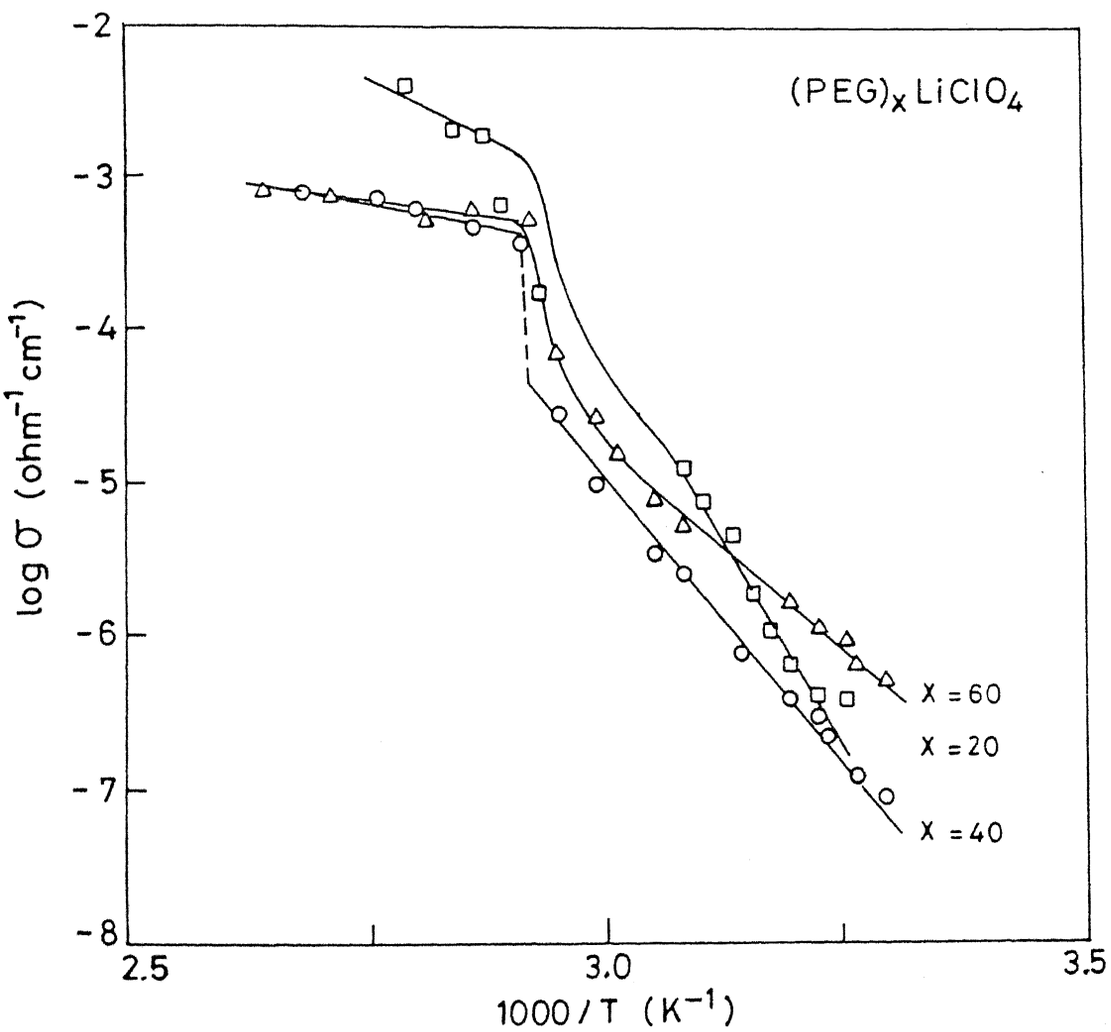

Figure 5.16: The $\log\sigma$ versus $10^3/T$ plots for various $(PEG)_xLiClO_4$ complexes x = 20, 40 and 60.

well behaved. Nevertheless, the log σ vs $10^3/T$ curves may be described roughly as superposition of two linear segments; a low temperature segment with low conductivity and high activation energy and a high temperature segment associated with a low activation energy. The temperature at which the log σ vs $10^3/T$ curve exhibits a discontinuity or a change in slope ,i.e., the transition temperature separating the two linear segments, is listed in Table 5.11 for the various compositions. It is seen that the transition temperature decreases initially, attains a minimum value of $\sim$ 50°C and then increases as the salt concentration decreases (or O/Li ratio increases). Unfortunately, the DSC measurements could not be carried out on these samples due to certain difficulties and thus it is not possible to make a detailed comment on the nature of these transitions.

However, the above results may be briefly discussed in view of, and compared with those on PEO–$LiClO_4$ system which has been thoroughly investigated (Fauteux and Robitaille, 1986). According to its phase–diagram (see also Fig. 2.2), there are two intermediate compounds of nominal compositions $(PEO)_3LiClO_4$ and $(PEO)_6LiClO_4$ (mpt. $\sim$ 65°C). The latter forms an eutectic with PEO at x $\sim$ 10 whose melting temperature is $\sim$ 50°C. At about the same composition a minimum value of transition temperature ($\sim$ 50°C) is observed in $(PEG)_xLiClO_4$ system. In fact there is a fair correlation between the observed transition temperatures (Table 5.11) in the $(PEG)_xLiClO_4$ complexs and the phase diagram of the $(PEO)_xLiClO_4$ system, which would suggest that the former has a similar phase diagram.

The Arrhenius activation energies, E_1, below and E_2 above the transition temperature, for the various complexes are given in Table 5.12. The value of E_1 decreases as x (or the O/Li ratio) increases upto $\sim$ 6, remains practically constant ($\sim 0.90 \pm 0.04$ eV) for x = 6–8, and then increases. On the other hand the activation energy E_2 above the transition temperature decreases almost continuously as x (or O/Li ratio) increases. Thus the polymer–salt complexes have lower activation energies (E_2) in the high temperature region at lower salt concentrations (or higher values of x) which is generally ascribed to

Table 5.11: Transition temperatures inferred from the log σ vs $10^3/T$ plots (Figs. 5.15 and 5.16) for various $(PEG)_xLiClO_4$ complexes

Composition (O/Li)	Transition Temperature (°C)
4*	72
5	59
6	58
7	71
8	48
10	50
20	61
40	70
60	67

*This composition is not shown in Fig. 5.15 to avoid loss of clarity.

Table 5.12: **Arrhenius activation energies, E_1 (low temperature region) and E_2 (high temperature region) for ion transport in $(PEG)_xLiClO_4$ complexes.**

Composition	Activation Energy (eV)	
(O/Li)	E_1	E_2
4	1.39	-
5	1.31	-
6	0.86	0.81
7	0.94	0.60
8	0.97	0.56
10	-	0.45
20	-	0.56
40	1.32	0.22
60	1.18	0.20

N.B. The blank indicates that the relevant log σ vs 1/T plot is not sufficiently linear so as to assign an activation energy.

the predominance of amorphous rather than crystalline phase. These results, viz., the transition temperature and the activation energies E_1 and E_2 and their variations with composition (x) are similar to some extent to those for PEO–$LiClO_4$ system and also consistent with its phase diagram.

A V-T-F fit of the conductivity–temperature data for various PEG–$LiClO_4$ complexes was also attempted. These results in the form of $[\ln (\sigma T^{1/2}/A')]^{-1}$ vs T plots are shown in Fig. 5.17 for some selected compositions, viz. x = 10, 40 and 60 at temperatures below the transition temperature. It is evident that the data do not fit very well the V-T-F equation either. For other compositions the fits are still worse. These studies lead to the only conclusion that the polymer/salt complexes with dilute salt concentrations (or higher values of O/Li or x) are more amorphous. Table 5.13 lists the best–fit V-T-F parameters, the apparent activation energy E_a and the glass transition temperature (T_{ox}),

Table 5.13: **The V-T-F best–fit parameters for ion transport below the transition temperature (see text and Table 5.11) for $(PEG)_xLiClO_4$ (x = 10, 40, 60) complexes.**

Composition (O/Li)	A' ($ohm^{-1}\ cm^{-1}\ K^{1/2}$)	E_a (eV)	T_o (K)
10	0.091	0.01	298
40	0.024	0.03	267
60	0.016	0.02	276

for the three compositions (x = 10, 40, 60). Within the limitations, these results indicate that the glass transition temperature increases as the salt concentration increases, while E_a is practically constant at a rather too low value (0.02 $\pm$ 0.01 eV).

5.3 Electrical Relaxation Studies

The frequency dependent conductivity, σ (ω), and the dielectric constant, ϵ (ω), studies are useful in discriminating between various ion transport mechanisms in solid electrolytes (Jr., Ditzenberger and Remeika, 1976; Wong, Brodwin, *et al.*, 1980). These studies have been found useful in polymeric electrolytes as well (Ansari, Brodwin, *et al.*, 1985; Fontanella, Wilson, *et al.*, 1992; Wintersgill, Fontanella, *et al.*, 1983). This section reports the dielectric loss and electric modulus (M) for some selected polymer–salt complexes.

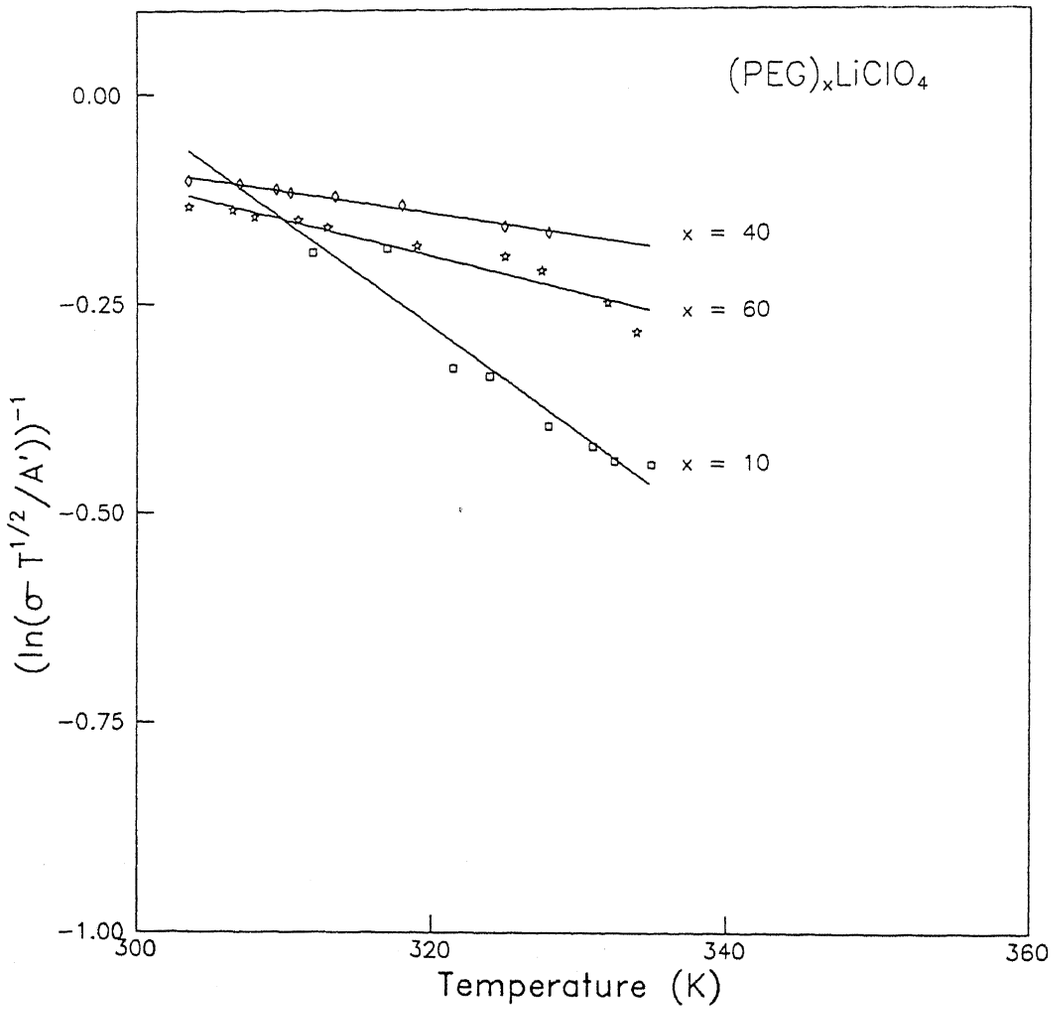

Figure 5.17: **The variation of $[\ln(\sigma T^{1/2}/A')]^{-1}$ vs T in the low temperature region for the $(PEG)_xLiClO_4$ complexes x = 10, 40 and 60.**

5.3.1 Dielectric loss studies

The complex admittance Y* is related to the resistance (R_p) and the capacitance (C_p) of the sample (in the parallel mode) by the relation

$$Y^* = Y\cos\theta + jY\sin\theta = 1/R_p + j\omega C_p \tag{5.20}$$

Thus we have,

$$1/R_p = Y cos\theta \tag{5.21}$$

$$\text{and } \omega C_p = Y sin\theta \tag{5.22}$$

The real (ϵ') and the imaginary (ϵ'') parts of the complex dielectric constant ϵ^* (since $\epsilon^* = \epsilon' - j\,\epsilon'' = Y^*/j\,\omega C_o$) are given by

$$\epsilon' = \frac{C_p}{C_0} = \frac{Y\sin\theta}{\omega C_o} \tag{5.23}$$

$$\epsilon'' = \frac{1}{\omega C_o R_p} = \frac{Y\cos\theta}{\omega C_o} \tag{5.24}$$

where $C_o = \epsilon_o A/d$ is the capacitance of the cell in vacuum or without sample (ϵ_o = permittivity of vacuum, A = area of the electrodes and d the separation between the electrodes or the thickness of the sample). Thus from the measured admittance (or impedance) data (Y,θ), and the known value of C_o, ϵ' and ϵ'' can be calculated.

The normalized dielectric loss,i.e., the ratio $\epsilon''/\epsilon''_{max}$, as a function of temperature over the range 180–300 K is shown in Fig. 5.18 at three different frequencies (500 Hz, 1 kHz and 5 kHz) for $(PEG)_{10}LiCl$ complex. Two relaxations are apparent in all the three curves. Similar results having two relaxations have been reported for the $(PEO)_{6.5}Ca(SCN)_2.4H_2O$ and $(PEO)_{6.5}Ba(SCN)_2.3H_2O$ complexes (Fontanella, Wintersgill and Calame, 1985) . The peak at the lower temperature (Fig. 5.18) has been assigned to the so called γ–relaxation attributed to a $tg^+\,t \rightleftharpoons tg^-\,t$ (conformational) transition usually responsible for ionic conductivity . This relaxation is therefore also referred to as conductivity relaxation. This γ relaxation may also be due to

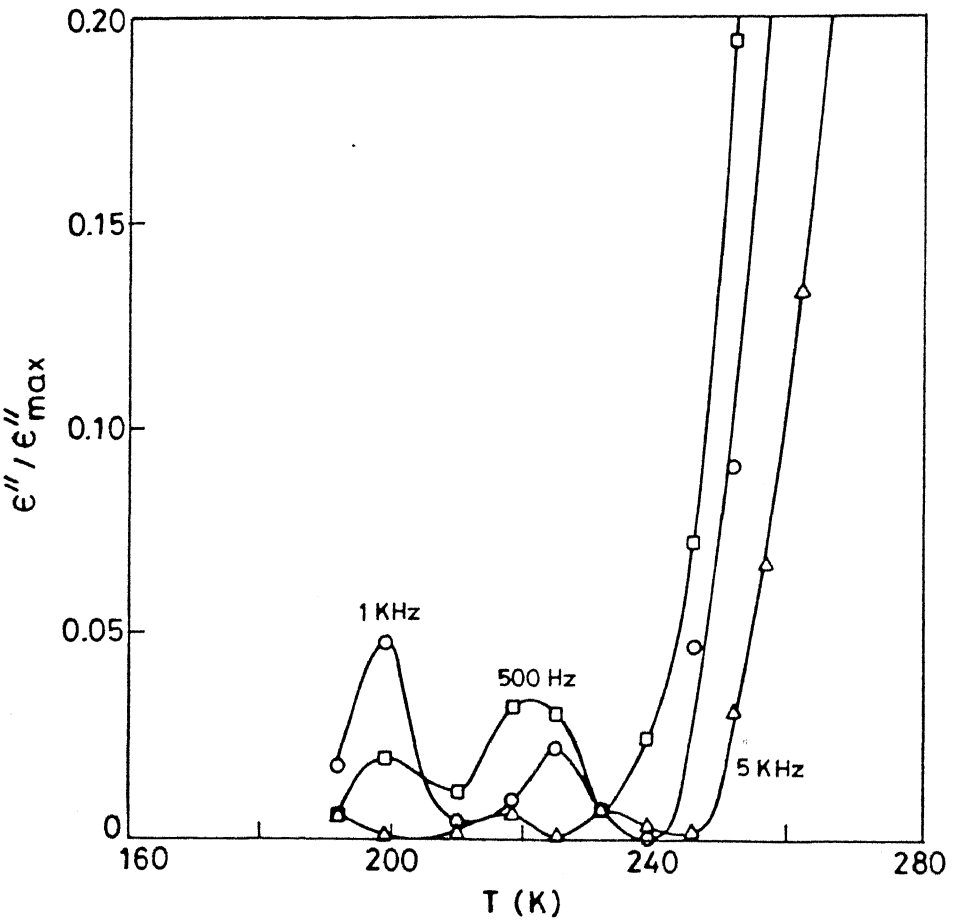

Figure 5.18: Plot of $\epsilon''/\epsilon''_{max}$ vs Temperature for the $(PEG)_{10}LiCl$ complex at 500 Hz, 1 kHz and 5 kHz.

Table 5.14: The relaxation frequencies at various temperatures obtained from the dielectric loss response for $(PEG)_{10}LiCl$.

A : High temperature relaxation frequency (ω_H)

f_H (kHz)	ln ω_H	T_{max} (K)	$10^3/T_{max}$ (K^{-1})
0.5	8.05	221	4.52
1	8.75	225	4.44
5	10.35	234	4.27

B : Low temperature relaxation frequency (ω_L)

f_H (kHz)	ln ω_H	T_{max} (K)	$10^3/T_{max}$ (K^{-1})
0.5	8.05	198	5.05
1	8.75	200	5
5	10.35	216	4.63

the end -OH groups which will be present in the PEG based complexes. The peak appearing at the higher temperature is due to so called α relaxation attributed to *mechanical* relaxation associated with the segmental motion in the pure polymer host (Fontanella, Wilson, *et al.*, 1992). The dielectric loss behavior for $(PEG)_{10}LiBr$ and $(PEG)_8LiClO_4$ complexes were also found to be similar to that of $(PEG)_{10}LiCl$.

The temperature corresponding to the maximum in $\epsilon''/\epsilon''_{max}$ vs T curve, i.e., T_{max}, is related to the relaxation frequency ω by the relation

$$\omega(T) = \omega_o \exp(-E/kT_{max}) \tag{5.25}$$

where ω_o and E are characteristic relaxation frequency (= inverse of relaxation time, $\tau_o=\omega_o^{-1}$) and activation energy for a particular relaxation process. The ω and T_{max} obtained from Fig. 5.18 which are listed in Table 5.14 for both the low and high temperature peaks, were fitted to Eq.(5.25). From the intercept and the slope of the linearized ln ω vs $10^3/T_{max}$ plots, the relaxation times for

the two processes (γ and α relaxation) and the corresponding activation energies have been calculated:
γ-Relaxation: $\tau_o = 1/\omega_o = 2.2\times10^{-15}$ s ; E = 0.43 eV
α-Relaxation: $\tau_o = 1/\omega_o = 1.1\times10^{-19}$ s; E = 0.68 eV

These values for the γ-relaxation are comparable to the corresponding values for $(PEO)_{6.5}Ba(SCN)_2.3H_2O$ (4.3×10^{-14} s and 0.37 eV). However our relaxation time for α relaxation appears too low in comparison to the reported values in PEO based complexes (Fontanella, Wintersgill and Calame, 1985).

5.3.2 Electric Modulus Studies

The electric modulus is another quantity which can be calculated from the basic measured quantities, viz., the impedance (Z^*) or the admittance ($Y^* = 1/Z^*$) data. The complex (electric) modulus (M^*) is defined as

$$M^* = \frac{j\,\omega C_o}{Y^*} = \frac{\omega C_o \sin\theta}{Y} + j\,\frac{\omega C_o \cos\theta}{Y} \tag{5.26}$$

so that its real (M') and imaginary (M'') parts are

$$M' = \omega C_o \sin\theta / Y \tag{5.27}$$

$$\text{and} M'' = \omega C_o \cos\theta / Y \tag{5.28}$$

By eliminating Y and θ from the above equations using Eqs. (5.23) and (5.24), M' and M'' can also be written as

$$M' = \frac{\epsilon'}{(\epsilon'^2 + \epsilon''^2)} \tag{5.29}$$

and

$$M'' = \frac{\epsilon''}{(\epsilon'^2 + \epsilon''^2)} \tag{5.30}$$

Thus M' and M'' can be calculated either from Eqs. (5.27) and (5.28) or from Eqs. (5.29) and (5.30). The modulus spectroscopy (M vs ω studies) was

perhaps introduced by (Schrama, 1957), and it is widely being used in recent times (Almond and West, 1981; Bruce, West and Almond, 1982; Macdonald and Cook, 1984). It has been pointed out that the modulus spectroscopy is more appropriate for highly conducting (lossy) materials and for investigating bulk properties. Here we breifly present the M″ vs temperature studies at a few different frequencies for some selected polymer–salt complexes.

Fig 5.19 shows the variation of M″ versus temperature over the range 180–300 K at three different frequencies for the same polymer–salt ,viz., $(PEG)_{10}LiCl$ whose ϵ'' results are shown in Fig. 5.18. As pointed out earlier, since $M^* = 1/\epsilon^* = j\omega C_o/Y^*$, all the four quantities (M′, M″, ϵ' and ϵ'') are generated from the same admittance/impedance data. Thus both the results, viz., ϵ'' vs T and M″ vs T shown in Figs. 5.18 and 5.19 respectively, are calculated from the same measured admittance data (Y, θ) on $(PEG)_{10}LiCl$ sample. In fact the curves at 1 kHz in both the figures are obtained from exactly the same data. It may be appreciated that the M″ vs T curves at different frequencies shown in Fig. 5.19 reveal only one but quite large and fairly sharp peak at higher temperatures. The other, presumably the low temperature side peak appears to have shifted out of the temperature range of investigation, except in case of the curve at 1 kHz. However, a closer inspection of the curve at 100 Hz might suggest that the two peaks have moved closer and perhaps merged into one, but the curves at 1 and 10 KHz deny this conjecture. Similar results were observed for the $(PEG)_{10}LiBr$ sample, as shown in the M″ vs Temperature plots at two different frequencies, 100 Hz and 1 kHz (Fig. 5.20).

The temperature, T_{max} corresponding to the peak position in M″ vs T curves at three different frequencies (100 Hz, 1 kHz and 10 kHz) for the $(PEG)_{10}LiCl$ complex are listed in Table 5.15.

The characteristic relaxation frequency ($\omega_o = 1/\tau_o$) and the activation energy (E) for the relaxation process have been calculated from the intercept and the slope of the linearized ln $(2\pi f)$ vs $1/T_{max}$ plot (eq. 5.25). Their values are :

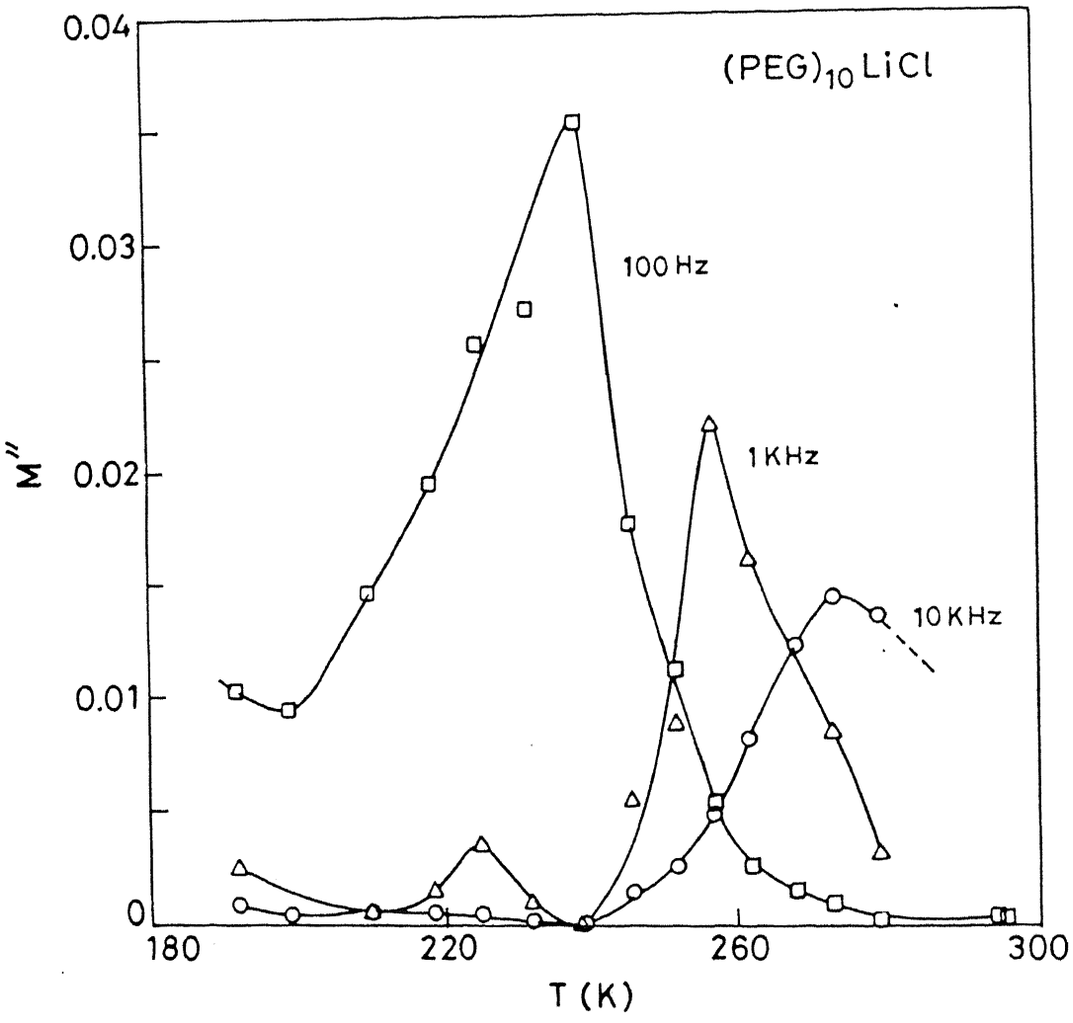

Figure 5.19: **Plot of M″ vs Temperature for the $(PEG)_{10}LiCl$ complex at 100 Hz, 1 kHz and 10 kHz.**

Table 5.15: The high temperature (α - relaxation) peak parameters viz., T_{max} and the corresponding frequency (ω) , obtained from M'' vs T curves for the $(PEG)_{10}LiCl$ complex.

frequency (f) (kHz)	ln (2πf)	T_{max} (K)	$10^3/T$ (K^{-1})
0.1	6.44	239	4.18
1	8.75	257	3.89
10	11.05	273	3.66

τ_o = 1.6×10^{-19} s; E = 0.76 eV.
which compare favorably with the high temperature, α-relaxation parameters (τ_o = 1.1×10^{-19} s; E = 0.68 eV) obtained from the ϵ'' vs T studies in the preceding section.

5.4 NMR measurements

NMR studies have been employed to investigate the polymer electrolytes in order to gain information about :

(a) the proportion of amorphous and crystalline phase present from T_2 (spin–spin relaxation time) measurements (Minier, Berthier and Gorecki, 1984).

(b) the nature of relaxation process as occurring in the system from the spin–lattice relaxation time (T_1) measurements (Sandahl, Schantz, *et al.*, 1989; Schantz, Kakikhana and Sandberg, 1990).

(c) diffusion coefficient of the mobile species and hence ion transport numbers t_+ and t_- from the pulsed–feild gradient measurements (Bhattacharjee, Smoot and Whitmore, 1986).

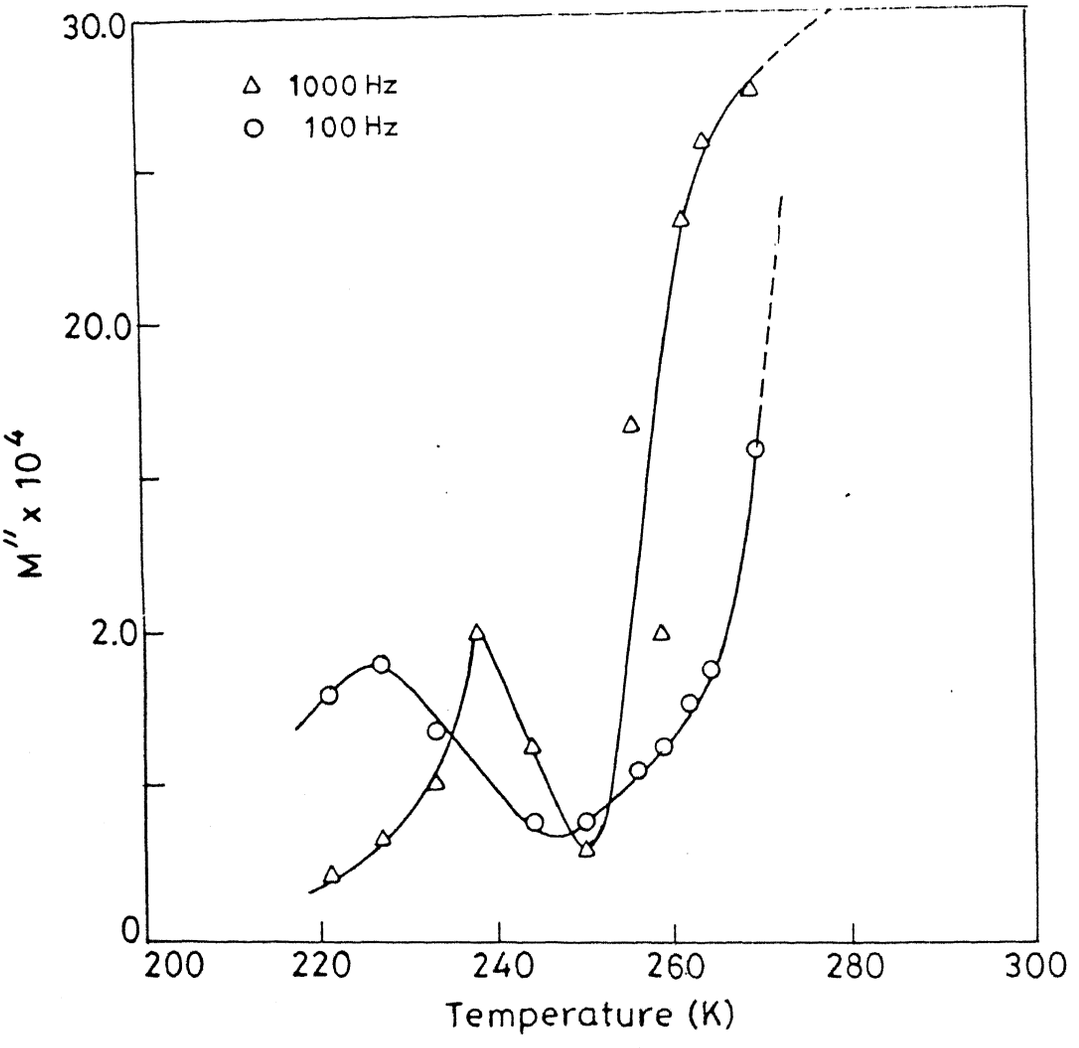

Figure 5.20: The plot of M'' vs Temperature for the $(PEG)_{10}LiBr$ complex

In this work the linewidth and the spin–lattice relaxation time (T_1) measurements have been carried out on the $(PEG)_{10}LiCl$ composition. The results are presented below.

Fig. 5.21 shows the ^7Li NMR spectra recorded at various temperatures in the range 160K - 370 K. Throughout the temperature range only one signal is observed which can be assigned to the $+1/2 \rightleftharpoons -1/2$ central transition of the quadrupolar split energy levels of the ^7Li nuclei. A broad background signal due to the satellite ($+3/2 \leftrightarrow +1/2$) transitions has sometimes been observed (Chung, Jefferey and Stevens, 1991; Panero, Scrosati and Greenbaum, 1992) in similar systems (e.g. $(PEG)_8LiClO_4$) at low temperatures. The absence of such a signal in the present work is probably due to the insufficient signal ratio.

The full-widths at half maxima (FWHM) of the signal are plotted as a function of temperature in Fig 5.22. The result suggests that the data can be analyzed in terms of two motional narrowing regions: one in the low temperature region (180-240 K) and another above the room temperature. The low temperature one can be associated with the glass transition. A number of studies have reported such a narrowing just above the glass transition temperature T_g and attributed it to the onset of segmental motion of the polymer chain (Chung, Jefferey and Stevens, 1991; Panero, Scrosati and Greenbaum, 1992). What is interesting in our result is the fact that this region of narrowing is fairly clearly separated from the second narrowing region (300-360 K), which is shown magnified in the inset of Fig. 5.22. The enhancement of conductivity also occurs in this region as shown in Fig. 5.7. Therefore we associate this narrowing with translational diffusion of the Li^+ ions.

An estimate of the motional parameters can be obtained from the line-width data using the modified BPP relation (Boyce and Huberman, 1979)

$$\tau_c = \frac{1}{2\pi\alpha\Delta H} \tan[\pi/2 \frac{(\Delta H)^2 - (\Delta H_r)^2}{(\Delta H_d)^2}] \qquad (5.31)$$

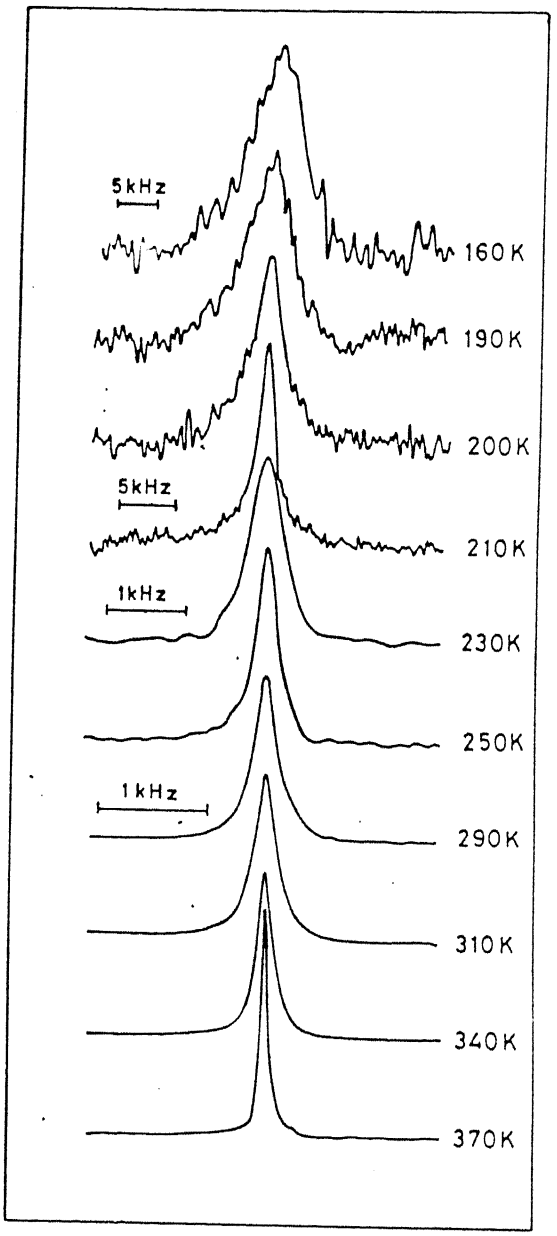

Figure 5.21: ^7Li NMR line-width for the $(PEG)_{10}LiCl$ at various temperatures

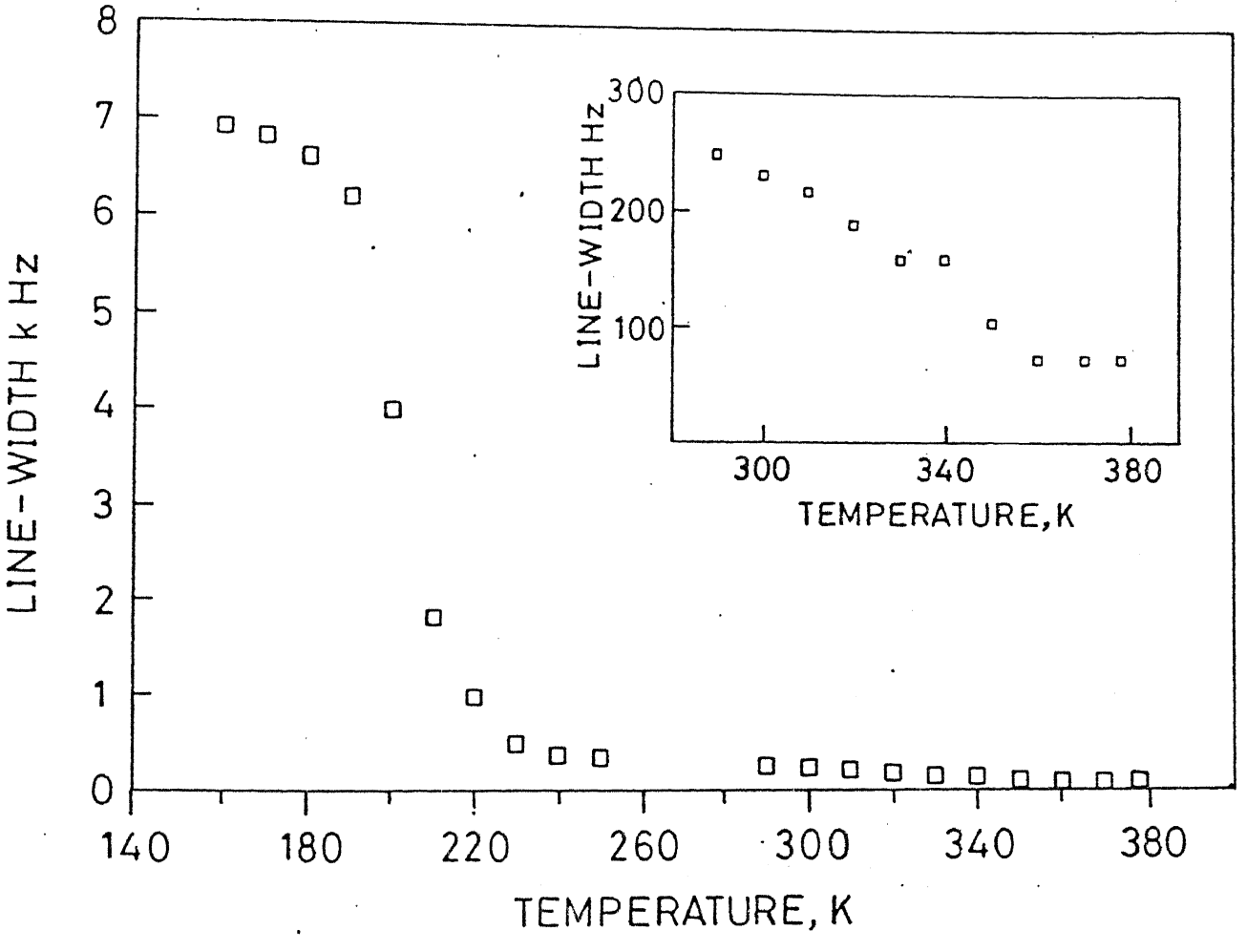

Figure 5.22: Variation of ^7Li NMR line-width with temperature

where ΔH is the line-width, ΔH_r is the residual line-width, ΔH_d is the rigid lattice line-width and α is a parameter of order unity, coupled with the Arrhenius relation:

$$\tau_c = \tau_o \exp(E_a/kT) \tag{5.32}$$

We obtain the following values from such an analysis:

E_a = 0.35 eV and $\tau_o = 2.4 \times 10^{-13}$ s; 180–420 K.
E_a = 0.37 eV and $\tau_o = 7.7 \times 10^{-9}$ s; 300–360 K.

An attempt to fit the data to VTF relation was not satisfactory. Similar observation has been made earlier by Chung, Jefferey and Stevens (1991).

While the values of the parameters in the low temperature region are reasonable , the value of τ_o in the high temperature region is orders of magnitude higher than expected value of 10^{-13}s. Such an anomalous prefactor has been observed in a number of inorganic fast ionic conductors (Slade, 1985) where translational diffusion is the cause of motional narrowing. The reason for this anomaly has been the subject of a large number of investigations (Jalamon, 1979). we are presently examining the applicability of such ideas to polymer systems. Fig. 5.23 shows the results of the spin-lattice relaxation time measurements.Similar to the line-width result, the relaxation behaviour is also seen to be separated into two regions on either side of $\sim$ 325 K. This is also the temperature around which a peak in the DSC is observed (see Chapter 4), indicating the melting of pure polymer. As a function of temperature, T_1 goes through two minima, a relatively broad one at 305 K and another sharp minimum at 340 K. Two distinct mechanisms of relaxation appear to be operative in the two regions.

We have analysed the low temperature data using the standard Bloembergen,Purcell and Pound (BPP) model and the fit gives the following values for the motional parameters:

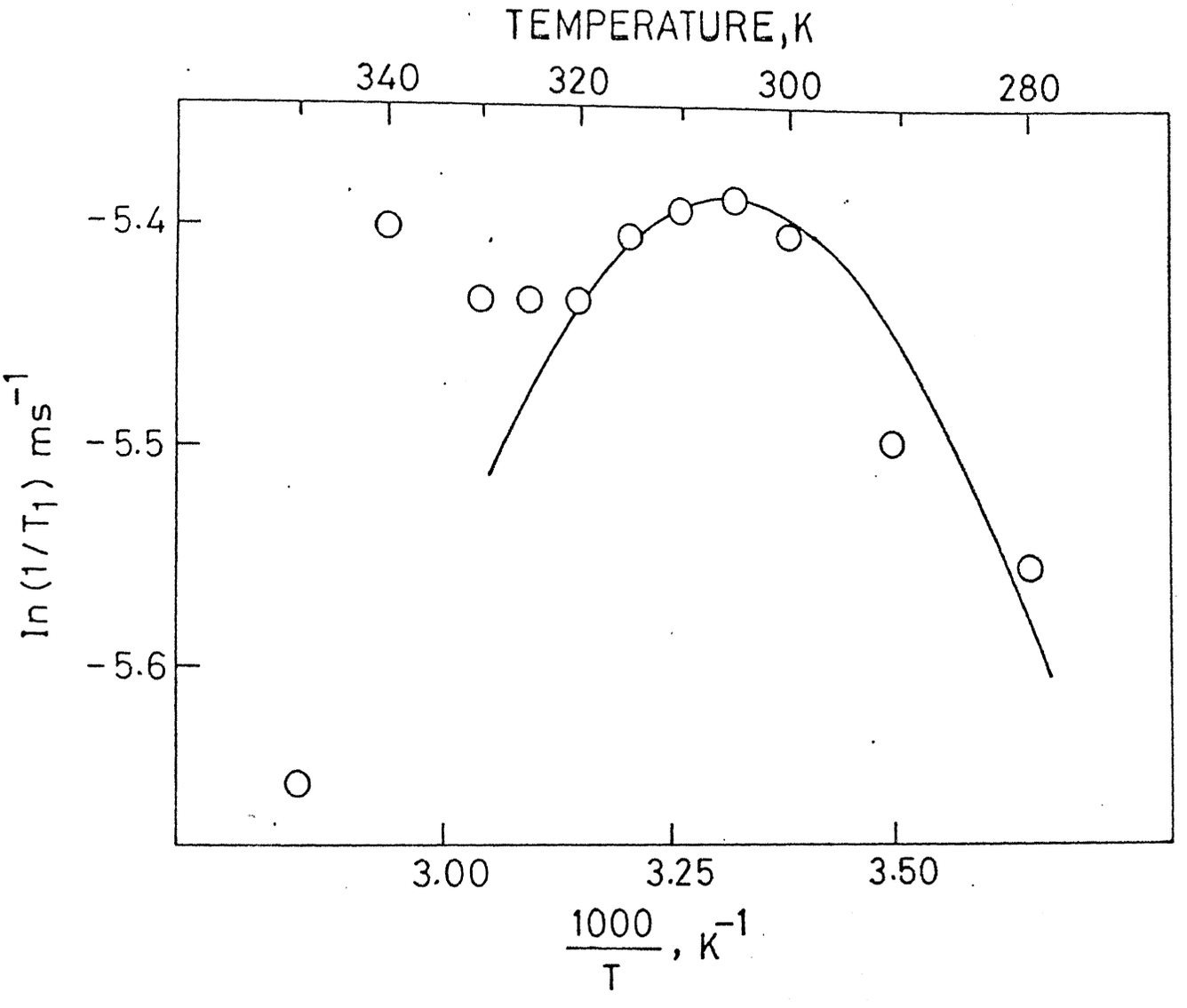

Figure 5.23: Variation of relaxation time,T_1 with temperature for the $(PEG)_{10}LiCl$ complex

$$E_a = 0.21\text{eV and } \tau_o = 2.9 \times 10^{-13}\text{s}$$

No attempt was made to fit the results beyond 325 K due to insufficient number of points.

5.5 Summary and Conclusion

The polyethylene glycol (PEG) forms complexes with lithium salts (LiX, X = Cl, Br and ClO_4) which exhibit enhanced electrical conductivity by orders of magnitude. The composition $(PEG)_8LiClO_4$ exhibits the highest conductivity ($\sim 2.5\times10^{-2}$ ohm^{-1} cm^{-1} at 105°C) which is comparable to PEO–$LiClO_4$ system. In view of their potential, PEG– based polymer electrolytes should be explored further.

The conductivity (σ) vs composition (X) characteristics of the polymer salt complexes can be classified into three categories; category I includes systems whose σ vs X (or log σ vs log X) isotherms are linear, category II in which the σ-X isotherms exhibit a single maximum and category III which feature a pair of maxima separated by a minimum in their σ-X isotherms. The PEG–LiX (X = Cl, Br and ClO_4) systems investigated in this work belong to the category III. It should be pointed out that the category I systems would be a sub-group of either category II or III.

Assuming that the polymer-salt complexes are essentially amorphous in nature and that the glass transition temperature ($T_{o\alpha}$) increases linearly with the salt concentration (X), the configurational entropy (CE) model has been extended to include the effect of the salt. This extended CE model predicts the salient features observed for category I and category III systems, viz., (i) the log σ vs log X isotherms in the low salt concentration regime ($X \rightarrow 0$) are linear with a slope of unity, (ii) the σ vs X isotherms exhibit a pair of maxima separated by a minimum, (iii) all the three extrema in the σ-X shift towards higher salt concentrations as the temperature increases,etc. Microscopically,

the formation of the neutral ion-pairs and the charged triple ion-pairs may be responsible for the observed σ vs X behaviour.

The extended CE model is found to be inadequate for category II systems, but at least some of these are suspected to comprise a large fraction of crystalline phases, while others are not carefully studied , especially at low salt concentrations. It has been reasoned that in general more careful measurements on some selected systems would be desirable to establish whether or not the extended CE model is satisfactory for all the polymer–salt systems.

The electrical conductivity (σ) vs temperature data generally consist of two linear segments; one below 60°C and the other above 60°C. The transition temperature ($\sim$ 60°) separating these two regions corresponds to the melting temperature of the host polymer (PEG). The discontinuous jump in the σ at the transition temperature is larger for complexes containing larger fraction of the host polymer, which is attributed to the fact that these samples produce larger fraction of amorphous phase on melting. The conductivity– temperature data could be described either by the Arrhenius or V-T-F relation for almost all the complexes investigated. The glass transition temperature (T_o) obtained from the V-T-F of σ vs T data are found to increase consistently with the salt concentration. A lowest Arrhenius activation energy (0.20 eV) was obtained for $(PEG)_{60}LiClO_4$ while a highest value of 1.91 eV was obtained for $(PEG)_6LiBr$.

The dielectric loss (ϵ'') and electric modulus (M″) studies as function of temperature and frequency show evidence of two distinct relaxation processes each. The low temperature relaxation process ($\tau_o \sim 10^{-15}$ s and E = 0.43 eV) has activation energy similar to that of ionic conductivity, and thus appears to be associated with the conformational transition in the polymer chain. The high temperature relaxation process ($\tau_o \sim 10^{-19}$ and E $\sim$ 0.7 eV) is associated with the segmental motion in the host polymer (PEG). The relaxation time for this process is anomalously low ($\sim 10^{-19}$) in comparison to that of PEO ($\sim 10^{-15}$).

The NMR measurements also reveal the presence of two distinct relaxation

processes; one of which involves activation parameter similar to that of translational motion of ion responsible for electrical conductivity while the other has anomalously low relaxation time ($\sim 10^{-9}$).

Chapter 6

Effect of ion size on conductivity of PEG–MX complexes

The thermodynamic processes involved in the polymer–salt complex formation have been described in Chapter 2. The complex formation can occur if the free energy change is negative, i.e.,

$$-\left\{\begin{array}{c}\text{Lattice energy of salt}\\ +\\ \text{Lattice energy of polymer}\end{array}\right\}+\left\{\begin{array}{c}\text{Solvation energy}\\ +\\ \text{Lattice energy of complex}\end{array}\right\}<0$$

Hence the solvation energy and the lattice energy are the main factors involved in competition to each other, in the complex formation. Both these factors are dependent on the ionic size and polarizability, and hence it may be expected that the ease of complex formation will depend upon both the cation and anion size. Smaller cations will have lower enthalpies of solvation and the trend for alkali metal ions is

Table 6.1: **Some Physical Constants for MX salts**

Cation	Ion size	Lattice Energy (kcal/mole)		
	(Å)	Cl^-	Br^-	I^-
Li^+	0.58	199.2	188.5	174.1
Na^+	0.99	183.1	174.5	163.9
K^+	1.37	165.4	159.3	150.8
Cs^+	1.67	152.2	146.3	139.1

$$Li < Na < K < Cs$$

The lattice energy values, on the other hand, are higher for smaller cations. Table 6.1 shows the lattice energy values for the various cations, with halide anions (Cl^-, Br^-, I^-).

In the case of anions the trend is opposite. The larger the anion, greater will be the ease of complex formation, as a larger anion will have lesser tendency to enter into competition with the ether oxygens on the polymer, to associate with the cation. The driving force for complex formation is the formation of the M–O bond, which has bond energy of about –75 kJ/mole for the Na^+ cation. Complexes of Na salts with PEO have been reported to be crystalline, whereas those of Rb and Cs salts have been found to be more or less amorphous when detected by XRD and microscopic studies. Three dimensional models of PEO complexes predict an open helical chain structure with the oxygen atoms directed inward. The smaller alkali metal ions like Na^+ and K^+ may reside within the helical cavity. In the case of Na^+ salt complexes the oxygen coordination number is estimated to be 4 (Papke, Ratner and Shriver, 1982a). Rb^+ and Cs^+ cations being too large are expected to lie outside the cavity. However, EXAFS studies have shown evidence of the formation of Rb–PEO complexes with a coordination number of four. The conductivity studies on $(PEO)_{10}MBF_4$ and $(PEO)_{10}$ MCF_3SO_3 (M = Li, Na, K,

Rb and Cs) indicate that the larger cations can also be effectively complexed with the polymer.

6.1 Effect of ion size on conductivity

In a previous work on PEO complexes with alkali metal salts (Chabagno, 1980), it has been reported that the conductivity at a given temperature and fixed concentration increases as one goes down the group IA in the periodic table of elements. This may be due to the fact that the polarizability and hence enthalpy of solvation is in this order. It may be difficult to imagine that larger cations like Cs^+ show higher conductivity than Na^+ and K^+ ions, but this may be explained in view of the conductivity mechanism. The barrier to ionic diffusion is the energy needed to change its solvation sphere from three to four. The rate determining steps are :

$$\underset{(1)}{M(O)_n} \rightarrow \underset{(2)}{M(O)_{n-1}} \rightarrow \underset{(3)}{O - M(O)_{n-1}}$$

The energy necessary to pass from the transition state (2) to (3) follows the order Li > Na > K > Cs. Hence the conductivity generally follows the order Cs > K > Na. In the case of Li^+ ion, the cation size is much too small and it is highly electropositive, hence in most cases its complexes show more conductivity than Cs salt complexes. That the order of increase or decrease in the conductivity is also dependent on the size of anion has been concluded in a later work (Reitman, Kaplan and Cava, 1985). The conductivity of the alkali metal tetra fluoroborate complexes, $(PEO)_{10}MBF_4$ followed the order : Na >> Li > K,Cs >> Li. This may be related to the crystalline or amorphous nature of the complexes. The MF_3SO_3.PEO, M = Cs and Rb complexes are also reported to be highly amorphous (Reitman, Kaplan and Cava, 1987).

With a view to investigate the cation size effect on the conductivity of PEG–based complexes, we have investigated the bromides and iodides of lithium,

sodium, potassium and cesium complexed with PEG. Further,the complexes of PEG with lithium chloride, bromide, iodide and perchlorate are examined to see the effect of the size of anions. These are discussed in the following sections.

6.1.1 Effect of Cation size on conductivity

Fig. 6.1 shows the variation of log σ versus $10^3/T$ for $(PEG)_{10}MI$ complexes with M = Li, Na, K and Cs. The polymer to salt ratio of 10 was chosen as it was found to give maximum conductivity in the PEG–LiX (X = Cl, Br, ClO_4 systems). It is evident that the linearity of the Arrhenius (log σ vs 1/T) plots in Fig. 6.1 is less than satisfactory. In any case, these conduction characteristics as usual, consist of nearly linear segments with two different slopes. The so called *knee* or transition temperature separating the two segments for all the systems except $(PEG)_{10}CsI$ is around 50°C, which is close to the melting temperature of the host polymer PEG. However, for the $(PEG)_{10}CsI$ the knee appears at a somewhat higher temperature ($\sim$ 62°C). The activation energy (E_1) in the low temperature region is generally higher than that (E_2) in the low temperature region for all the four complexes examined in this work. The knee temperature, the activation energies E_1 and E_2 below and above the knee temperature and the electrical conductivities at two different temperatures (30° and 60°C) for all the four systems are given in Table 6.1.

Below the transition temperature,it is observed that the NaI complex has the lowest conductivity over the entire temperature range which is expected as the sodium complexes have been found to be most crystalline and hence least conducting. Below the transition temperature the lithium and potassium complexes have similar σ values while the Cs–complex has a lower value. Above the transition temperature, however, the σ value of $(PEG)_{10}CsI$ increases much more drastically than that of the $(PEG)_{10}KI$. Thus, in the high temperature region $(PEG)_{10}LiI$ and $(PEG)_{10}CsI$ have similar σ values while $(PEG)_{10}CsI$ shows a slightly higher σ value. As for the activation energies (E), the Cs–complex

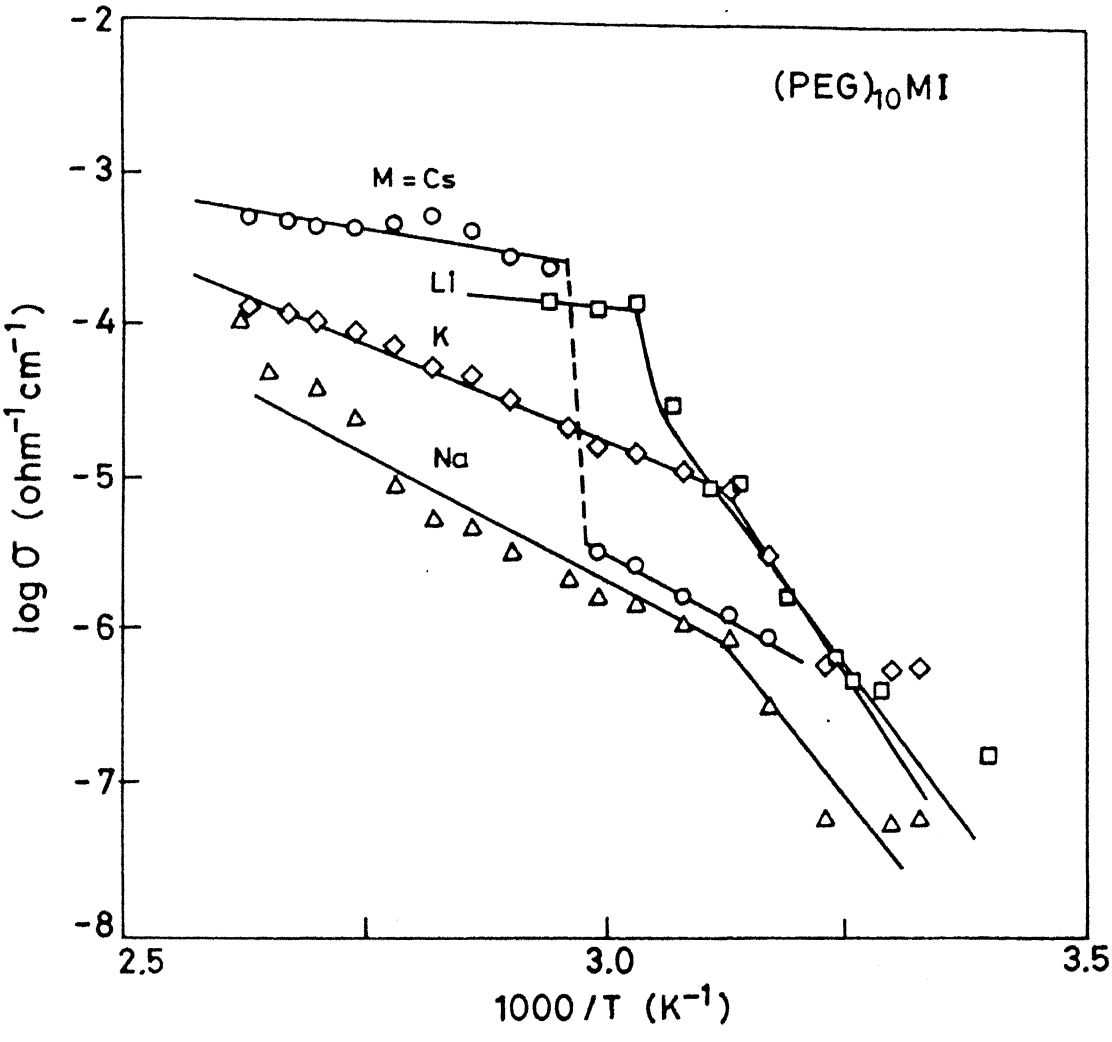

Figure 6.1: The log σ versus 1000/T plots for the $(PEG)_{10}MI$ complexes (M = Li, Na, K and Cs)

Table 6.2: **Ionic transport parameters for $(PEG)_{10}MI$ (M = Li, Na, K and Cs) complexes**

Complex	Knee Temp. (T_N)	Activation Energy		Conductivity	
$(PEG)_{10}MI$	(K)	E_1 (eV)	E_2 (eV)	(ohm^{-1} cm^{-1})	
		(below T_N)	(above T_N)	65°C	30°C
LiI	330	1.28	-	1.5×10^{-4}	4.1×10^{-7}
NaI	320	1.36	0.66	2.2×10^{-6}	5.62×10^{-8}
KI	319	1.23	0.50	2.3×10^{-7}	5.6×10^{-7}
CsI	335	0.84	0.20	2.4×10^{-4}	4.5×10^{-7}

has the lowest value (0.20 eV) in the high temperature region. This may be expected due to the low energy barrier encountered in passing through the transition states, as explained earlier. Although the activation energy (E_1) in the low temperature region is similar for $(PEG)_{10}NaI$ and $(PEG)_{10}KI$, that in the high temperature (E_2) for K^+ is lower. Our values may be compared with those reported for $(PEO)_{10}MBF_4$ complexes (Reitman, Kaplan and Cava, 1987):

$$\begin{aligned} M = Cs, &\quad E_1 = 1.30 \text{ eV} ; E_2 = 0.17 \text{ eV} \\ M = K, &\quad E_1 = 1.39 \text{ eV} ; E_2 = 0.21 \text{ eV} \\ M = Na, &\quad E_1 = 1.42 \text{ eV} ; E_2 = 0.42 \text{ eV} \end{aligned}$$

Thus it is evident that our results on PEG–MI (M = Li, Na, K and Cs) complexes are consistent with those of PEO–MBF_4 (Reitman, Kaplan and Cava, 1987) inasmuch as the activation energies in both high and low temperature regions (E_1 and E_2) decrease as the cation size increases, with the exception of lithium salt complexes.

The PEG complexes with MBr (M = Li, Na, K and Cs) are found to exhibit a different trend (Fig. 6.2). The complexes with Na, K and Cs show much lower conductivity values than the lithium bromide complex. The trend within this group is Li >> Cs > K > Na. This is expected keeping in view the conductivity values for the $(PEG)^{10}MBr$ complexes are less than those of

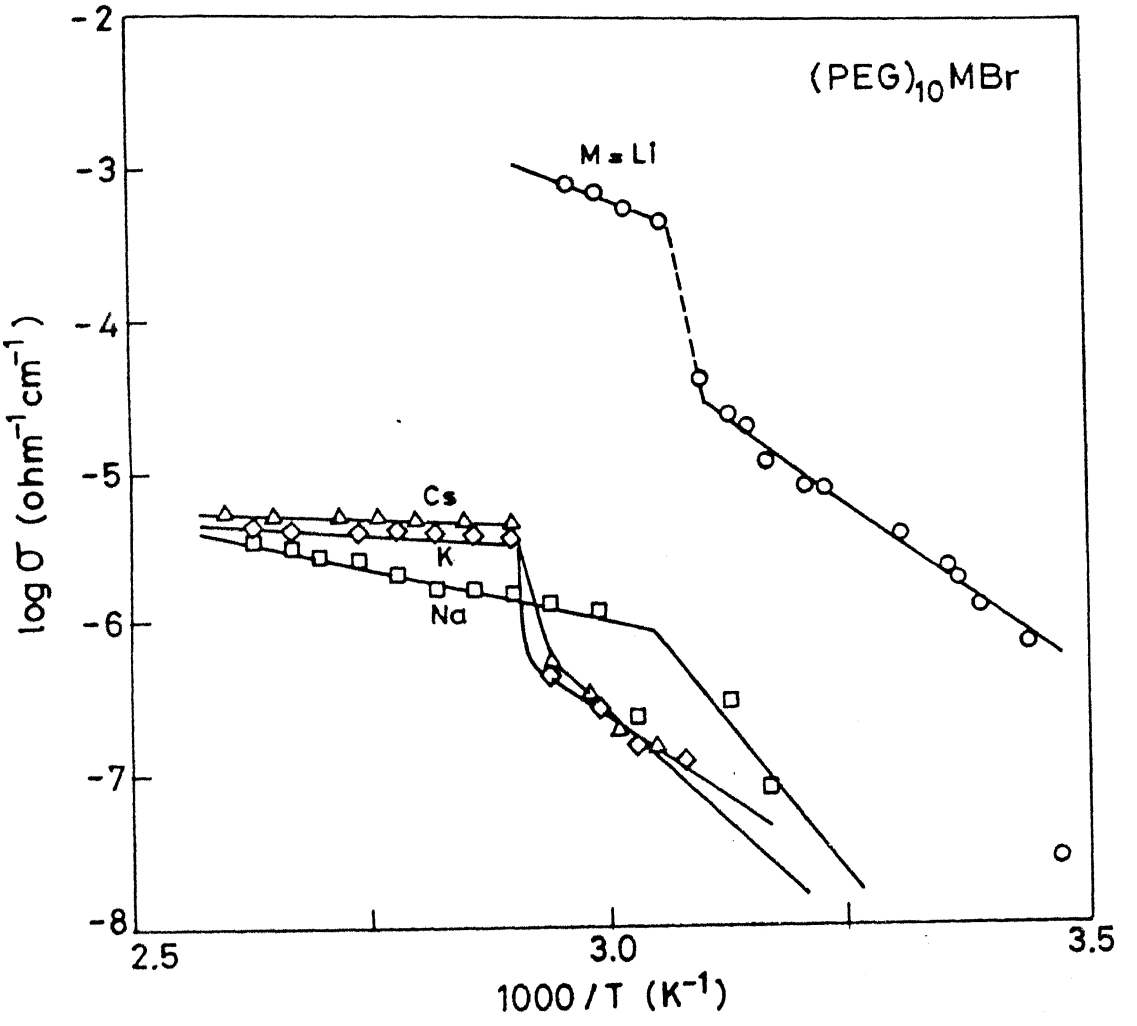

Figure 6.2: The log σ versus 1000/T plots for the $(PEG)_{10}MBr$ complexes (M = Li, Na, K and Cs)

$(PEG)_{10}MI$ complexes. This may indicate that the complex formation is not complete in case of bromide salts. This is supported by the XRD patterns of these complexes which showed peaks corresponding to the pure MBr salts, indicating the presence of uncomplexed salts. The SEM micrographs also showed regions of crystallized MBr salts. These results are consistent with Chabagno's (1980) , who found that only LiBr and NaBr could form complexes with PEO. However, with PEG even KBr and CsBr have complexed, although to a limited extent. This may be inferred as there is a definite enhancement in the conductivity of the complexes over pure PEG.

6.1.2 Effect of anion size on conductivity

It has been reported previously (Reitman, Kaplan and Cava, 1985; MacCallum and Vincent, 1987) that the *hard* anions give the best conductivity results. The anions with a large delocalization of charge like ClO_4 and CF_3SO_3 show higher conductivity. In the case of small cations like Li^+, larger and more polarizable anions will have lesser tendencies to form ion–pairs and hence lead to higher conductivities. Results on several complexes of the series $(PEO)_{4.5}LiX$ (X = Cl, Br, I, NO_3^-, etc.; Reitman, Kaplan and Cava (1985)) show that there is a vast difference in activation energy values for different anions. Thus the role of the anion is no less significant. Analysis of detailed impedance measurements on PEO–LiSCN (Sorensen and Jacobsen, 1982) shows the transport number of Li^+ to be $\sim$ 0.54. For the PEO–$LiClO_4$ system, the Li^+ ion transference number was found to be $\sim$ 0.27 for the fully amorphous state (Weston and Steele, 1981). It has been reported in the past that complexes with anions containing oxygen are more susceptible to the effects of water. The order of hydrogen bond energy is

$$Cl > I > ClO_4$$

indicating that the effect of moisture would be maximum in the case of ClO_4.

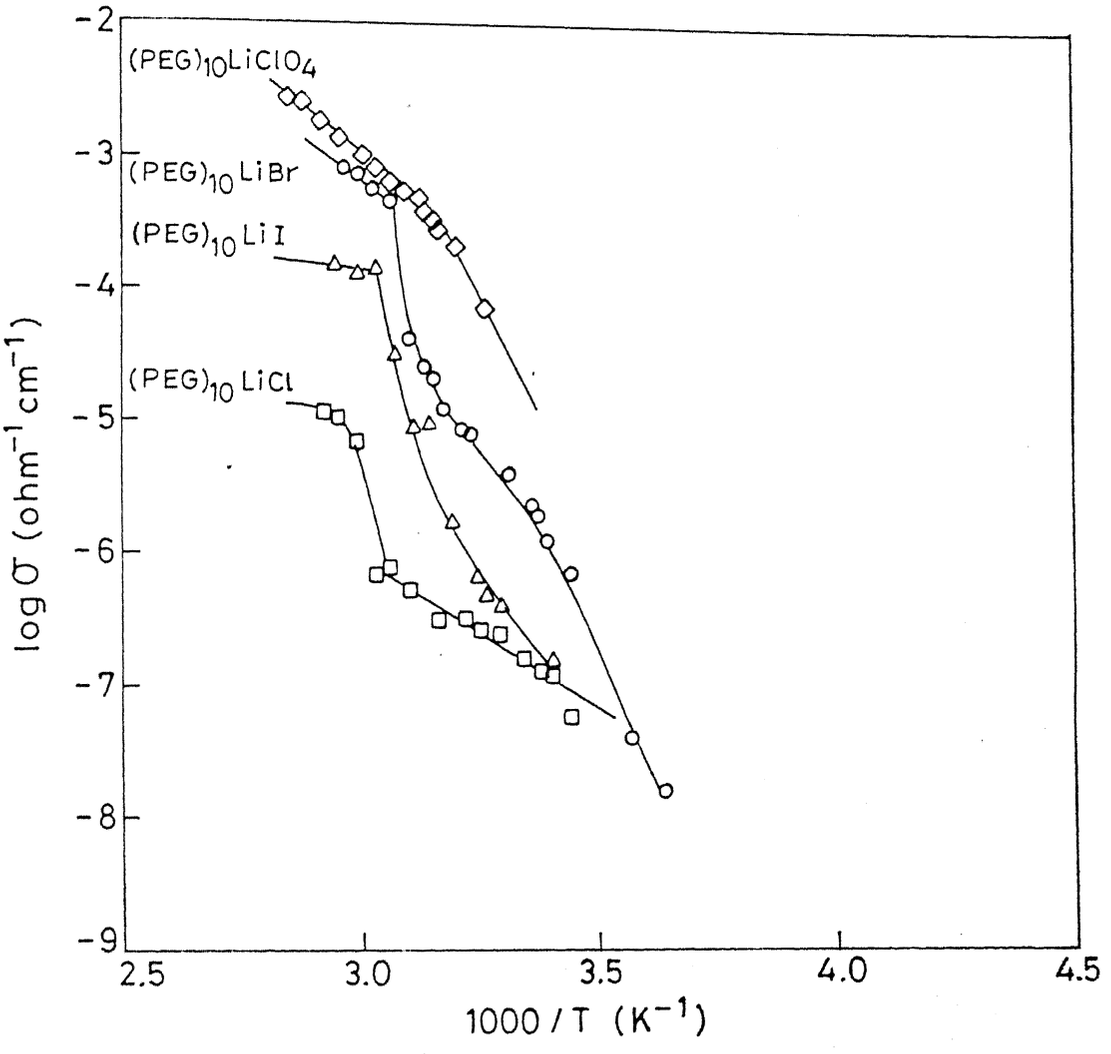

Figure 6.3: The log σ versus 1000/T plots for the $(PEG)_{10}LiX$ complexes (X = Cl, Br, I and ClO_4)

The Li^+ salts,viz., –LiCl, LiBr, LiI and $LiClO_4$ were complexed with PEG to study the effect of anion size. The ClO_4^- ion has the highest radii and thus $(PEG)_{10}LiClO_4$ is expected to show best conductivity. Fig. 6.3 shows the log σ vs 1000/T plots for the complexes $(PEG)_{10}LiX$ (X = Cl, Br, I and ClO_4). The complexes of LiCl are crystalline at room temperature and hence show the least conductivity. The $(PEG)_{10}LiBr$ complex shows higher conductivity than the LiI complex. Although this is not expected in view of the anionic size, the $(PEO)_{4.5}LiBr$ complex has also been reported to follow an unusual behavior (Reitman, Kaplan and Cava, 1985). The $LiClO_4$ complex shows the maximum conductivity, this is in accordance with large anionic size and high delocalization of charge on this anion.

6.2 Effect of dispersion of Al_2O_3

Weston and Steele (1981) have investigated the effect of dispersion of Al_2O_3 in polymer electrolytes mainly with a view to improve the mechanical properties. Small increase in the conductivity due to the addition of γ– Al_2O_3 (grain size = 40 μm) in the PEO–$LiClO_4$ system has also been reported (Przyluski and Wieczorek, 1989). For higher concentration of the ceramic powder the conductivity dropped down rapidly due to the formation of low conducting ceramic regions in the polymer matrix. The dispersion of γ – alumina in PEO–NaSCN was found to increase the σ values by about 5 times and a conductivity as high as 1.2×10^{-5} ohm^{-1} cm^{-1} at 30 °C was thus obtained (He, Chen, *et al.*, 1986). The conductivity was found to increase upto $\sim$ 30 w% of γ–alumina. Weiczorek, Such, *et al.* (1989) have studied the $(PEO)_{10}NaI$ complex containing dispersion of θ–Al_2O_3, and have obtained a maximum σ value at 10 wt% composition. The increase in the conductivity by about one order of magnitude was observed near the room temperature for the particle size of 2 μm. Polymer complexes containing alumina of particle size greater than 2 μm did not show any enhancement. Such studies have been done with NASICON fillers also (Weiczorek, Such, *et al.*, 1989).

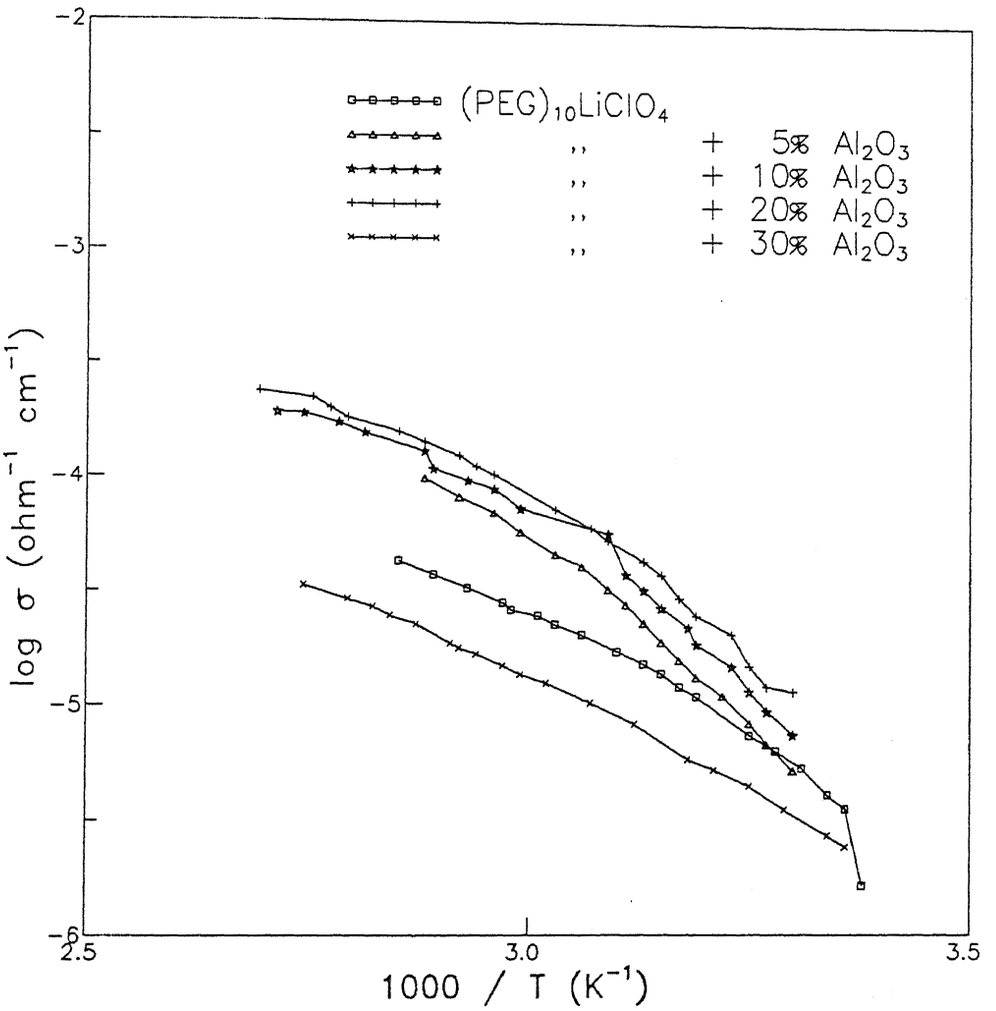

Figure 6.4: The log σ versus 1000/T plots for the $(PEG)_{10}LiClO_4$ complex containing dispersion of γ Al_2O_3 (0.3 μ)

In this work the $(PEG)_{10}LiClO_4$ complex was mixed with various concentrations of γ–alumina of particle size 0.3 μm. The concentrations used are 5, 10, 20 and 30 wt% of Al_2O_3. The composition with 20 wt% Al_2O_3 was found to show the maximum conductivity. The enhancement in σ was by a factor of about 3 at 30°C. This may be explained by the fact that the addition of the ceramic powder increases the amorphous phase content of the polymer. Fig. 6.4 shows the log σ vs 1000/T plots for the various compositions. The ceramic additive was found to improve the mechanical strength of the complex as well.

6.3 Summary and Conclusion

The electrical conductivity (σ) on the PEG–MI (M = Li, Na, K and Cs) complexes reveal that the size of cations as well as anions does influence the conduction characteristics. At higher temperatures, i.e., above the knee (T_N)/ transition temperature ($\sim$ 60°C) , the trend is that the σ is higher for larger cations, with the exception of lithium ion. Thus the conductivity above T_N is in the following order

$$Li,Cs > K > Na$$

However, below the knee or transition temperature (T_N), the trend is rather different. The Li and K complexes have similar σ values while the Cs–Complex has a lower σ value. As for the activation energies, there is a clear trend that the activation both above and below the knee temperature increases as the cation size increases, with the exception of Li– complexes again.

The results on PEG–MBr (M = Li, Na, K and Cs) complexes, show more or less a similar trend, viz., the conductivity is higher for larger cations with the exception of lithium ion. However, the bromide complexes generally exhibit a lower σ than the iodide complexes. It is concluded that the complexation

is less complete in bromide than iodide complexes. The above results are generally consistent with earlier studies on PEO–based complexes and also with the ion diffusion mechanism involving transition solvation sphere from three to four.

The conductivity studies on PEG–LiX (X = Cl, Br, I and ClO_4) complexes indicate that larger and more polarized anions generally lead to higher conductivity. Thus PEG–$LiClO_4$ exhibits the highest conductivity while $(PEG)_{10}LiCl$ the lowest. However, this trend is interrupted by the (Li) bromide and iodide complexes. Finally, the dispersion of Al_2O_3 particles are found to enhance both electrical and mechanical properties.

III. It should be pointed out that the category I systems would be a sub-group of either category II or III.

Assuming that the polymer-salt complexes are essentially amorphous in nature and that the glass transition temperature ($T_{o\sigma}$) increases linearly with the salt concentration (X), the configurational entropy (CE) model has been extended to include the effect of the salt. This extended CE model predicts the salient features observed for category I and category III systems, viz., (i) the log σ vs log X isotherms in the low salt concentration regime ($X \rightarrow 0$) are linear with a slope of unity, (ii) the σ vs X isotherms exhibit a pair of maxima separated by a minimum, (iii) all the three extrema in the σ-X shift towards higher salt concentrations as the temperature increases,etc. Microscopically, the formation of the neutral ion-pairs and the charged triple ion-pairs may be responsible for the observed σ vs X behaviour.

The extended CE model is found to be inadequate for category II systems, but at least some of these are suspected to comprise a large fraction of crystalline phases, while others are not carefully studied , especially at low salt concentrations. It has been reasoned that in general more careful measurements on some selected systems would be desirable to establish whether or not the extended CE model is satisfactory for all the polymer–salt systems.

The electrical conductivity (σ) vs temperature data generally consist of two linear segments; one below 60°*C* and the other above 60°C. The transition temperature ($\sim$ 60°) separating these two regions corresponds to the melting temperature of the host polymer (PEG). The discontinuous jump in the σ at the transition temperature is larger for complexes containing larger fraction of the host polymer, which is attributed to the fact that these samples produce larger fraction of amorphous phase on melting. The conductivity– temperature data could be described either by the Arrhenius or V-T-F relation for almost all the complexes investigated. The glass transition temperature (T_o) obtained from the V-T-F of σ vs T data are found to increase consistently with the salt concentration. A lowest Arrhenius activation energy (0.20 eV) was obtained

for $(PEG)_{60}LiClO_4$ while a highest value of 1.91 eV was obtained for $(PEG)_6LiBr$.

The dielectric loss (ϵ'') and electric modulus (M″) studies as function of temperature and frequency show evidence of two distinct relaxation processes each. The low temperature relaxation process ($\tau_o \sim 10^{-15}$ s and E = 0.43 eV) has activation energy similar to that of ionic conductivity, and thus appears to be associated with the conformational transition in the polymer chain. The high temperature relaxation process ($\tau_o \sim 10^{-19}$ and E $\sim$ 0.7 eV) is associated with the segmental motion in the host polymer (PEG). The relaxation time for this process is anomalously low ($\sim 10^{-19}$) in comparison to that of PEO ($\sim 10^{-15}$).

The NMR measurements also reveal the presence of two distinct relaxation processes; one of which involves activation parameter similar to that of translational motion of ion responsible for electrical conductivity while the other has anomalously low relaxation time ($\sim 10^{-9}$).

The electrical conductivity (σ) on the PEG–MI (M = Li, Na, K and Cs) complexes reveal that the size of cations as well as anions does influence the conduction characteristics. At higher temperatures, i.e., above the knee (T_N)/ transition temperature ($\sim$ 60°C) , the trend is that the σ is higher for larger cations, with the exception of lithium ion. Thus the conductivity above T_N is in the following order

$$Li,Cs > K > Na$$

However, below the knee or transition temperature (T_N), the trend is rather different. The Li and K complexes have similar σ values while the Cs–Complex has a lower σ value. As for the activation energies, there is a clear trend that the activation both above and below the knee temperature increases as the cation size increases, with the exception of Li– complexes again.

The results on PEG–MBr (M = Li, Na, K and Cs) complexes, show more or

less a similar trend, viz., the conductivity is higher for larger cations with the exception of lithium ion. However, the bromide complexes generally exhibit a lower σ than the iodide complexes. It is concluded that the complexation is less complete in bromide than iodide complexes. The above results are generally consistent with earlier studies on PEO–based complexes and also with the ion diffusion mechanism involving transition solvation sphere from three to four.

The conductivity studies on PEG–LiX (X = Cl, Br, I and ClO_4) complexes indicate that larger and more polarized anions generally lead to higher conductivity. Thus PEG–$LiClO_4$ exhibits the highest conductivity while $(PEG)_{10}LiCl$ the lowest. However, this trend is interrupted by the (Li) bromide and iodide complexes. Finally, the dispersion of Al_2O_3 particles are found to enhance both electrical and mechanical properties.

Bibliography

Adam, G. and Gibbs, J.H. (1965). *J. Chem. Phys.*, **43**:159.

Albensson, I., Jacobsson, P., *et al.* (1992). *Solid Stae Ionics*, **53–56**:1059.

Almond, D.P. and West, A.R. (1981). *Solid State Ionics*, **3/4**:73.

Angell, C.A. (1967). *J. Chem. Phys.*, **46**:4673.

Angell, C.A. and Sichina, W. (1976). *Ann. NY Acad. Sci*, **279**:53.

Angell, C.A., Liu, C. and Sanchez, E. (1993). *Nature*, **362**:137.

Angell, C.A., Pollard, L.J. and Strauss, W. (1969). *J. Chem. Phys.*, **50**:2694.

Ansari, S.M., Brodwin, M., *et al.* (1985). *Solid State Ionics*, **17**:101.

Armand, M.B. (1980). Lithium non-aqueous batteries electrochemistry. *The Electrochem. Soc. ed. Pennington*, **80**:261.

Armand, M.B. (1983). *Solid State Ionics*, **9/10**:745.

Armand, M.B. (1987). *High Conductivity Solid Ionic Conductors recent trends and applications.* World Scientific Publishing Co. Ltd., Singapore.

Armand, M.B. and Gandini, A. (1991). *Proceedings of the 3 rd International Symposium on Polymer Electrolytes (ISPE3)*, Annecy, France.

Armand, M.B., Chabagno, J.M. and Duclot, M.J. (1979). *Fast Ion Transport in Solids*, page 131. North Holland, New York.

Armstrong, R.D. and Clarke, M.D. (1984). *Electrochim. Acta.*, **29-10**:1443.

Bermudez, V. De Zea, Armand, M.B., *et al.* (1992). *Electrochimica Acta*, **37**:1603.

Berthier, C., Gorecki, W., *et al.* (1983). *Solid State Ionics*, **11**:91.

Bhattacharjee, S., Smoot, S.W. and Whitmore, D.H. (1986). *Solid State Ionics*, **18/19**:306.

Blonsky, P.M. and Shriver, D.F. (1984). *J. Am. Chem. Soc.*, **106**:6854.

Bonino, F., Ottaviani, M. and Scrosati, B. (1988). *J. Electrochem. Soc.*, **135**:12.

Boukamp, B.A. (1986). *Solid State Ionics*, **18/19**:136.

Bouridah, A., Dalard, F., *et al.* (1985). *Solid State Ionics.*

Boyce, J.B. and Huberman, B.A. (1979). *Physics Reports*, **51**:189.

Bradley, J.N. and Greene, P.D. (1967). *Trans. Farad. Soc.*, **63**:434.

Bruce, P.G., West, A.R. and Almond, D.P. (1982). *Solid State Ionics*, **7**:57.

Cai, H., Hu, R., *et al.* (1992). *Solid State Ionics*, **52**:333.

Camaron, G.G., Ingram, M.D. and Sorrie, G.A. (1986). *J. Electrochem. Soc.*, **198**:205.

Cameron, G., Harrie, J., *et al.* (1988). *British Polym. Jr.*, **20**:199.

Cameron, G., Ingram, M. and Sarmouk, K. (1990). *European Polymer Journal*, **26**:1097.

Catlow, C.R.A., Chadwick, V., *et al.* (1983). *Solid State Ionics*, **9/10**:1107.

Chabagno, J.M. (1980). PhD thesis, Univ. of Grenoble.

Chandra, S. (1981). *Superionic Solids-Principles and Applications.* North-Holland,Amsterdam.

Chandra, S., Hashmi, S.A. and Prasad, G. (1990). *Solid State Ionics*, **40/41**:651.

Chawdari, B.V.R., Chandra, S., *et al.* (1992). *Proceedings of the 3rd Asian Conference on Solid State Ionics, Materials and Applications*, Varanasi, India.

Chiang, C.K., Davis, G.T., *et al.* (1983). *Solid State Ionics*, **9/10**:1121.

Chung, S.H., Jefferey, K.R. and Stevens, J.R. (1991). *J. Chemical Physics*, **94**:1803.

Cohen, H.H. and Turnbull, D.J. (1959). *J. Chem. Phys.*, **31**:1164.

Davidson, W.H.T. (1955). *J. Chemical Society*, page 3270.

Davis, T. and Chiang, C.K. (1984). Oakland University MI. Meadow Brook Conference on Conducting Polymers.

Doolittle, A.K. (1951). *J. Appl. Physics*, **22**:471.

Doolittle, A.K. and Doolittle, D.B. (1957). *J. Appl. Phys.*, **26**:901.

Druger, S.D., Nitzan, A. and Ratner, M.A. (1983). *J. Chem. Phys.*, **79**:3133.

Druger, S.D., Ratner, M.A. and Nitzan, A. (1986). *Phys. Rev.*, **B31**:3939.

Dupon, R., Papke, B.L., *et al.* (1982). *J. Am. Chem. Soc.*, **104**:247.

Dupon, R., Papke, B.L., *et al.* (1984). *J. Electrochem. Soc.*, **131-3**:586.

Farrington, G.C. and Linford, P. (1987). *Polymer Electrolyte Review, Vol.1,2.* Elsevier, London.

Fauteux, D. and Robitaille, C. (1986). *J. Electrochem. Soc.*, **133**:307.

Fauteux, D., Prud'homme, J. and Harvey, P.E. (1988). *Solid State Ionics*, **28-30**:923.

Fenton, B.E., Parker, J.M. and Wright, P.V. (1973). *Polymer*, **14**:589.

Ferloni, P., Chiodelli, G., *et al.* (1986). *Solid State Ionics*, **18/19**:265.

Ferry, J.D. (1970). *Viscoelastic Properties of Polymers*, page 316. New York.

Feuillade, G. and Perche, Ph (1975). *J. Appl. Electrochem.*, **5**:63.

Fontanella, J.J., Wilson, J.J., *et al.* (1992). *Solid State Ionics*, **50**:259.

Fontanella, J.J., Wintersgill, M.C. and Calame, J.P. (1985). *J. Polymer Sci.:Polymer Phys. Ed.*, **23**:113.

Forsyth, M., Payne, V.A., *et al.* (1992). *Solid State Ionics*, **53-56**:1011.

Fuoss, R.M. and Krauss, C.H. (1933). *J. Am. Chem. Soc.*, **55**:2387.

Gang, W., Roos, J., *et al.* (1992). *Solid State Ionics*, **53-56**:1102.

Gauthier, M., Fauteux, D., *et al.* (1985). *J. Electrochem. Soc.*, **132**:1333.

Geller, S. (1967). *Science*, **157**:301.

Geller, S. (1975). *Topics in Applied Physics : Solid Electrolytes.* Springer-Verlag, Berlin.

Gibbs, J.H. and DiMarzio, E.A. (1958). *J. Chem. Phys.*, **28**:373.

Glasse, M.D., Latham, R.J., *et al.* (1992). *Solid State Ionics*, **53-56**:1111.

Gorecki, W., Andreani, R., *et al.* (1986). *Solid State Ionics*, **18/19**:295.

Goulart, G., Sanchez, J.Y. and Armand, M. (1992). *Electrochimica Acta*, **37**(9):1589.

Gray, F.M. (1990). *Solid State Ionics*, **40/41**:637.

Greenbaum, S.G. (1985). *Solid State Ionics*, **15**:259.

Hagenmuller, P. and VanGool, W. (1977). *Solid Electrolytes : General Principles, Characterization, Materials, Applications.* Academic Press, New York.

Hardy, L.C. and Shriver, D.F. (1984). *Macromolecules*, **17**:977.

He, Y., Chen, Z., *et al.* (1986). *Chem. J. Chinese Univ.*, **2**:97.

Hibma, T. (1983). *Solid State Ionics*, **9/10**:1101.

Hooper, A. and North, J.M. (1983). *Solid State Ionics*, **9/10**:1160.

Huang, W. and Frech, R. (1992). *Solid State Ionics*, **53-56**:1095.

Huq, R. and Farrington, G.C. (1988). *Solid State Ionics*, **28-30**:990.

Huq, R., Saltzberg, M. and Farrington, G.C. (1989). *J. Electrochem. Soc.*, **136**:1260.

Ichikawa, K. and MacKnight, W.J. (1992). *Polymer*, **33**:4693.

Ichikawa, K., Dickinson, L.C., *et al.* (1992). *Polymer*, **33**:4699.

Ito, Y., Syakushiro, K., *et al.* (1986). *Solid State Ionics*, **18/19**:277.

Jalamon, M.B. (1979). *Topics in Current Physics, Vol. 15*,Physics of Superionic Conductors. Springer-Verlag.

Jr., A.S. Barker, Ditzenberger, J.A. and Remeika, J.P. (1976). *Phys. Rev.*, B **14**:4254.

Kelly, I.E., Owen, J.R. and Steele, B.C.H. (1984). *J. Electroanal. Chem.*, **168**:467.

Ketlaar, J.A.A. (1934). *Z. Physik Chem.*, **B26**:327.

K.Funke (1987). *Z. Physik. Chem.*, **154**:25.

Killis, A., LeNest, J.F., *et al.* (1982). *Makromol. Chem.*, **183**:2835.

Killis, A., LeNest, J.F., *et al.* (1984). *Macromolecules*, **17**:63.

Klug, H.P. and Alexander, L.E. (1974). *X-Ray diffraction Procedures for Polycrystalline and Amorphous Materials.*

Kobayashi, N., Uchiyama, M., *et al.* (1985). *J. Phys. Chem.*, **89**:987.

Kuroda, Y. and Kubo, M. (1955). *J. Polymer Science*, **24**:323.

Kuroda, Y. and Kubo, M. (1959). *J. Polymer Science*, **26**:453.

Latimer, W.H. (1952). *Oxidation Potentials,2nd edition.* Prentice Hall, Englewood cliff,NJ.

Lee, C.C. and Wright, P.V. (1982a). *Polymer*, **23**:681.

Lee, C.C. and Wright, P.V. (1982b). *Polymer*, **23**:690.

Lee, Y.L. and Crist, B. (1986). *J. Appl. Phys.*, **60**:2683.

LeNest, J.F., Cheradame, H. and Gandini, A. (1988). *Solid State Ionics*, **28–30**:1032.

Linden, E. and Owen, J.R. (1988). *Solid State Ionics*, **28-30**:995.

Liu, K.J. and Parson, J.L. (1969). *Macromolecules*, **2**:529.

MacCallum, J.R. and Vincent, C.A. (1987). *Polymer Electrolyte Review, Vol.1,2.* Elsevior, London.

MacCallum, J.R., Smith, M.J. and Vincent, C.A. (1984). *Solid State Ionics*, **11**:307.

Macdonald, J.R. (1986). *Solid State Ionics*, **13**:147.

Macdonald, J.R. and Cook, J.R. (1984). *J. Electroanal. Chem.*, **168**:335.

Macdonald, J.R., Schoonman, J. and Lehnen, A.P. (1982). *J. Electroanal. Chem.*, **72-75**:131.

Matsui, Y., Kubota, T., *et al.* (1965). *J. Polymer Science*, **A3**:2275.

Mendolia, M.S. and Farrington, G.C. (1992). *Solid State Ionics*, **53-56**:1059.

Miller, H. (1966). *The Structure of Polymers.* Reinhold,New York.

Minier, M., Berthier, C. and Gorecki, W. (1983). *Solid State Ionics*, **9/10**:1125.

Minier, M., Berthier, C. and Gorecki, W. (1984). *J. Physique*, **45**:739.

M.Minier and Berthier, C. (1983). Proceedings of the 3rd solid state ionics conference , also in solid state ionics (1984), Grenoble.

Nagae, S., Nekoomanesh, H.M., *et al.* (1992). *Solid State Ionics,* **53-56**:1118.

Owens, B.B. and Argue, G.R. (1967). *Science,* **157**:308.

Panero, S., Scrosati, B. and Greenbaum, S.G. (1992). *Electrochimica Acta.,* **37**:1533.

Papke, B.L., Ratner, M.A. and Shriver, D.F. (1981). *J. Phys. Chem. Solids,* **42**:493.

Papke, B.L., Ratner, M.A. and Shriver, D.F. (1982a). *J. Electrochem. Soc.,* **129**:1694.

Papke, B.L., Ratner, M.A. and Shriver, D.F. (1982b). *J. Electrochem. Soc.,* **129**:1434.

Przyluski, J. and Wieczorek, W. (1989). *Solid State Ionics,* **36**:165.

Purohit, H.D. and Sengwa, R.J. (1991). *J. Polym. Mater.,* **8**:317.

Ratner, M.A. (1987). *Polymer Electrolyte Review, Vol 1,* page 173. Elsevier.

Reitman, E.A., Kaplan, M.L. and Cava, R.J. (1985). *Solid State Ionics,* **17**:67.

Reitman, E.A., Kaplan, M.L. and Cava, R.J. (1987). *Solid State Ionics,* **25**:41.

Reuter, B. and K.Hardel (1961). *Natureweissenschaften,* **48**:161.

Robitaille, C., Marques, S., *et al.* (1987). *Macromolecules,* **20**:3023.

Rossi, C. and Magnasco, V. (1962). *J. Polymer Science,* **58**:977.

Sanchez, S.Y. (1992). in *Proceedings of the 3rd Asian Conference on Solid State Ionics, Materials and Applications* (edited by Chawdari, B.V.R., Chandra, S., *et al.*), Varanasi, India.

Sandahl, J., Schantz, S., *et al.* (1989). *J. Chem. Physics,* **91**:123.

Schantz, S., Kakikhana, M. and Sandberg, M. (1990). *Solid State Ionics,* **40/41**:645.

Schrama, J. (1957). PhD thesis, Leiden.

Scrosati, B. (1988). Proceedings of the international seminar on solid state ionic devices, Singapore.

Seanor, D.A. (1982). *Electrical Properties of Polymers.* Academic Press,London.

Shahi, K. (1977). *Phys. Stat. Sol.(a),* **41**:11.

Shahi, K. (1983). *Lithium Batteries,* page 407. Academic Press, New York.

Shahi, K. and Chandra, S. (1975). *Phys. Stat. Sol.(a),* **28**:653.

Shriver, D.F., Papke, B.L., *et al.* (1981). *Solid State Ionics,* **5**:83.

Slade, R.C.T. (1985). *Solid State Commun.,* **54**:1035 and references cited therein.

Sonderegger, M., Roos, J., *et al.* (1992). *Solid State Ionics,* **53-56**:849.

Sorensen, P.R. and Jacobsen, T. (1982). *Electrochimica Acta,* **27**:1671.

Stainer, M., Hardy, L.C., *et al.* (1985). *J. Electrochem. Soc.,* **131**:784.

Strock, L.W. (1934). *Z. Physik. Chem.,* **B25**:411.

Takahashi, T. and Yamamoto, O. (1966a). *Electrochimica Acta.,* **11**:779.

Takahashi, T. and Yamamoto, O. (1966b). *Electrochimica Acta,* **11**:911.

Takahashi, Y. and Tadokoro, H. (1973). *Macromolecules,* **6**:672.

Teeters, D. and Norton, J.C. (1990). *Solid State Ionics,* **40/41**:648.

Thomas, J.O. (1992). Proceedings of the 3rd asian conference on solid state ionics, materials and applications, Varanasi, India.

Torell, L.M. and Angell, C.A. (1988). *Br. Polymer Journal,* **20**:173.

Tsunemi, K., Ohno, H. and Tsuchida, E. (1983). *Electrochem. Acta.,* **28**:833.

Tubandt, C. and Lorenz, E. (1914). *Z. Physik. Chem.,* **87**:513.

Tubandt, C. and Reinhold, H. (1934). *Z. Physik Chem.*, **B24**:22.

Watanabe, M. (1992). in *Proceedings of the 3rd Asian Conference on Solid State Ionics, Materials and Applications* (edited by Chawdari, B.V.R., Chandra, S., *et al.*), Varanasi, India.

Watanabe, M., Itoh, M., *et al.* (1987). *Macromolecules*, **20**:569.

Watanabe, M., Togo, M., *et al.* (1984). *Macromolecules*, **17**:2908.

Watanabe, M., Waganaka, H., *et al.* (1992). *Electrochimica Acta*, **37**(9):1521.

Weiczorek, W., Such, K., *et al.* (1989). *Solid State Ionics*, **36**:255.

Weston, J.E. and Steele, B.C.H. (1981). *Solid State Ionics*, **2**:347.

White, H.F. and Lovell, C.M. (1962). *J. Polym. Science*, **58**:977.

Williams, M.L., Landel, R.F. and Ferry, J.D. (1955). *J. Amer. Chem. Soc.*, **77**:3701.

Wilson, A. and Prosser, H.J. (1982). *Developments in Ionic Polymers.* Applied Science Publishers, London.

Wintersgill, M.C., Fontanella, J.J., *et al.* (1983). *Solid State Ionics*, **11**:151.

Wong, T., Brodwin, M., *et al.* (1980). *Solid State Commun.*, **35**:591.

Wright, P.V. (1975). *Br. Polymer Journal*, **7**:319.

Wright, P.V. (1976). *Br. Polymer J.*, **7**:319.

Xie, L. and Farrington, G.C. (1993). *Solid State Ionics*, **60**:19.

Xue, R. and Angell, C.A. (1987). *Solid State Ionics*, **25**:223.

Yanagida, S., Takahashi, K. and Okahara, M. (1978). *Bull. Chem. Soc. Japan*, **51**:1294.

Bibliography for Table 1.1

Andeen, M., Ravaina, D. and Souquet, J.L. (1976). *C.R. Acad. Sci. Paris,Ser C*, **282**:499.

Baurle, J.E. (1966). *J. Chem. Phys.*, **45**:4162.

Bradley, J.N. and Greene, P.D. (1967). *Trans. Farad. Soc.*, **63**:434.

Chabagno, J.M. (1980). PhD thesis, Univ. of Grenoble.

Chaklanobis, S., Shahi, K. and Syal, R.K. (1990). *Solid State Ionics*, **44**:107.

Dudney, N.J. (1988). *Solid State Ionics*, **28-30**:1065.

Etsell, T.H. and Fleugas, S.N. (1970). *Chem. Rev.*, **70**:339.

Farrington, G.C., Frase, K.G. and Thomas, J.O. (1984). *Advances in Materials Science.*

Fujitsu, S., Koumoto, K. and Yanagida, H. (1986). *Solid State Ionics*, **18/19**:1146.

Geller, S. and Owens, B.B. (1972). *J. Phys. Chem. Solids*, **33**:1241.

Ghosal, B., Mangle, E.A., *et al.* (1983). *Solid State Ionics*, **9/10**:273.

Gratzer, W., Bittner, H., *et al.* (1971). *Z. Kristallograph.*, **133**:260.

Hartwig, R., Rabenau, A. and Weppner, W. (1981). *J. Less-Common Metals*, **78**:227.

Huggins, R.A. (1977). *Electrochimica Acta*, **22**:773.

Jackson, J.H. and Young, D.A. (1969). *J. Phys. Chem. Solids*, **30**:1973.

Kawamoto, Y., Nagura, N. and Tsuchikashi, S. (1974). *J. Amer. Ceramic Soc.*, **57**:489.

Kennedy, J.H., Meles, R. and Hunter, J. (1973). *J. Electrochem. Soc.*, **120**:1441.

Ketlaar, J.A.A. (1938). *Trans. Farad. Soc.*, **34**:874.

Khandkar, A. and Wagner, J.B. (1986). *Solid State Ionics*, **20**:257.

Kummer, J.T. (1972). *Prog. Solid State Chem.*, **7**:141.

Lunze, D. (1972). *Fast Ion Transport in Solids.*